SENSING AND MODELLING
FOR OXYGEN LEAD SOFTENING

by

JOËL PATRICK THIERRY KAPUSTA

Maîtrise de Science, Université de LYON I, France, 1985
Diplôme d'Etudes Approfondies, Université de NANCY I, France, 1986

A THESIS SUBMITTED IN PARTIAL FULFILLMENT OF

THE REQUIREMENTS FOR THE DEGREE OF

DOCTOR OF PHILOSOPHY

in

THE FACULTY OF GRADUATE STUDIES

(Department of Metals & Materials Engineering)

We accept this thesis as conforming
to the required standard

THE UNIVERSITY OF BRITISH COLUMBIA

August 1995

In presenting this thesis in partial fulfilment of the requirements for an advanced degree at the University of British Columbia, I agree that the Library shall make it freely available for reference and study. I further agree that permission for extensive copying of this thesis for scholarly purposes may be granted by the head of my department or by his or her representatives. It is understood that copying or publication of this thesis for financial gain shall not be allowed without my written permission.

(Signature)

Department of Metals and Materials Engineering

The University of British Columbia
Vancouver, Canada

Date Sept. 15, 1995

DE-6 (2/88)

ABSTRACT

Lead ores generally contain significant amounts of arsenic and antimony. The process of lead softening, corresponding to the removal of these hardening impurities, is therefore of necessity in any pyrometallurgical lead refining circuit. Even in a smelter where electrorefining is used, a partial softening might be required. The treatment of silver bearing concentrates, while providing additional revenues, also introduces additional amounts of arsenic and antimony into the circuit. The efficiency of the Betts electrorefining process depends on the stability of the corroding lead anodes. Anode slime stability is directly related to the antimony and arsenic content of the anodes. Thus, control of bullion quality prior to anode casting is key to optimization of the electrorefining operations, improvement of lead production, and addition of revenues. The (partial) softening stage is the ideal location in a smelter for such a control. When composition spikes are regular occurrences, the batch softening circuit tends to become somewhat complicated to reduce their effects. In this thesis work, the option of continuous single pass softening has been explored. In particular, the two critical components to this revision, i.e. a method of continuously monitoring bullion quality, and a control strategy, were investigated.

An oxygen probe for continuous measurements in molten lead has been designed in the laboratory prior to being tested in an industrial environment. A commercially available yttria stabilized zirconia serves as solid electrolyte. The reference system is composed of a Cu-Cu_2O mixture. Both lead wire and conducting lead (probe housing) are made of 316 stainless steel. Sealing is achieved by means of a high temperature magnesia cement. An additional plug of copper powder, isolated from the reference system by a layer of alumina powder, serves as oxygen getter

to eliminate oxygen ingress from the atmosphere. The extremity of the lead wire that is inserted into the probe is coated with cement to avoid any short-circuit with the Cu plug. These features were decisive in the success of the probe which provides a continuous measurement for several consecutive days. Once it was established that the probe was giving satisfactory measurements in the laboratory, i.e. quick response, proper response to temperature changes and oxygen potential changes, a testing campaign was carried out in the plant. The campaign was successful and a correlation between measured emf and As+Sb bullion content was established.

Since any control decision would be based on the probe readings, it is crucial to regularly ensure the proper functioning of the probe. A method based on the thermal arrest technique has been tested and calibrated to provide for a quick assessment of the probe reliability.

A thermodynamic model of the current semi-batch process was developed. An analysis of the process showed that a thermodynamic model can be used to represent process operation, and an equilibrium analysis gave a reasonable fit to operating data. The model developed for semi-batch softening was modified to continuous softening in order to simulate continuous single pass softening. The preliminary calculations showed that the concept of continuous single pass softening will meet the target set for lead softening, assuming the process operates close to thermodynamic equilibrium. A slag high in As+Sb can be produced at bullion compositions in the target range for electrorefining. Based on the data presented in this thesis, a simple feedback control algorithm could be developed to regulate O_2 injections to a continuous softener on the basis of the measured level of As+Sb in output bullion.

TABLE OF CONTENTS

	Page
ABSTRACT	ii
TABLE OF CONTENTS	iv
LIST OF TABLES	viii
LIST OF FIGURES	x
LIST OF NOMENCLATURE	xiv
ACKNOWLEDGEMENTS	xvii
CHAPTER 1	
INTRODUCTION: LEAD REFINING	1
1.1 Lead Softening Practices	3
1.2 Cominco's Lead Softening Practice	13
CHAPTER 2	
LITERATURE REVIEW: OXYGEN PROBES AND PROCESS CONTROL	23
2.1 Oxygen Probes	24
2.1.1 Oxygen Probe Principle	25
2.1.2 Oxygen Probe Applications in Process Control	30
2.1.2.1 Steelmaking Industry	30
2.1.2.2 Non-Ferrous Industry	32
2.1.3 Oxygen Probe Applications in Molten Lead	39

2.2 Process Modelling 44
2.2.1 Thermodynamic Models 45
2.2.2 Kinetics Models 48
2.2.3 Conclusions 49

CHAPTER 3

SCOPE AND OBJECTIVES 51

CHAPTER 4

OXYGEN PROBE DESIGN 55
4.1 Selection of Probe Components 56
4.1.1 Solid Oxide Electrolyte 56
4.1.2 Reference System 60
4.1.3 Lead Wire and Conducting Lead 67
4.1.4 Conclusions 68
4.2 Probe Development in Laboratory 70
4.2.1 Experimental Apparatus 70
4.2.2 Cell Assembly 75
4.2.3 Measurements in Molten Lead 84

CHAPTER 5

INDUSTRIAL TRIALS 94
5.1 Softening Process Investigations 95
5.1.1 Preliminary Sampling Campaign 95
5.1.2 Softening Chemistry and Oxygen Efficiency 103

5.1.3 Conclusions 106
5.2 Oxygen Probe Plant Tests 110
5.2.1 Oxygen Potential Measurements 110
5.2.2 Results and Discussion 112
5.2.3 Conclusions 118
5.3 Thermal Arrest Technique 120

CHAPTER 6

SOFTENING PROCESS MODELLING AND CONTROL STRATEGY 127
6.1 Model Formulation 128
6.1.1 Assumptions 128
6.1.2 Computation of Equilibrium Composition 130
6.1.3 Solution Modelling 134
6.2 Model Validation and Calibration 138
6.2.1 Solution Modelling Validation 138
6.2.2 Model Calibration 139
6.2.3 Analysis of the Batch Process 144
6.2.4 Batch Process Operation 151
6.3 Continuous Single Pass Softening Process 153
6.3.1 Assumptions 153
6.3.2 Process Analysis 155
6.3.3 Control Strategy 164

CHAPTER 7

SUMMARY AND RECOMMENDATIONS 166

7.1 Summary 166

6.3 Recommendations 168

REFERENCES 169

APPENDIX 1 EXPERIMENTAL EQUIPMENT 176

APPENDIX 2 PLANT DATA 181

LIST OF TABLES

Table 1.1	Typical assays of lead bullion and slag in the softening circuit (early 1992).	15
Table 2.1	Characteristics of emf cells used for oxygen measurements in molten lead.	43
Table 4.1	Equilibrium oxygen pressure of various metal-metal oxide systems at temperatures between 500 and 700°C.	65
Table 4.2	Properties of Y_2O_3 fully stabilized zirconia from Coors Ceramic Co.	68
Table 4.3	Assays for Cu and Cu_2O powders from Cerac Inc.	69
Table 4.4	Computed values of $P_{O_2\,(Pb/PbO)}$, $P_{O_2\,(Cu/Cu_2O)}$, and E_{th}.	81
Table 4.5	Comparison of theoretical and measured emf for various probes immersed in oxygen saturated molten lead.	88
Table 4.6	Measured emf in laboratory tests and corresponding lead bullion assays.	93
Table 5.1	Assays of softener bullion for vertical gradient assessment (measurement #1).	100
Table 5.2	Assays of softener bullion for vertical gradient assessment (measurement #2).	101
Table 5.3	Assays of softener bullion for vertical gradient assessment (measurements #3 and #4).	101
Table 5.4	Assays of softener slag from opposite sides of the vessel for vertical gradient assessment (measurements #5 and #6).	102
Table 5.5	Process parameters and assays of softener slag and bullion for softener chemistry assessment (test #1, June 1994).	108
Table 5.6	Process parameters and assays of softener slag and bullion for softener chemistry assessment (test #2, October 1994).	109
Table 5.7	Measured emf in softener vessel and corresponding lead bullion assays.	117
Table 6.1	Equilibrium reactions representing the oxygen softening process.	129

Table 6.2	Molar balance equations of the chemical system representing the oxygen softening process.	129
Table 6.3	Expressions for the temperature dependence of the standard Gibbs free energies of all species.	135
Table 6.4	Oxygen saturation in liquid lead at different temperatures. Comparison between the model computations and the relationship from Alcock and Belford (1964, ref. 42).	139
Table 6.5	Batch softening model parameters (June plant data and corresponding model calculations).	142
Table 6.6	Batch softening model parameters (October plant data and corresponding model calculations).	143
Table 6.7	Batch softening model parameters.	144
Table 6.8	Equilibrium constants of As and Sb oxidation (Reactions (III) and (IV)).	150
Table 6.9	Continuous softening model parameters.	154
Table 6.10	Continuous softening model parameters.	155

LIST OF FIGURES

Figure 1.1	Lead production flowchart (Adapted from Davey, 1980, ref. 1).	2
Figure 1.2	Pyrometallurgical lead refining flowchart (Adapted from Davey, 1980, ref. 1).	4
Figure 1.3	Harris machine (From Leroy *et al.*, 1970, ref. 7).	5
Figure 1.4	Batch refining kettle (Adapted from Bowers and Johnston, 1984, ref. 9).	8
Figure 1.5	Simplified view of a reverberatory softening furnace (Adapted from Gilges *et al.*, 1981, ref. 10).	9
Figure 1.6	Softening rate as a function of bullion composition (Adapted from Green, 1950, ref. 13).	10
Figure 1.7	Oxygen-assisted kettle (Adapted from Blanderer, 1984, ref. 14).	12
Figure 1.8	Cominco's lead refining process flowchart.	16
Figure 1.9	Scale drawing of Cominco's original softener (Adapted from de Groot *et al.*, 1989, ref. 16).	17
Figure 1.10	Cominco's original lead softening circuit.	18
Figure 1.11	Cominco's current lead softening circuit.	19
Figure 1.12	Schematic drawing of Cominco's current softener.	22
Figure 2.1	Schematic representation of pure zirconia and calcia stabilized zirconia.	26
Figure 2.2	Schematic diagram of emf generation in an oxygen concentration cell using calcia stabilized zirconia as solid oxide electrolyte.	29
Figure 2.3	Schematic drawing of a typical oxygen probe for application in molten metal.	31
Figure 2.4	Progress of silicon-deoxidation recorded by the electromotive force measurements of an oxygen probe at 1600°C (From Turkdogan and Fruehan, 1972, ref. 26).	33

Figure 2.5	Sublance system for automatic dipping of oxygen sensors into a steelmaking converter (From Goto, 1988, ref. 37, after Ariga and Ogawa, 1977, ref. 35).	34
Figure 2.6	Computing system to control the content of soluble aluminum in Al-Si killed steel and the magnitude of the deoxidation of Si-semi-killed steel (From Goto, 1988, ref. 37, after Hiromoto *et al.*, 1977, ref. 36).	35
Figure 2.7	Improvements in deviation from target value of the content of soluble aluminum in Al-killed steels before and after the use of oxygen sensors (From Goto, 1988, ref. 37, after Hiromoto *et al.*, 1977, ref. 36).	36
Figure 2.8	Feed-back control system for continuous casting of tough pitch copper billet using an oxygen probe at the exit of the launder (From Dompas and Lockyer, 1972, ref. 39).	37
Figure 2.9	Schematic illustration showing how the oxygen content in flowing molten copper is continuously measured in the launder (From Goto, 1988, ref. 37).	38
Figure 2.10	Correlation between oxygen partial pressure in the slag and lead content of the slag (From Fontainas *et al.*, 1985, ref. 52).	41
Figure 3.1	Continuous single pass softening circuit.	52
Figure 4.1	Schematic drawing showing the effect of temperature and oxygen pressure on the conductivity of a solid oxide electrolyte (Adapted from Patterson, 1971, ref. 74).	58
Figure 4.2	Schematic representation of (a) partial electrical conductivities, (b) ionic transference number in Y_2O_3 - doped ThO_2, and (c) effect of dopant concentration on partial conductivities in ThO_2 - Y_2O_3 solid solutions (Adapted from Choudhary *et al.*, 1980, ref. 75).	59
Figure 4.3	Conductivity of various solid oxide electrolytes as a function of temperature (Adapted from Choudhary *et al.*, 1980, ref. 75).	61
Figure 4.4	Electrolytic domain of various zirconia solid oxide electrolytes as a function of temperature and oxygen partial pressure (Adapted from De Schutter *et al.*, 1991, ref. 57).	62
Figure 4.5	Characteristics of commercial zirconia solid electrolytes (Adapted from Nippon Kagaku Togyo Co. Ltd. marketing pamphlet, 1991, ref. 83).	63
Figure 4.6	Overvoltage versus current for various metal-metal oxide systems at 900°C (Adapted from Worrel and Iskoe, 1973, ref. 84).	66

Figure 4.7	Schematic representation of the experimental set-up for laboratory tests.	71
Figure 4.8	Temperature profile along the vertical axis of the chamber with location and length of the hot zone (± 1°C) for a temperature set point of 610°C using the outer thermocouple (S-type).	72
Figure 4.9	Schematic representation of the chamber with measuring devices in position for laboratory tests.	74
Figure 4.10	Schematic representation of the possible cell assembly geometries for oxygen probes.	76
Figure 4.11	Schematic representation of the first design of cell assembly used in the early experiments.	77
Figure 4.12	Scale drawing of the steel sleeve used as housing for the probe tip (35 mm long zirconia thimble shown in position).	78
Figure 4.13	Emf and temperature readings recorded during a test with a probe fabricated according to the design adopted in the early tests.	83
Figure 4.14	Schematic representation of the improved design of cell assembly. ..	85
Figure 4.15	Schematic representation of the probe and the probe holding device.	86
Figure 4.16	Typical probe response upon immersion into an oxygen saturated lead melt at 697°C ± 1°C.	89
Figure 4.17	Probe response to a temperature change. Initial temperature 683°C, intermediate temperature 730°C, and final temperature back to 683°C.	91
Figure 4.18	Probe response to additions of antimony at temperatures around 625°C.	92
Figure 5.1	Close-up of softener circuit.	96
Figure 5.2	Dimensions of the softener unit as of June 1994.	99
Figure 5.3	Typical recording of emf and temperature measured in the softener vessel.	113
Figure 5.4	Plot of plant and laboratory emf measurements versus total impurity content of lead bullion.	115
Figure 5.5	Plot of plant and laboratory emf measurements versus As+Sb content of lead bullion.	116

Figure 5.6	Schematic representation of a probe tip with a steel cup for sludge protection.	119
Figure 5.7	Thermal arrest apparatus.	121
Figure 5.8	Cooling curve of pure lead.	122
Figure 5.9	Cooling curve of "North Pot" bullion containing 2 wt% total impurity.	123
Figure 5.10	Calibration curve for thermal arrest technique.	124
Figure 5.11	Plot of As+Sb content in output bullion versus total impurity content.	126
Figure 6.1	Simplified flow diagram of the whole algorithm.	132
Figure 6.2	Simplified flow diagram of the minimization routine.	133
Figure 6.3	As+Sb removal during a softening cycle in batch and continuous slag removal modes.	145
Figure 6.4	Oxygen partition during a softening cycle in batch mode.	147
Figure 6.5	Evolution of the slag composition during a softening cycle in batch and continuous slag removal modes.	148
Figure 6.6	Effect of temperature on the slag composition during a softening cycle in batch mode.	149
Figure 6.7	Effect of impurity level and O_2 injection rate on output bullion quality (615°C, 15.5 tph input bullion).	157
Figure 6.8	Relationship between slag composition and impurity level in output bullion (615°C).	158
Figure 6.9	Variation of $P_{O_2}^{3/4}$ with impurity level in output bullion (615°C).	159
Figure 6.10	Sensitivity of impurity removal rate to O_2 injection rate (615°C, 15.5 tph input bullion).	160
Figure 6.11	Effect of bullion flow rate on impurity level in output bullion (615°C).	162
Figure 6.12	Effect of temperature on impurity level in output bullion (40 Nm^3/h O_2, 15.5 tph bullion).	163

LIST OF NOMENCLATURE

$a_{i,j}$	Activity of species i in phase j
B_i	Absolute mobility of species i
c_i	Concentration of species i
e	Elementary charge
E	Electromotive force
E_{meas}	Measured electromotive force
$E_{O.C.}$	Open circuit electromotive force
E_{th}	Theoretical electromotive force
F	Faraday constant
$G^{0}_{i,j}$	Standard Gibbs free energy of species i in phase j
$\overline{G}^{ex}$	Excess Gibbs free energy
G^{*}	Reduced Gibbs free energy
j_i	Flux of particle i
K	Equilibrium constant
$n_{i,j}$	Number of moles of species i in phase j
p_{O_2}	Oxygen partial pressure
R	Gas constant
T	Temperature
$T_{bullion}$	Bullion temperature
T_{slag}	Slag temperature
t_i	Transference number of species i

$t_{electron}$	Transference number of electrons
t_{ion}	Transference number of ions
$X_{i,j}$	Mole fraction of species i in phase j
z_i	Valency of species i

Greek Symbols

$\gamma_{i,j}$	Activity coefficient of species i in phase j
γ_i^0	Activity coefficient of species i at infinite dilution
ε_O^O	Self interaction coefficient of oxygen
η_i	Electrochemical potential of species i
μ_i	Chemical potential of species i
σ_i	Electrical conductivity of species i
σ_n	Electron free conduction
σ_{ion}	Ionic conduction
σ_p	Positive hole conduction
ϕ	Electrostatic potential

Subscripts

(s)	solid phase
(l)	liquid phase
(g)	gas phase

Other Symbols

Nm^3	Normal cubic meter

min	Minute
tph	Tonne per hour
at%	Atom percent
emf	Electromotive force
$\underline{X}_{(Bullion)}$	Dissolved element X in lead bullion

ACKNOWLEDGEMENTS

I would like to express my sincerest thanks to Dr. Greg Richards for his confidence in me and inspiration to me. I would like to extend my utmost gratitude to Dr. Ray Meadowcroft who graciously offered his help part way through this project and generously dealt with most of my worrying and complaining. Special thanks to my wife, Radka, for her patience, support, and help all along this research work. I am also very grateful to my daughter, Claire, who convinced me to complete my thesis, and successfully motivated me to do so.

I would also like to acknowledge the assistance of Cominco personnel, and in particular, Gerry Toop, Tom De Groot, Mark Plamondon, Wayne Teague and Dan Brew without whom the plant trials would not have been possible.

The financial assistance of Cominco Ltd., the B.C. Science Council, and the Natural Sciences and Engineering Research Council is gratefully acknowledged.

Thanks are also due to those members of the Department of Metals and Materials Engineering who helped in this endeavor, and in particular to Peter Musil for his invaluable contributions to the manufacturing and maintenance of my experimental apparatus. Special thanks to my office mates, Cornelius Muojekwu and Sunil Kumar, and to Bernardo Hernandez Morales for their friendship, support, and helpful discussions.

J'aimerais aussi remercier très sincèrement mes parents pour leur aide, leur soutien, et leurs encouragements répétés durant toutes mes longues années d'étude.

CHAPTER 1

INTRODUCTION: LEAD REFINING

In the course of the production of lead from ore to refined product, each stage can be considered as a refining operation since impurities are separated from the valuable product in each of these steps, as shown in Figure 1.1. However, in this figure, Davey[1] restricts the term "refining" to the operations carried out downstream of the smelting stage. Lead refining usually involves a number of different steps depending on the type and amount of impurity elements present in the molten metal. Copper, arsenic, antimony, sulphur, tin, bismuth, silver and gold are the main impurities present in crude lead. Most of the copper is removed from the lead by cooling the molten bullion to near its freezing point and precipitating the copper and the copper compounds in a dross or matte. Since there is no practical alternative to the pyrometallurgical process for copper removal, lead bullion is always thermally drossed as a first refining step[2]. Following copper drossing, two alternative routes are possible: either electrolytic or pyrometallurgical refining. Electrolytic refining is the only process that can adequately produce refined lead with a low level of bismuth (less than 10 ppm). Due to its high capital cost, this route is less attractive and is adopted only where high-purity metal (low bismuth level) is required by the market[2] or where there is cheap power. In most of the lead refineries around the world, operations are entirely pyrometallurgical, with a few exceptions such as Cominco Ltd. (British Columbia)[3], Monteponi & Montevecchio Co. (Sardinia)[4], Cerro de Pasco Co. (Peru)[5], or Shenyang Smelter (China)[6] where electrolytic techniques are used. Pyrometallurgical refining, which involves reacting the impurity elements with sulphur, oxygen, zinc, calcium, etc., in order to produce various slags or drosses, is reasonably selective in impurity

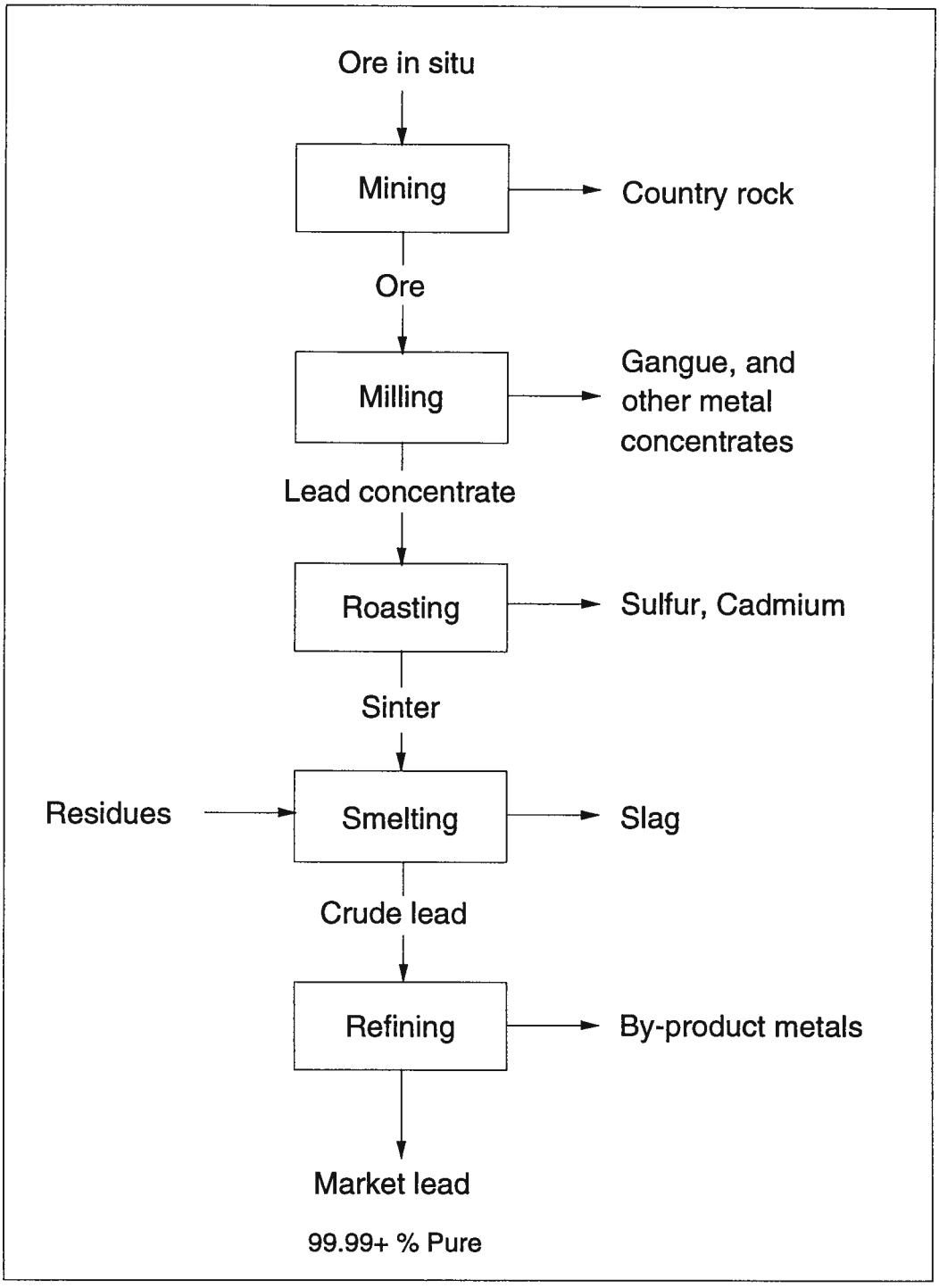

Figure 1.1 - Lead production flowchart (Adapted from Davey, 1980, ref. 1).

removal and the refined metal can meet the majority of the market requirements[2]. A typical pyrometallurgical route for lead refining is shown in Figure 1.2. In each successive step, the impurity level of one or more elements is decreased to trace level. Of particular interest for this project, the softening step corresponds to the removal of the hardening impurity elements, namely antimony, arsenic and tin, by selective oxidation due to differences in the free energies of formation of the oxides of these elements and lead. Current lead softening practices are reviewed and discussed in the following section. Details of Cominco's softening process are then presented to provide the industrial background of the project.

1.1 Lead Softening Practices

When lead bullion from a smelter is refined via an electrolytic route, antimony and arsenic are commonly added to the bullion prior to anode casting in order to achieve the desired hardness level required in the refinery. Removal of antimony, arsenic and tin, or softening, is usually performed in pyrometallurgical refineries. The preferential oxidation of the hardening elements can be accomplished at either low or high temperature.

In the low temperature alternative, softening is carried out in a kettle at about 450°C by adding a strong oxidizing agent, such as sodium nitrate, and absorbing the resulting sodium antimonate, arsenate and stannate into a caustic soda melt. This softening variant is commonly called the Harris process[1,7,8]. At the Metallurgie Hoboken refinery[7], lead softening is performed in Harris machines as shown in Figure 1.3. A reaction cylinder rests above a holding pot with its lower part immersed in liquid lead. The softening cycle starts by pouring molten caustic soda into the reaction cylinder. Then lead is pumped from the pot and injected into the cylinder where it migrates through the

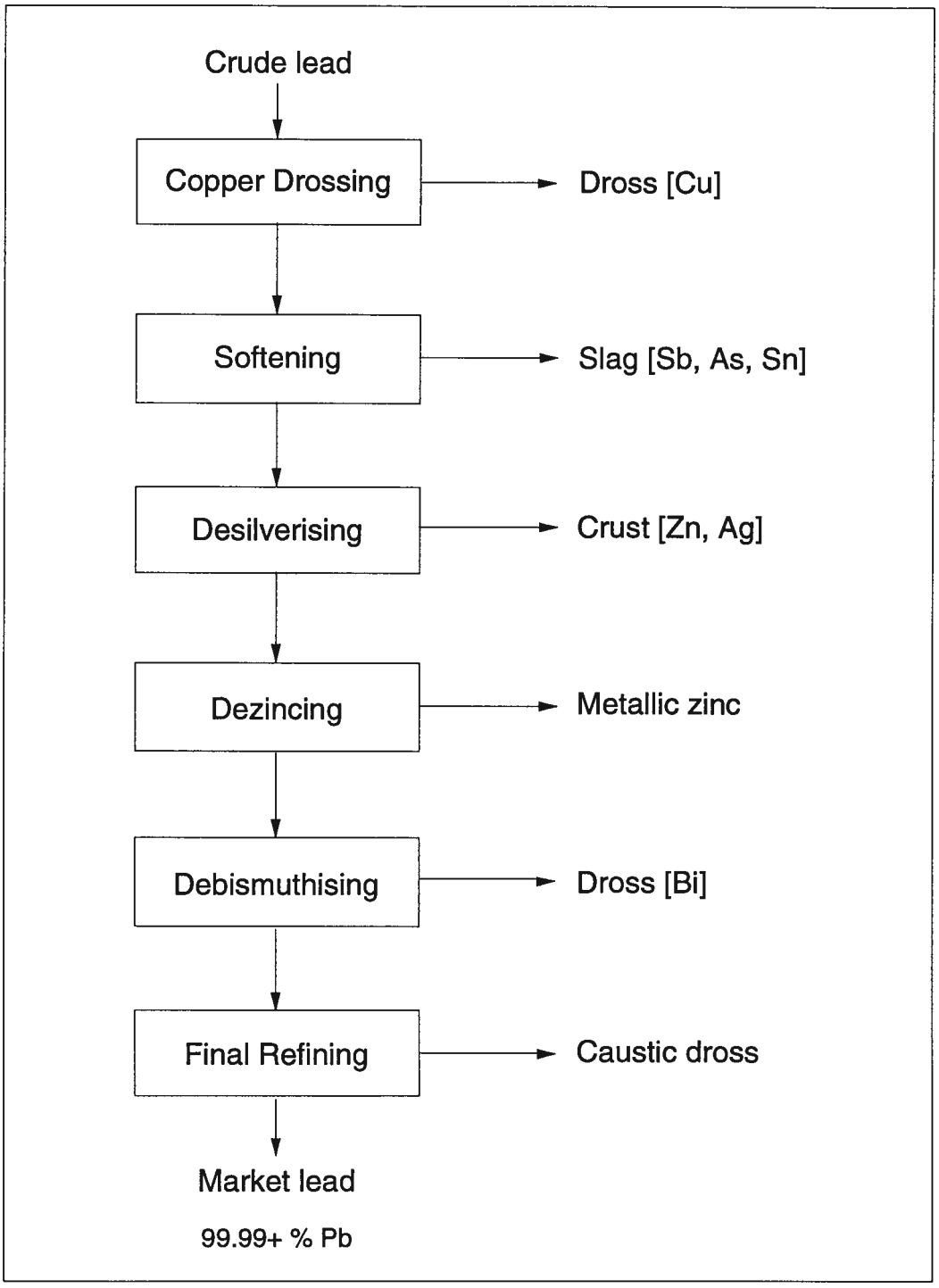

Figure 1.2 - Pyrometallurgical lead refining flowchart (Adapted from Davey, 1980, ref. 1).

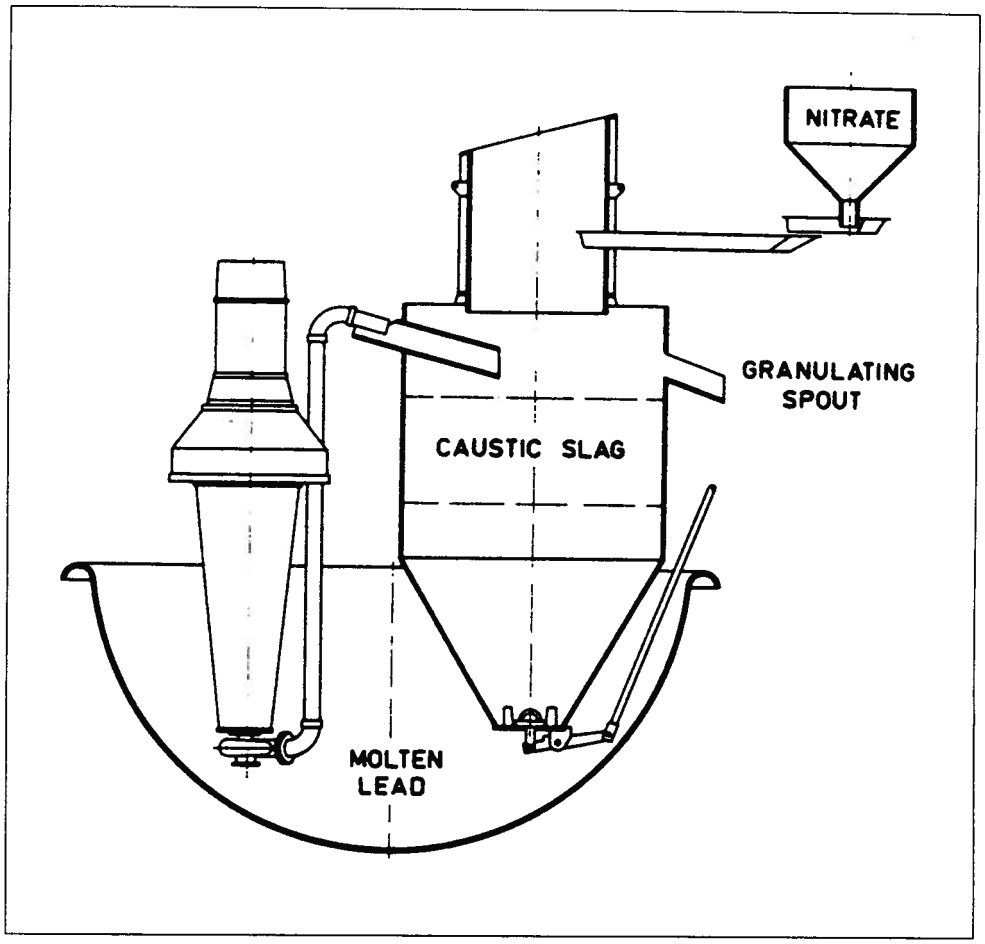

Figure 1.3 - Harris machine (From Leroy *et al.*, 1970, ref. 7).

caustic slag before returning to the pot through the valve located at the bottom of the cylinder. Each time lead flows through the slag, dissolved tin, arsenic or antimony together with some lead react with air or sodium nitrate and collect in the caustic slag layer. The reaction involving antimony, for example, can be described as follows:

$$2\,\underline{Sb}_{(Bullion)} + 2\,NaNO_3 + 4\,NaOH \leftrightarrow 2\,Na_3SbO_4 + N_2 + 2\,H_2O$$

The Harris process oxidizes very little lead and can be operated selectively for arsenic and tin with respect to antimony[2]. This selective softening can be achieved by means of several Harris machines in series, the first machines removing arsenic and tin with traces of antimony, provided the sodium nitrate is added in the appropriate proportion, the last machines removing the remaining antimony. The caustic soda, which can be regenerated by evaporation, not only participates in the oxidation reactions but also acts as a suspension medium for the reactants, facilitating their separation from the lead bullion[1].

The high temperature alternative involves oxidation by injecting air or oxygen into the molten lead at 600°C to 750°C to form a liquid slag containing most of the hardening impurities[9-13]. The basic reactions involved are the following:

$$1/2\,O_{2\,(g)} \leftrightarrow \underline{O}_{(Bullion)}$$

$$Pb_{(l)} + \underline{O}_{(Bullion)} \leftrightarrow PbO_{(Slag)}$$

$$\underline{Sb}_{(Bullion)} + 3/2\,\underline{O}_{(Bullion)} \leftrightarrow SbO_{1.5\,(Slag)}$$

$$\underline{As}_{(Bullion)} + 3/2\,\underline{O}_{(Bullion)} \leftrightarrow AsO_{1.5\,(Slag)}$$

This softening variant can be performed in batch or continuous mode. Batch softening is usually carried out in kettles of up to 350-tonne capacity, with most medium sized refineries (30,000 tons/year) having kettles of about 50 to 100-tonne capacity with a diameter of 2 to 3 metres (see Figure 1.4). Reverberatory furnaces (see Figure 1.5) are usually used for continuous softening in refineries with large bullion throughput (over 100,000 tons/year).

The BHAS refinery at Port Pirie, Australia, is well known for its high performances as a result of continuous efforts devoted to research[11-13]. Their softening process is the most efficient process in the world and serves as a reference and a source of inspiration for many refineries, including Cominco's. For that reason, it seems legitimate to provide more details of this particular operation. Softening at Port Pirie is carried out continuously in a reverberatory furnace to reduce the antimony content of the bullion from about 0.8 % to about 0.03 %, and the arsenic from about 0.2% to less than 0.001%. The oxidation of the hardening impurities is enhanced by the strong agitation of the bath accompanying the air injection. The temperature of crude lead bullion is about 400°C to 450°C while the temperature of the softener bath is in the range 700°C to 760°C. The oxidation reactions contribute largely to the heat requirements of the process. The rate of input bullion into the furnace and the amount of air injected are adjusted in such a manner that the impurity level in the bath remains in the composition range corresponding to the shaded area in Figure 1.6. This is to take advantage of the effect of varying antimony concentration on the rate of oxidation. As Green[13] points out, only a continuous process can gain the greatest advantage of the oxidation rate phenomenon by oxidizing the antimony as fast as it is supplied. The slag produced has roughly the following composition: 75% Pb, 12% Sb and 2% As. Removing the last traces of antimony is usually performed in a final refining step using caustic soda.

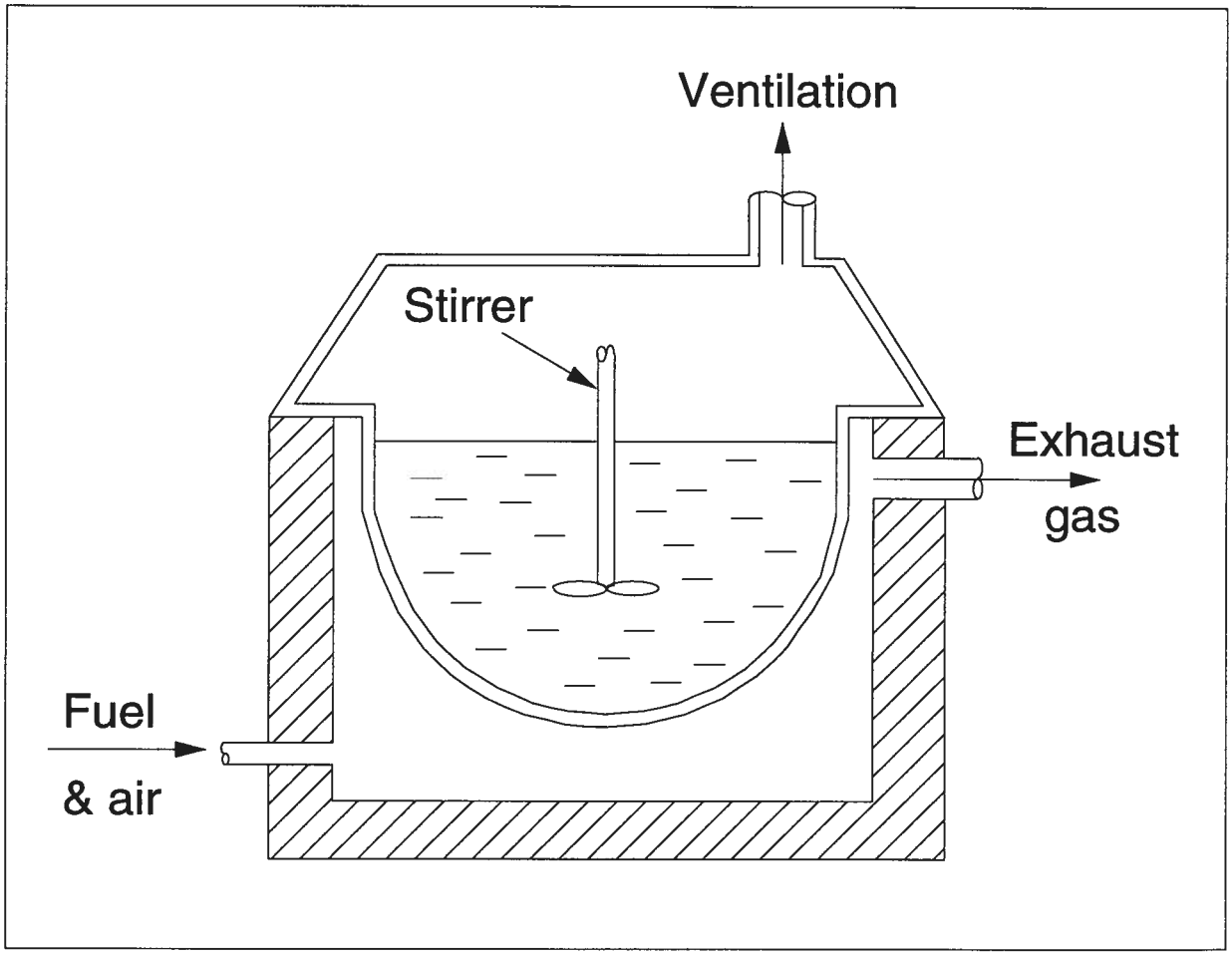

Figure 1.4 - Batch refining kettle (Adapted from Bowers and Johnston, 1984, ref. 9).

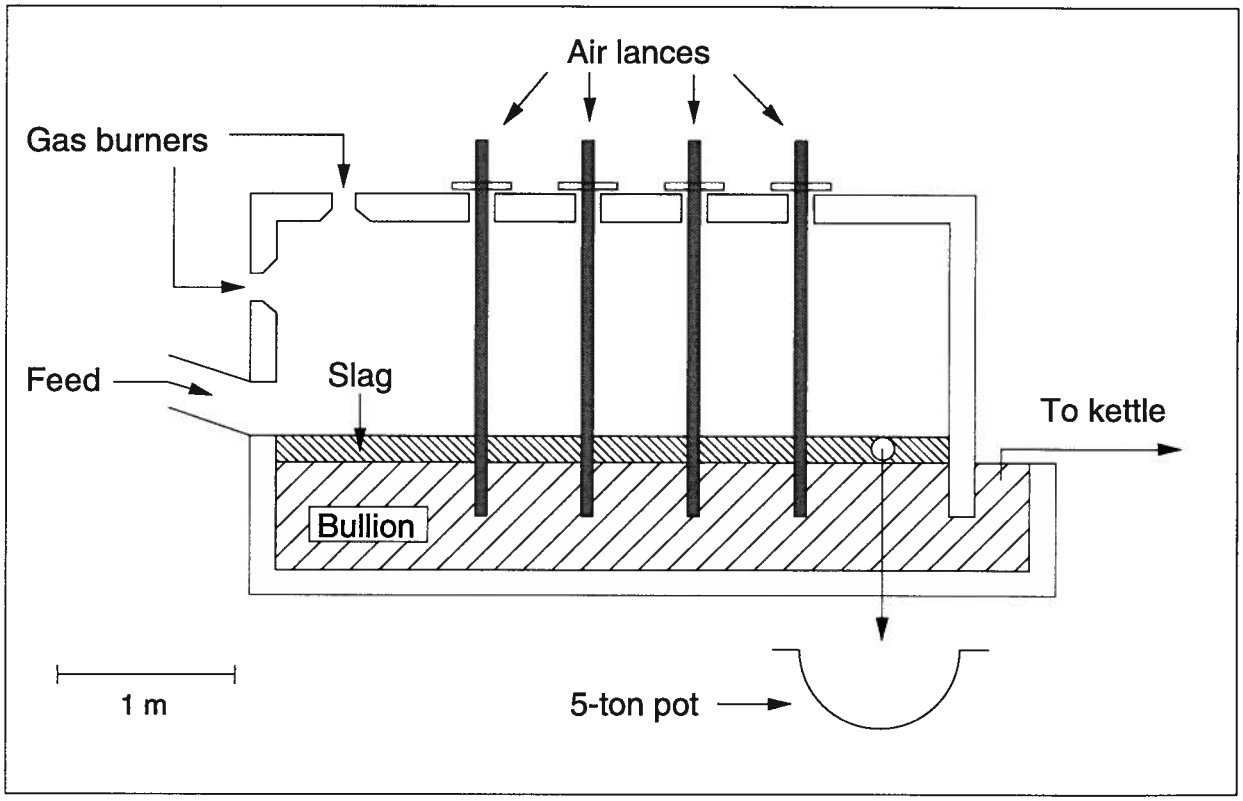

Figure 1.5 - Simplified view of a reverberatory softening furnace (Adapted from Gilges *et al.*, 1981, ref. 10).

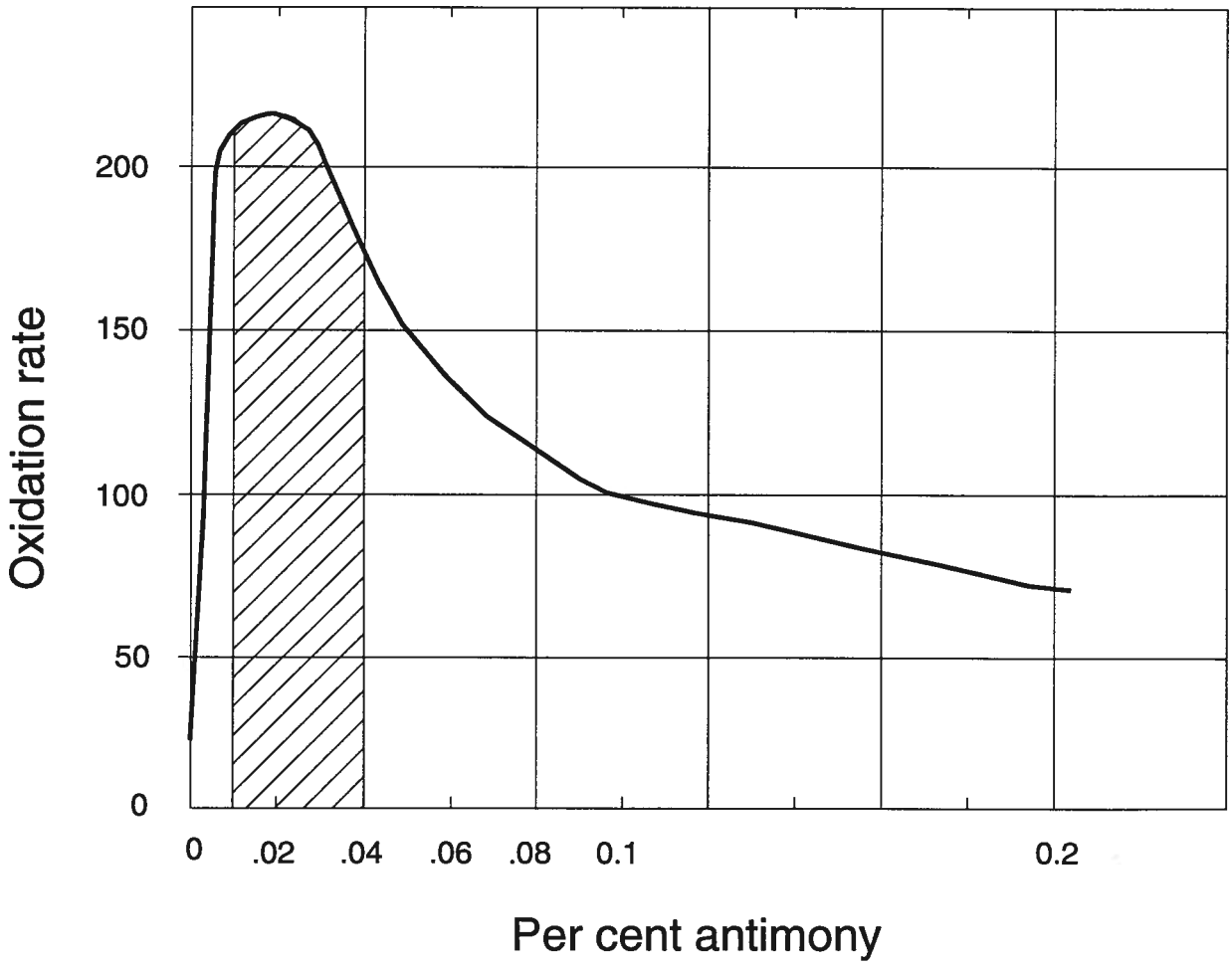

Figure 1.6 - Softening rate as a function of bullion composition (Adapted from Green, 1950, ref. 13).

A third alternative combines the use of caustic soda and high temperature. It is usually carried out in a stirred kettle at a temperature of about 630°C by addition of caustic soda into molten lead to form a dross which can be either dry or sticky. Air injection assists the process and promotes high softening rates. Blanderer[14], who patented a softening method using caustic soda in a kettle, claims to be able to achieve efficiencies close to those obtained in Port Pirie by injecting additional pure oxygen and adjusting the stirrer speed. A schematic drawing of Blanderer's oxygen-assisted kettle is given in Figure 1.7. With good control, i.e. limited arsenic vaporization, appropriate proportion of caustic soda, Quigley and Happ[15] report that selective oxidation of arsenic with respect to antimony can be achieved. The arsenic removal reaction can be described as follows:

$$\underline{As}_{(Bullion)} + 5\,NaOH + 5/2\,O_2 \leftrightarrow Na_3AsO_4 . 2\,NaOH + 3/2\,H_2O$$

The caustic soda requirements can be calculated from this reaction. Quigley and Happ[15] also observe that the selective extraction of arsenic occurs at the beginning of the process when the caustic slag is liquid. Once the slag is saturated with $Na_3AsO_4.2NaOH$, its viscosity increases and the selectivity decreases.

The choice between batch and continuous softening is site dependent since both have advantages and drawbacks. Batch softening requires that large holding pots or kettles are held at high temperature for long periods of time, which is costly in terms of energy requirements. It has, however, the advantage of being able to treat bullion of "abnormal" composition, such as high impurity feed bullion, by simply adjusting the operating conditions for the duration of the "abnormality". The number of kettles required depends on the throughput of the refinery. Large

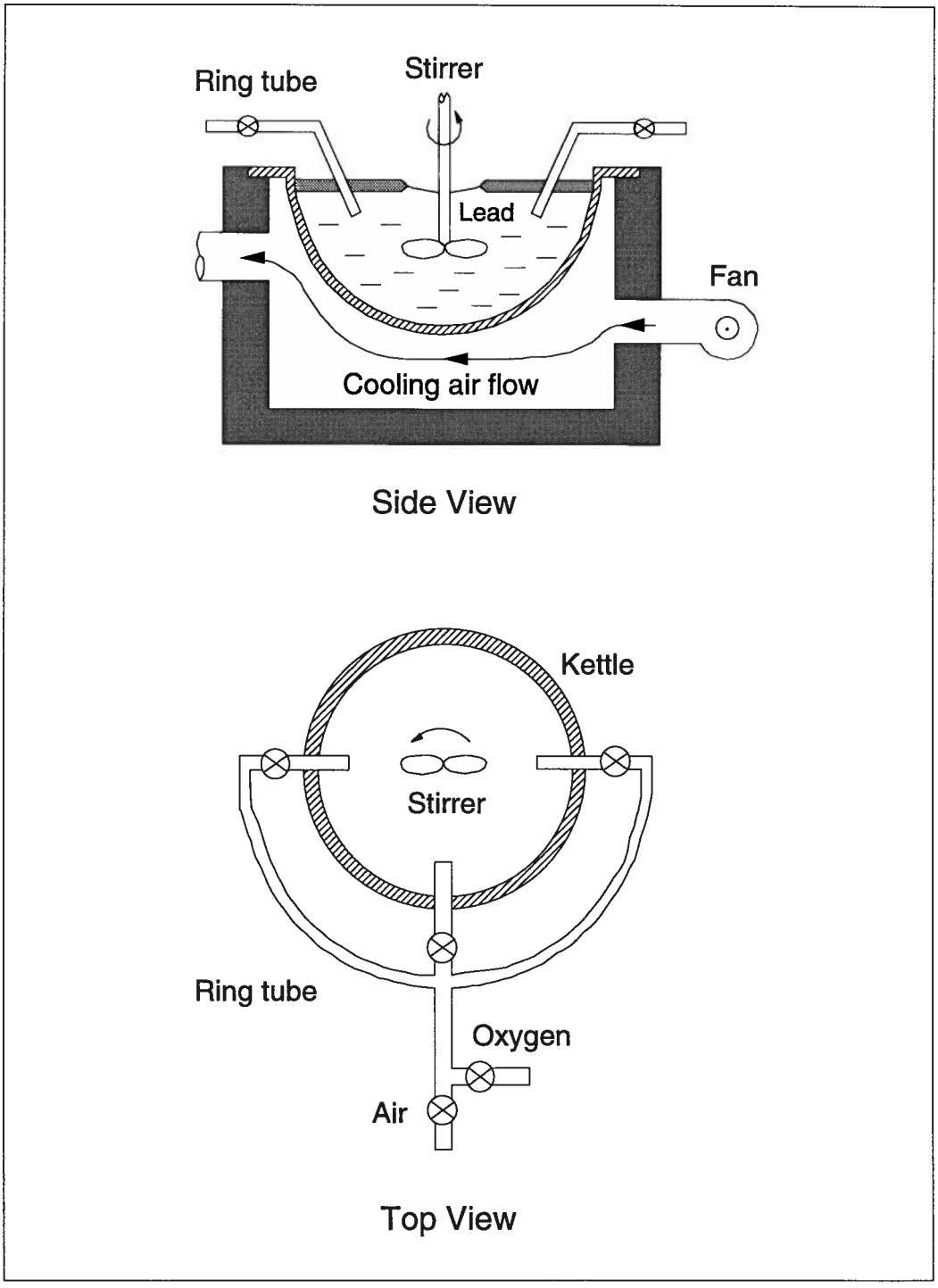

Figure 1.7 - Oxygen-assisted kettle (Adapted from Blanderer, 1984, ref. 14).

refineries may employ up to 5 kettles. Continuous softening on the other hand can be performed for large throughputs using smaller vessels at very high extraction rates. Since the process is controlled by the feed rate, the bullion and slag composition, the temperature and the degree of agitation, any "abnormal" bullion composition cannot be easily handled. When it comes to hygiene, it is difficult to assess whether the batch or continuous alternative is better since hygiene depends on temperature (higher temperature favors large amounts of flue gases and dusts), vessel size (larger vessels produce larger amounts of by-products), and on the type of by-product (manual dross skimming or automatic slag tapping).

1.2 Cominco's Lead Softening Practice

At the Trail smelter of Cominco, lead is produced in blast furnaces from sinter made from a mixed feed of concentrates and zinc plant residues. In the subsequent electrolytic refining by the Betts process, certain impurities contained in the anodes, such as copper, antimony, arsenic, bismuth, silver and gold, remain on the corroding anode surface as an adhering layer of porous slime, while zinc, cadmium, nickel and cobalt dissolve into the electrolyte. High current efficiencies and the production of high-purity refined lead depend on the stability of the slime[3]. In order to ensure that the slime remains on the anode surface, specific levels of antimony and arsenic in the cast anodes are required. The optimum content of combined antimony and arsenic is in the range 1.5 to 2.0%. Historically, antimony and arsenic were supplemented downstream of the blast furnaces to maintain an appropriate composition of the anodes. Mainly due to increasing levels of antimony and arsenic in the Sullivan concentrate in the mid 1980s and the purchase of larger quantities of silver bearing concentrate inherently rich in antimony and arsenic, the content of antimony and arsenic has

exceeded the limits required for the Betts process. Removing the excess antimony and arsenic in the bullion became necessary. After reviewing the various options currently available for lead softening, a choice was made at Cominco to undertake partial softening with pure oxygen.

The original partial softening vessel, commissioned in 1986 and installed downstream of the Continuous Drossing Furnace (C.D.F.), as shown in Figure 1.8, was designed to operate semi-continuously[16]. It consists of a 20-tonne capacity vessel built from a blast furnace settler with a metal depth of about 0.8 meters (see Figure 1.9). It is serviced with four to six oxygen lances each fitted with an oxygen flow meter and carrying up to 20 normal cubic meters per hour of 98% oxygen. The impurities, mainly antimony and arsenic, together with some lead are oxidized and form a slag which is kept fluid at about 700°C by means of a natural gas burner. A schematic representation of the original softening circuit is shown in Figure 1.10. Copper is removed from the crude bullion in the C.D.F. Two 200-tonne capacity holding pots, called "North" and "South" pots due to their geographical positions in the plant, allow mixing of crude bullion from the C.D.F. with partially softened lead from the softener. In the summer of 1991, the circuit was modified in an attempt to increase the softening capacity and increase control on the anode composition. The new lay-out is given in Figure 1.11. The desired target of 1.5 to 2.0% combined antimony and arsenic in the anodes is achieved by intermittent pumping between the two pots. During the process, the bullion temperature in the softener increases due to the exothermic character of the oxidation reactions. A pump is interlocked with a thermocouple in order to maintain the temperature at the bottom of the vessel between 615°C and 625°C. At the upper limit of the temperature cycle, the pump is turned on and lead bullion at 450°C is drawn from the "North" pot, while partially softened bullion and slag are discharged, the bullion returning to the same pot. When the temperature drops to the lower limit, the pump is turned off, the bullion and slag discharge ceases, and softening proceeds. The

time duration between the two pumping actions corresponds to a softening cycle and lasts about 20 minutes. The slag is produced at a rate of about 15.8 metric tons per day, corresponding to about 220 kg per cycle. Typical assays of the various bullions and the slag are shown in Table 1.1.

Table 1.1 - Typical assays of lead bullion and slag in the softening circuit (early 1992). Lead constitutes the balance together with minor amounts of tin and silver.

Location	**Sb** (wt%)	**As** (wt%)	**Bi** (wt%)	**Cu** (wt%)
C.D.F. Bullion	3.00	0.46	0.10	0.19
South Pot Bullion	1.37	0.18	0.10	0.14
North Pot Bullion	1.19	0.14	0.10	0.14
Softener Bullion	0.76	0.07	0.11	0.14
Softener Slag	26.8	5.4	0.01	0.10

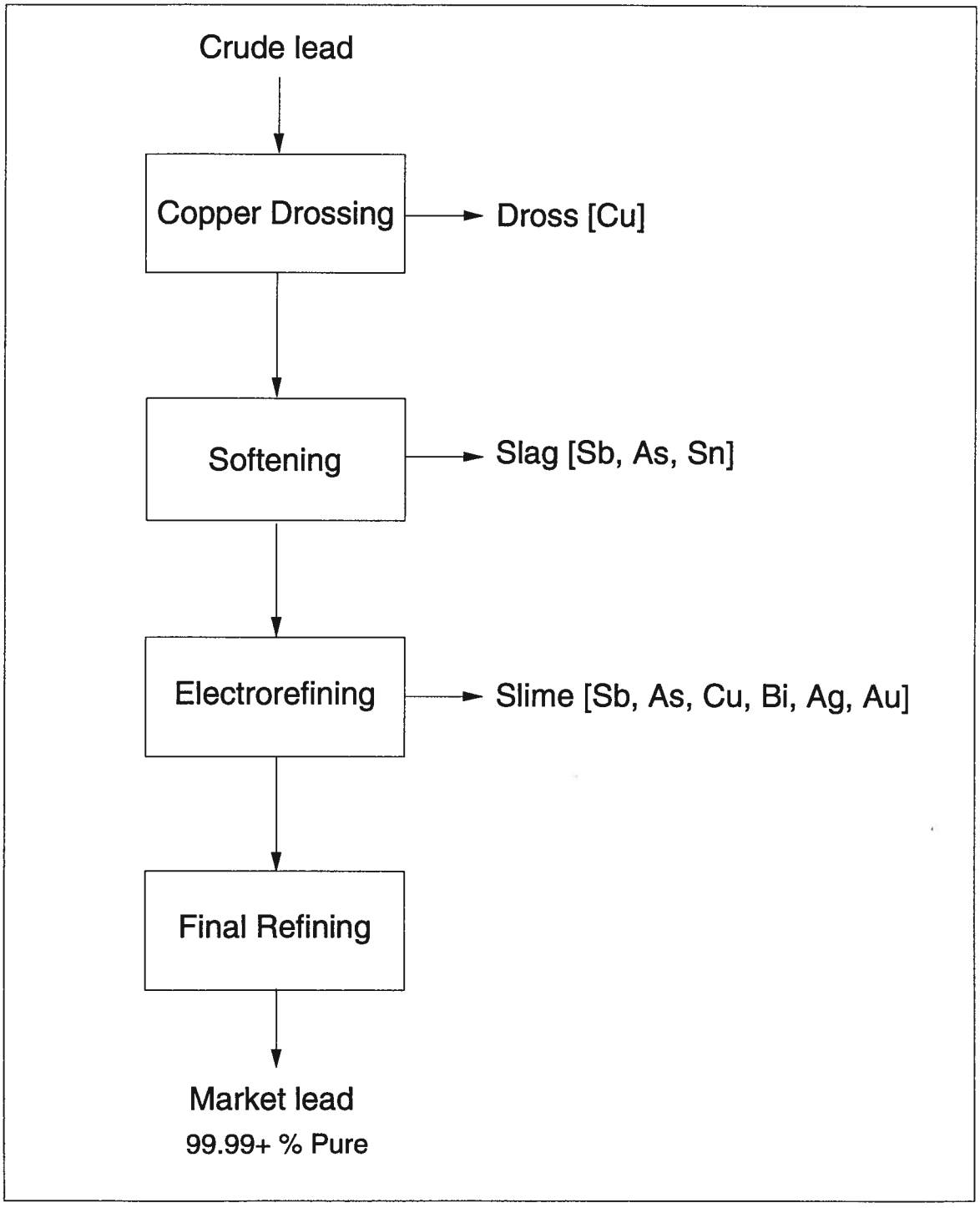

Figure 1.8 - Cominco's lead refining process flowchart.

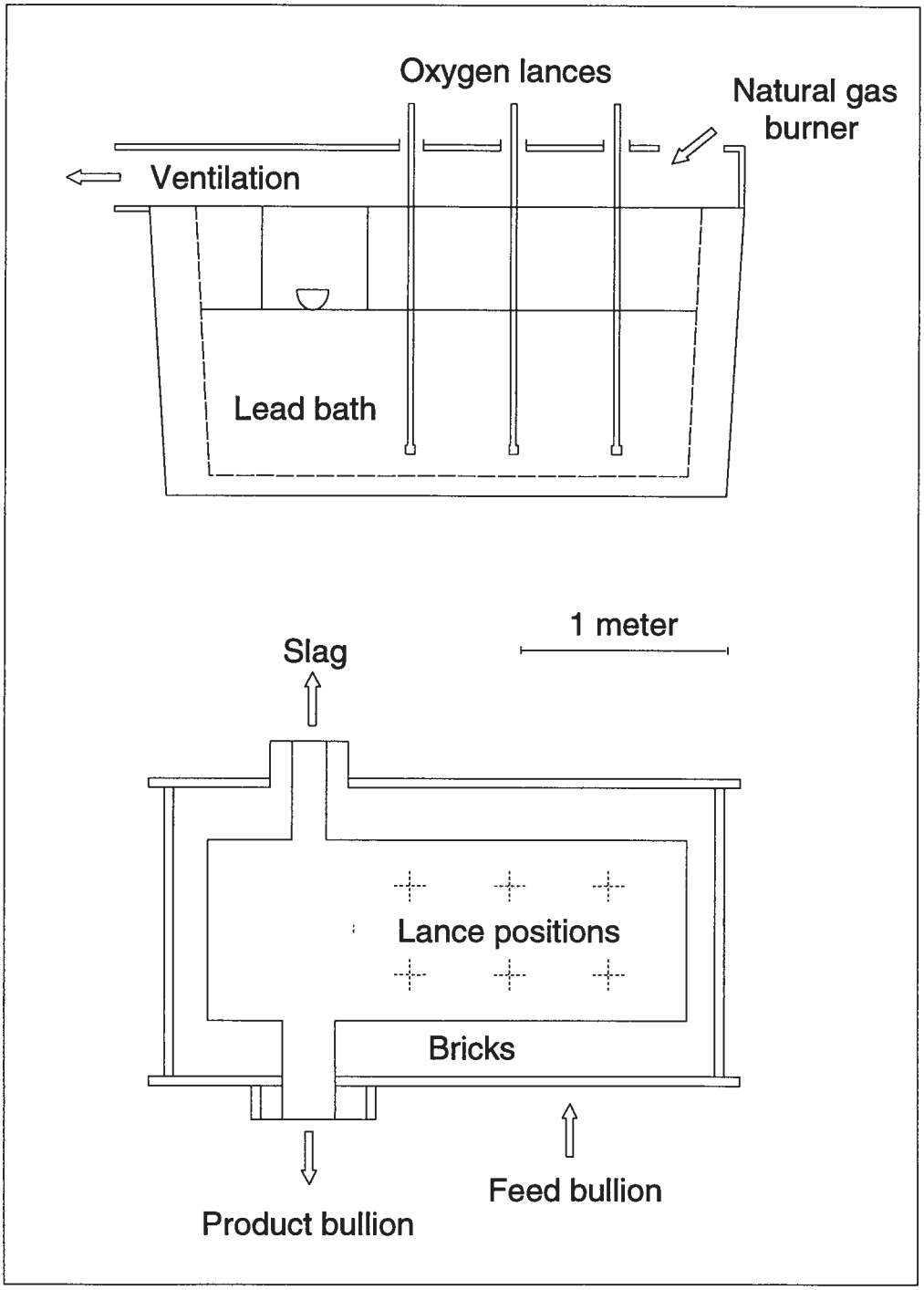

Figure 1.9 - Scale drawing of Cominco's original softener (Adapted from de Groot *et al.*, 1989, ref. 16).

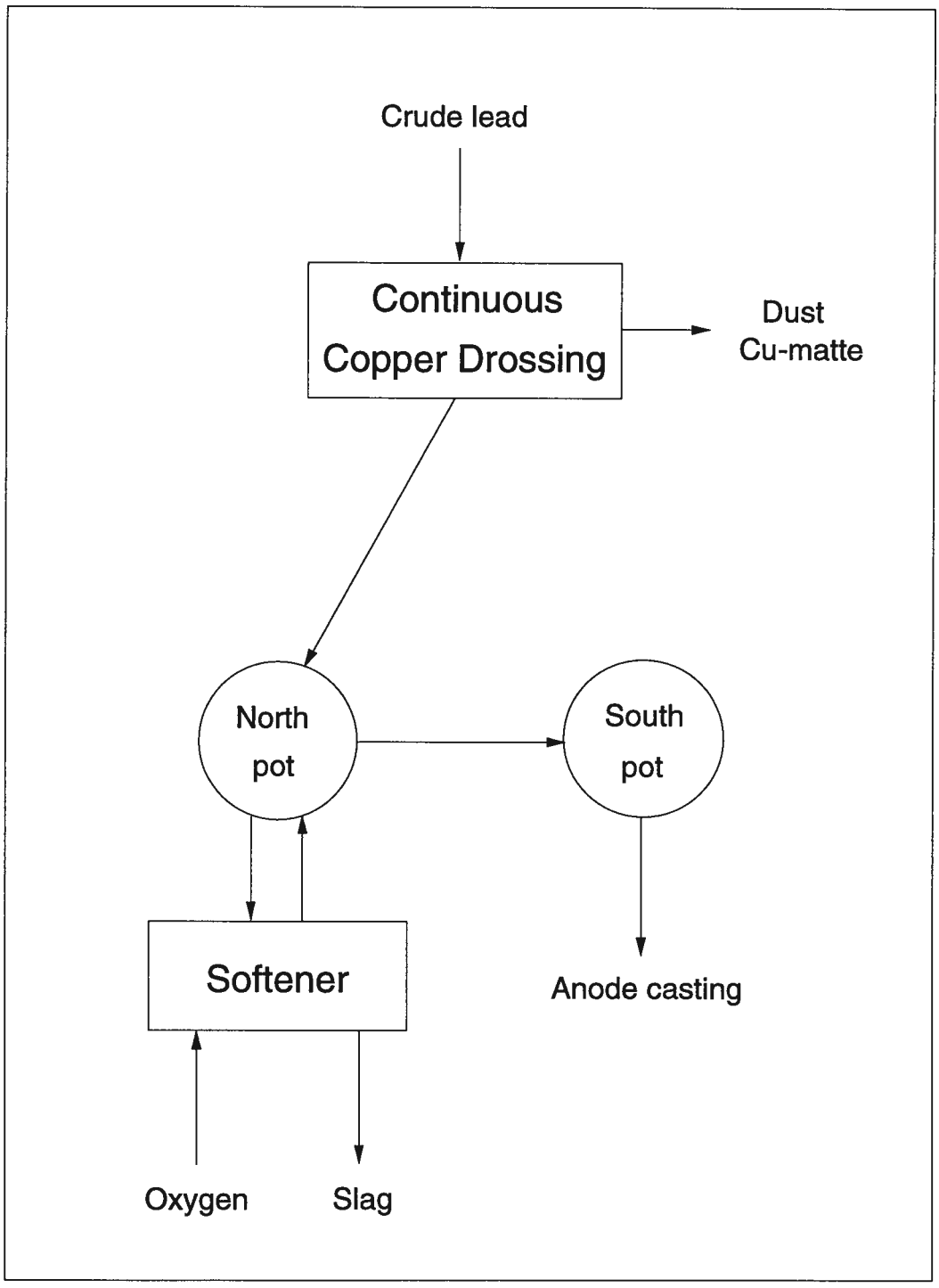

Figure 1.10 - Cominco's original lead softening circuit.

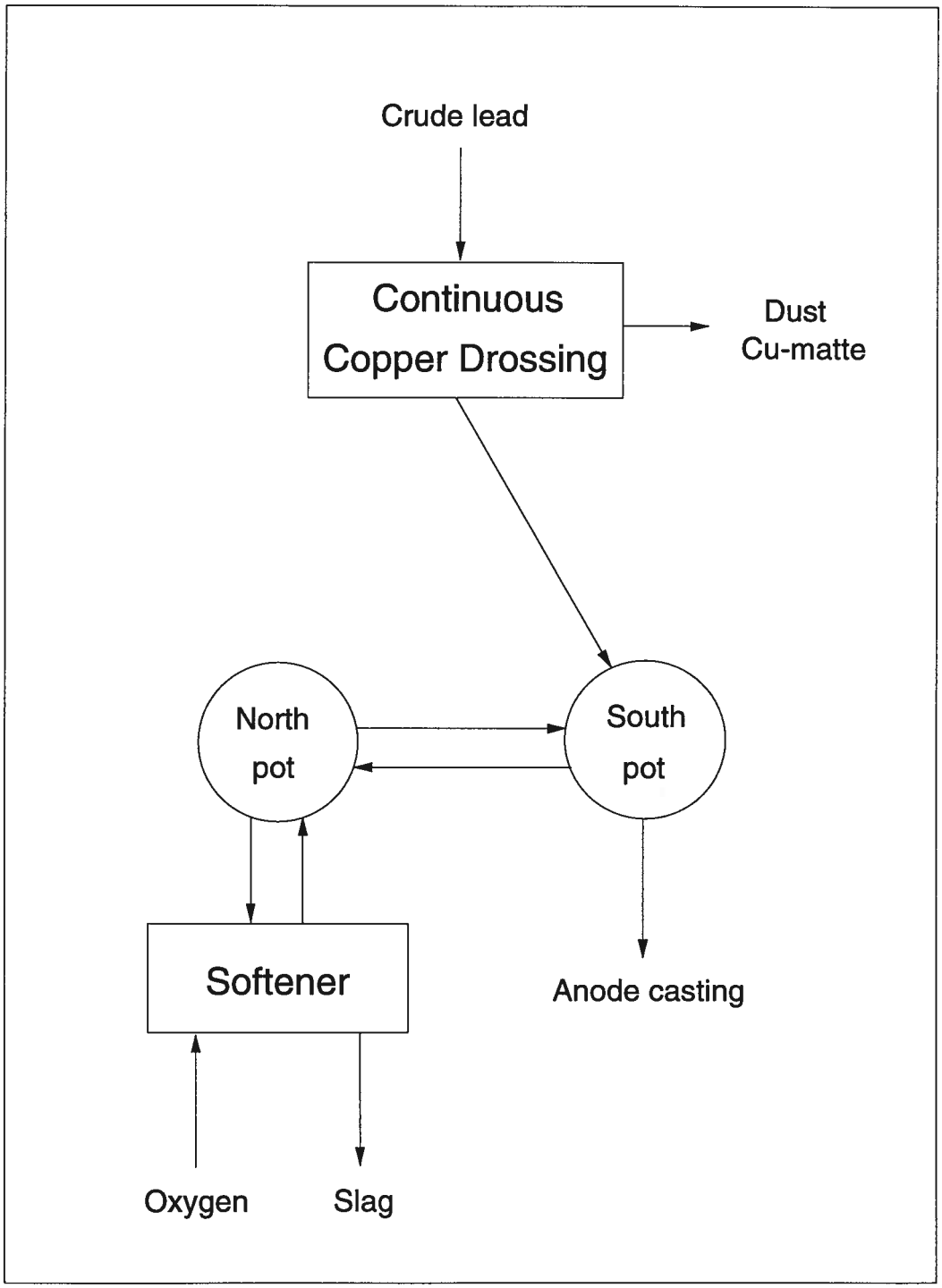

Figure 1.11 - Cominco's current lead softening circuit.

To accommodate the treatment of increasing quantities of silver bearing concentrate, a larger softener unit was commissioned and installed in 1992. The new unit consists of a circular 100-tonne capacity vessel serviced with up to eight oxygen lances (see Figure 1.12). A steel pipe, with a diameter of about 25 cm, is submerged into the molten lead and acts as the outlet for the softened bullion. A thermocouple, immersed one metre inside the pipe, serves as temperature controller to maintain the bullion temperature between 615°C and 630°C. Thus, the softener operates in a similar cyclic manner as the original unit. Two natural gas burners keep the slag fluid. As for the softening circuit, it remains unchanged with the exception that continuous pumping, rather than intermittent pumping, between the two holding pots was initiated to improve control over the anode composition.

Since the plant-scale softener was commissioned in 1989, Cominco lead furnaces staff have had to continuously modify and adapt the process to better respond to the changing operating conditions in the drossing plant: long term increase of bullion hardness due to the treatment of increasing amounts of silver concentrate, as well as daily fluctuations of incoming bullion composition due to changing operating conditions in the smelter. Holding a composition target is crucial in ensuring proper production in the refinery. Whatever the improvements achieved in the configuration of the process circuit or in the design of softening vessels, added revenues from silver recovery with good control of the production requires an ability to treat harder bullion with appropriate control of the output bullion composition from the softening stage. On-line composition control presents the best potential to achieve this goal.

Such a control requires an understanding of process fundamentals, and in particular process chemistry. Although much work as been devoted to the softener, no quantitative analysis of the process has been done. A number of fundamental questions are unanswered. For example, it is

not known whether composition and temperature gradients are present in the vessel. The oxygen efficiency has only been assessed qualitatively on the basis of the number of bubbles breaking the surface of the bath. The influence of bullion composition, and in particular high versus low As+Sb level and the ratio As/Sb, has been assessed based on an improper analysis of oxidation rate such as represented on Figure 1.6. Lower levels of As+Sb are believed to favor higher process efficiency. No characterization of the temperature effect on slag quality during normal operation, as opposed to during start-up, has been attempted. Moreover, only limited data are available in the literature on the chemical system Pb-Sb-As-O.

The following Chapter presents, on one hand, a review on sensors used in pyrometallurgy for process control purposes, and on the other hand, a review on process modelling.

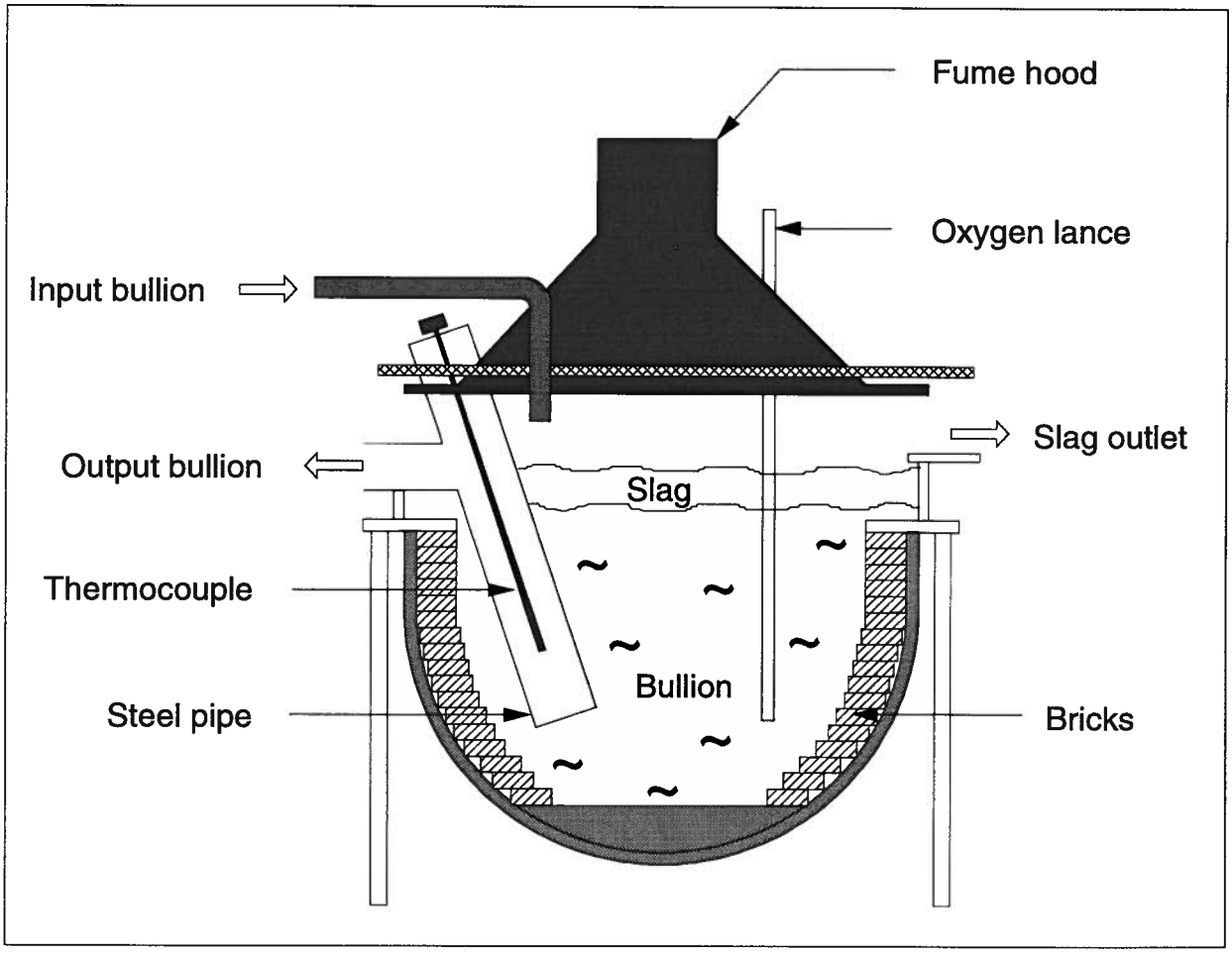

Figure 1.12 - Schematic drawing of Cominco's current softener.

CHAPTER 2

LITERATURE REVIEW: OXYGEN PROBES AND PROCESS CONTROL

A knowledge of the behavior of solutes such as oxygen, nitrogen or sulphur in metallic solutions is important for numerous chemical and metallurgical processes. In particular, the behavior of oxygen in molten metals governs industrial refining practices such as steel deoxidation, copper deoxidation or lead softening. In these refining operations, temperature and oxygen activity are the most important thermodynamic parameters. Consequently, the control of a refining process requires the monitoring of these two parameters. Temperature measurement has long been a common practice in ferrous and non-ferrous pyrometallurgy with the use of thermocouples. On the other hand, ***on-line*** oxygen determination without the need for sampling hot metals was not possible until the development of galvanic cells using solid oxide electrolytes. Since the pioneering work of Kiukkola and Wagner[17], tremendous progress has been achieved in improving the characteristics of solid oxide electrolytes and designing oxygen probes for rapid and accurate measurements of oxygen in molten metals.

A literature survey has been carried out covering the multiple aspects of oxygen probes: principle, design, and applications, and is presented in the first section. Even though the literature was extensively analyzed to elucidate the various design concepts, it is believed that it is best suited to present these concepts in Chapter 4, which specifically deals with the design, construction and testing of an oxygen probe for application in lead softening. The scope of the review in this Chapter is thus limited to the principle and the applications of oxygen probes.

The chemistry and kinetics of numerous pyrometallurgical processes were poorly understood at the time the first furnaces were built. Improvements in process efficiency were usually made by gradually implementing modifications in a process based on plant observations and experience. In this manner, new practices evolved, frequently leading to new furnace designs. The lead softening process in use at BHAS in Port Pirie, Australia, is a case in point. Over several years, a number of furnace designs were constructed and tested in the production circuit at very high costs until a satisfactory furnace was obtained[11-13]. With the development of computers, attempts at quantitatively analyzing pyrometallurgical processes in terms of chemistry and kinetics were made. Starting with simple assumptions, mathematical models of various processes were developed and gradually expanded as a better understanding of process fundamentals was gained. Since the advent of personal computers in the 1980s, mathematical modelling has become an integral part of the analysis of metallurgical processes. Richards *et al.*[18] described modelling as a very powerful tool when combined with industrial measurements in the elucidation of process kinetics, troubleshooting and optimization.

A review of the mathematical modelling of pyrometallurgical processes is presented in the second section of this Chapter. The objective is not to provide an exhaustive review of mathematical models available but rather to discuss, illustrated with some examples, the approach and purposes of process modelling.

2.1 Oxygen Probes

This section is composed of three main parts. First, the operating principle of an oxygen probe is briefly introduced. The most prominent applications of oxygen probes in process control

of ferrous and non-ferrous metallurgy are then presented to demonstrate that oxygen probes have become an indispensable tool in pyrometallurgy. In the last section, the emphasis is set onto reviewing the state-of-the-art of the oxygen probe applications in molten lead environments.

2.1.1 Oxygen Probe Principle

An oxygen probe is an electrochemical cell with a solid oxide electrolyte that operates as an oxygen concentration cell. Consider the generalized electrochemical cell written in concise notation as follows

$$\text{Pt, } O_2\,(P'_{O_2}) \;\mid\; \text{MO} \;\mid\; O_2\,(P''_{O_2}),\ \text{Pt} \qquad \text{(A)}$$

where MO is a solid oxide electrolyte in which oxygen ions, O^{2-}, are mobile. Calcia stabilized zirconia, ZrO_2 - CaO, is a typical example of solid oxide electrolyte. The addition of calcia into pure zirconia generates oxygen ion vacancies within the lattice which compensate for the difference of valency between zirconium and calcium ions (see Figure 2.1). These vacancies facilitate the transport of oxygen ions through the electrolyte. Further details on the conduction properties of solid oxide electrolytes are given in Chapter 4.

When there exists a gradient of oxygen partial pressure between P'_{O_2} and P''_{O_2}, cell (A) generates an electromotive force. The electrochemical phenomenon involved can be explained following the derivation of Jacob and Mathews[19]. Due to the difference of oxygen chemical potential between the two sides of the cell, there exists a flux of charged particles in the solid

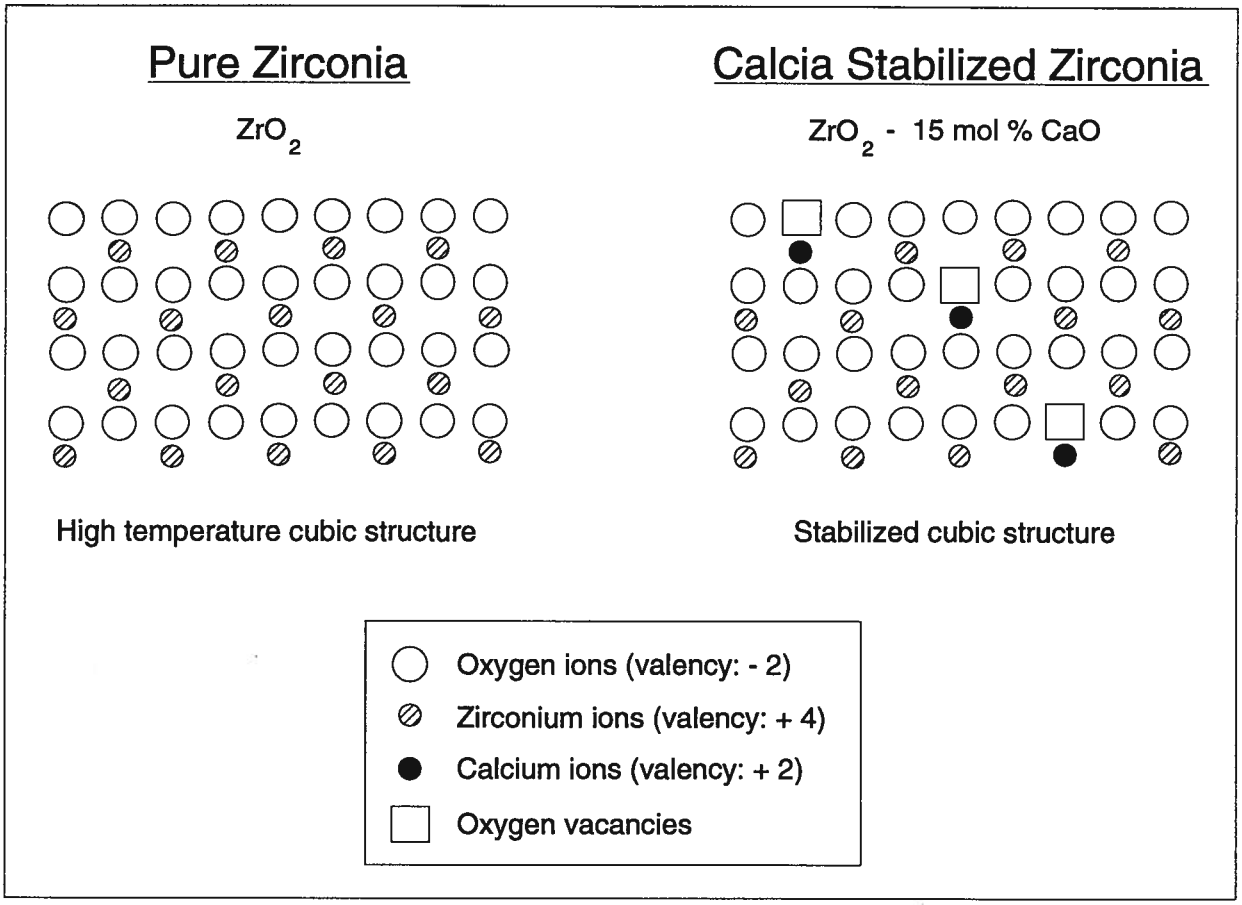

Figure 2.1 - Schematic representation of pure zirconia and calcia stabilized zirconia.

electrolyte along the gradient. The particle flux for diffusion of a mobile species i in an activity gradient and electrical field is given by

$$j_i = - c_i B_i \; grad \, \eta_i \tag{2.1}$$

where c_i, B_i, and η_i are the concentration, absolute mobility and electrochemical potential of the mobile species i, respectively. If no current is drawn from the solid electrolyte, under steady state conditions, maintaining the charge neutrality at every point requires that

$$\sum_i z_i j_i = 0 \tag{2.2}$$

where z_i is the valency of the mobile species i. Combining the Equations (2.1) and (2.2), it follows

$$- \sum_i c_i z_i B_i \; grad \, \eta_i = 0 \tag{2.3}$$

The absolute mobility of species i can be expressed as

$$B_i = \sigma_i / (z_i^2 c_i e^2) \tag{2.4}$$

where σ_i and e are the electrical conductivity and elementary charge respectively, and the electrochemical potential can be written as

$$\eta_i = \mu_i + z_i F \phi \tag{2.5}$$

where μ_i and ϕ are the chemical potential of species i, and the electrostatic potential, respectively. Substituting Equation (2.4) and (2.5) into (2.3) and rearranging yields

$$grad\ \phi \;=\; -\frac{1}{F}\ \sum_{i}\ (t_i/z_i)\ grad\ \mu_i \qquad (2.6)$$

where $t_i = \sigma_i / \sum_i \sigma_i$ is the transference number of species i. For an oxygen concentration cell using a solid oxide electrolyte, the mobile species are mainly oxygen ions and electrons. It is seen, from Equation (2.6), that the tendency of the mobile species to diffuse along the chemical potential gradient is compensated by an electric field that opposes ionic motion. As a consequence, in response to an oxygen potential gradient, an oxygen concentration cell generates an ***open-circuit*** emf, $E_{O.C.}$. This emf is an integral quantity measured between the left and right-hand side of the cell, and proportional to the difference of oxygen potential as expressed by the following equation

$$E_{O.C.} \;=\; \phi^r \;-\; \phi^l \;=\; -\frac{1}{F}\ \int_l^r\ \sum_i\ (t_i/z_i)\ d\mu_i \qquad (2.7)$$

where *r* and *l* stand for right and left. This electrochemical phenomenon is schematically illustrated in Figure 2.2. In electrochemical probes, predominantly ionic conducting solid electrolytes are used, i.e. only oxygen ion is mobile and its transference number is equal to unity, then the emf of cell (A) is given by the well-known ***Nernst*** equation as follows

$$E_{O.C.} \;=\; \frac{RT}{4F}\ \ln\ \frac{P''_{O_2}}{P'_{O_2}} \qquad (2.8)$$

The above oxygen pressures P'_{O_2} and P''_{O_2} can be exerted by pure oxygen gas, by a gas mixture, by a metal/metal oxide mixture or by oxygen dissolved in a molten metal. A measure of the open-circuit emf, $E_{O.C.}$, generated by an oxygen concentration cell in which the oxygen potential of one electrode is known (reference electrode), will provide a determination of the unknown oxygen

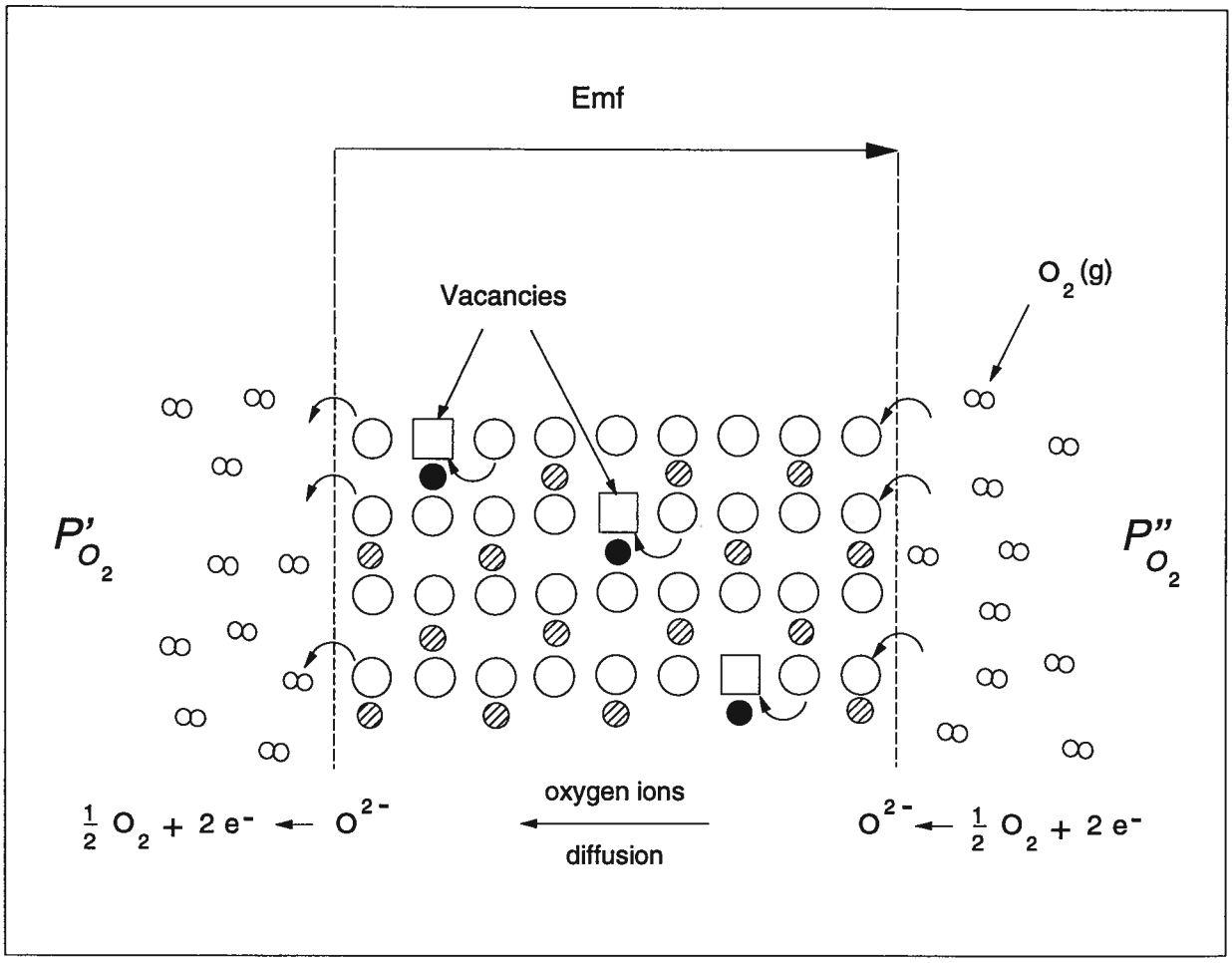

Figure 2.2 - Schematic diagram of emf generation in an oxygen concentration cell using calcia stabilized zirconia as solid oxide electrolyte.

potential of the other electrode. In this manner, the cell operates as an ***oxygen probe*** which can be used to measure the oxygen content of a molten metal. Oxygen probes based on this principle have been used in various ferrous and non-ferrous pyrometallurgical processes where oxygen control is required. These processes include steelmaking, copper smelting, copper refining, and nickel smelting. A schematic drawing of a typical oxygen probe is given in Figure 2.3. The next section presents some of the most significant applications of oxygen probes in process control.

2.1.2 Oxygen Probe Applications in Process Control

Oxygen probes have increasingly been used in pyrometallurgy to either investigate the process mechanisms or even to control certain operations. This section presents some of the main applications of these probes in process control. The first part covers the steelmaking industry while the second part deals with the non-ferrous industry.

2.1.2.1 Steelmaking Industry

Investigations of the potential application of oxygen probes in steelmaking operations have been reported as early as the mid-sixties by Fitterer and co-workers[20-22]. The first work on in-situ application of oxygen probes was published by U.S. Steel researchers in the early seventies[23-26], followed by numerous Japanese and German papers in the seventies and eighties[27-36]. Resulting from tremendous efforts devoted to designing oxygen probes for process control purposes, disposable devices for single readings were produced and commercialized[24,25]. Such devices have contributed significantly to the improvements made in the steelmaking industry over the last twenty years. These probes have made possible better monitoring and control of metal processing practices

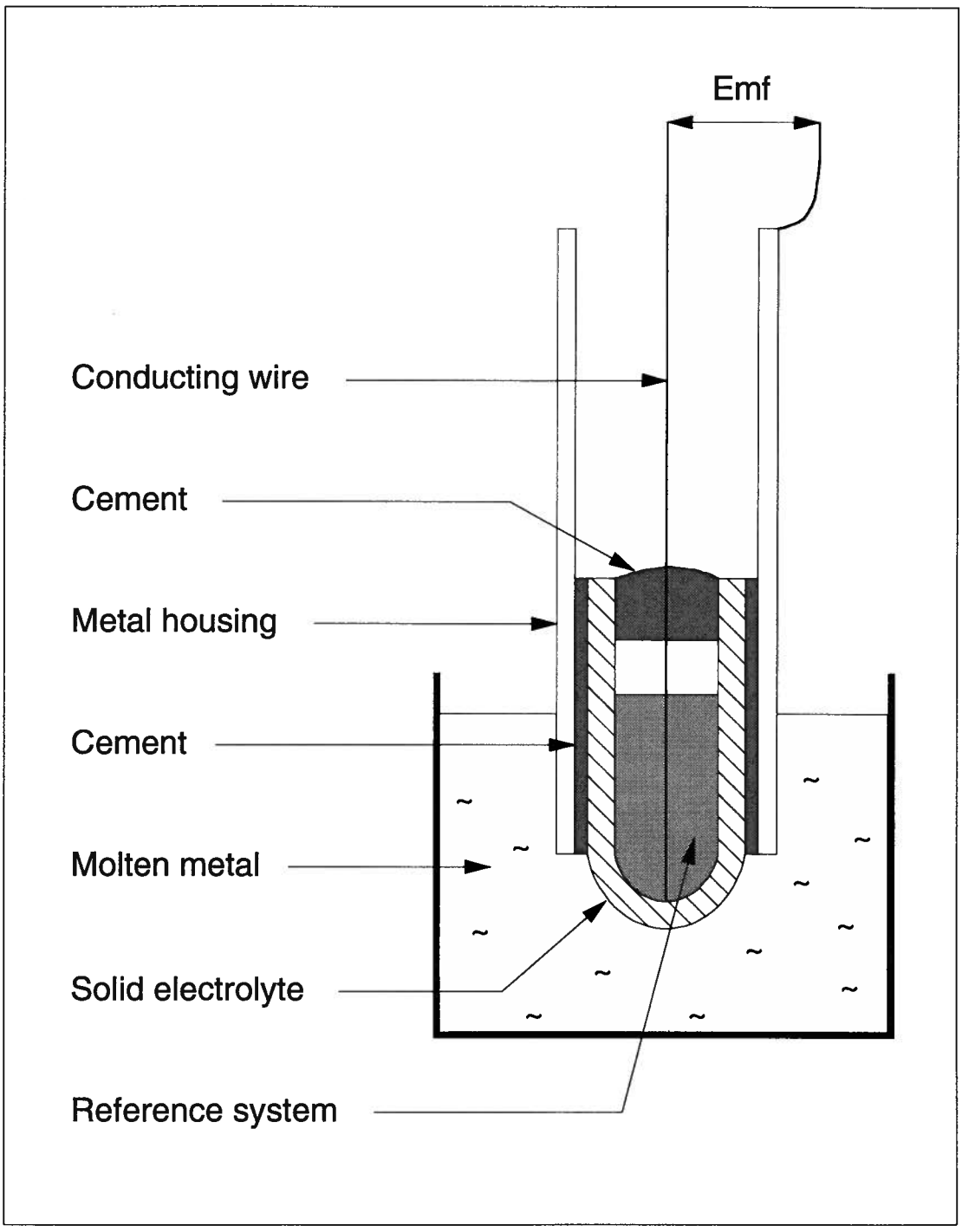

Figure 2.3 - Schematic drawing of a typical oxygen probe for application in molten metal.

such as decarburization, dephosphorization or deoxidation, as well as slag formation and composition. The progress of silicon-deoxidation recorded by oxygen probes is shown in Figure 2.4. The measurement of the dissolved oxygen can be carried out by manually dipping the probe into molten steel. Performing this measurement just after refining in a converter provides a measure of the dissolved oxygen remaining in the liquid steel. This information is extremely valuable in deciding whether or not to proceed with further processing. When the use of oxygen probes became standard in Japan, more sophisticated systems such as the sublance system shown in Figure 2.5 were incorporated into steelmaking practices. Figure 2.6 shows a computing system to control the content of soluble aluminum in Al-Si-killed steel. The improvements in the deviation from target values for soluble aluminum in Al-killed steels before and after the use of oxygen probes are shown in Figure 2.7.

2.1.2.2 Non-Ferrous Industry

The most successful oxygen probe application to date in non-ferrous metallurgy is in copper refining[38-41]. Dompas and Lockyer [39] report on how copper deoxidation prior to continuous casting at Metallurgie Hoboken (Belgium) is monitored by oxygen probe measurements. Oxygen potential measurements in flowing copper in the launder is used to control deoxidizer additions and combustion air to the launder heater (see Figures 2.8 and 2.9).

The copper industry also provides examples of the application of oxygen probes for investigating the mechanism involved in a process. Kemori *et al.*[42] measured the oxygen potential of the matte in a copper flash smelting furnace using disposable oxygen probes. The oxygen potential

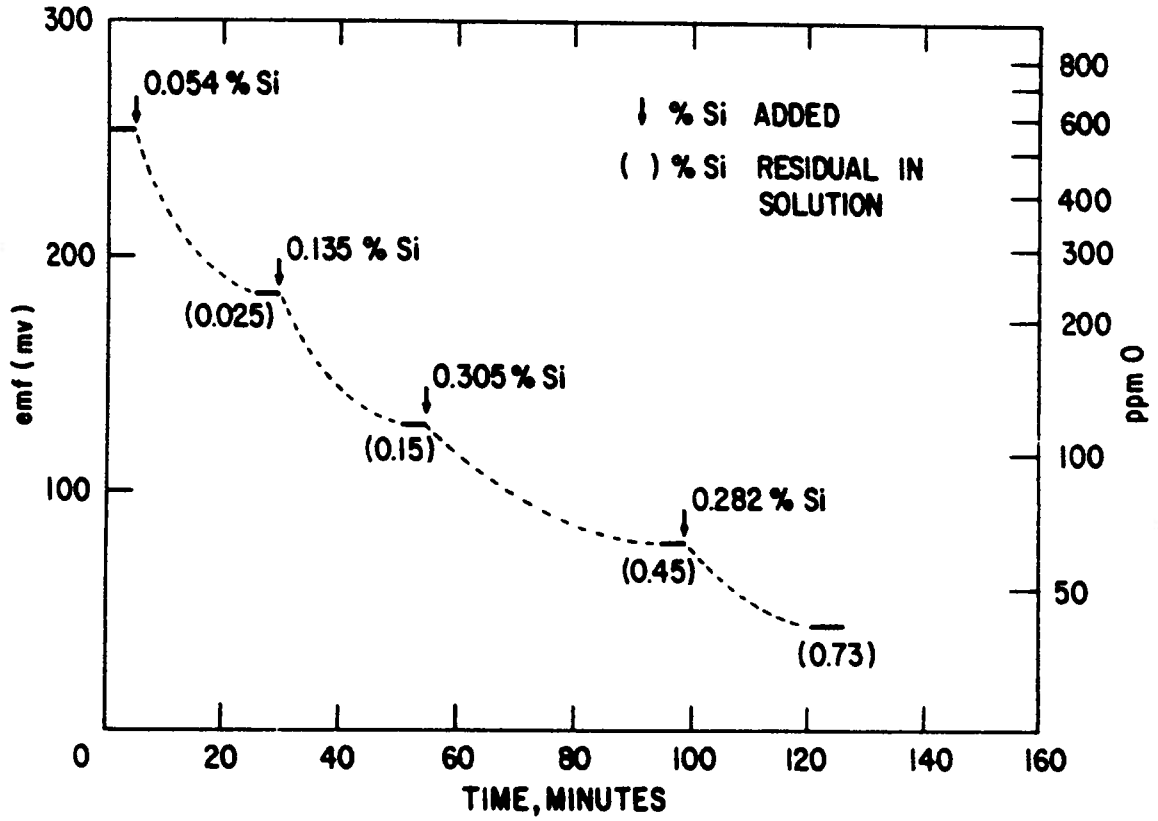

Figure 2.4 - Progress of silicon-deoxidation recorded by the electromotive force measurements of an oxygen probe at 1600°C (From Turkdogan and Fruehan, 1972, ref. 26).

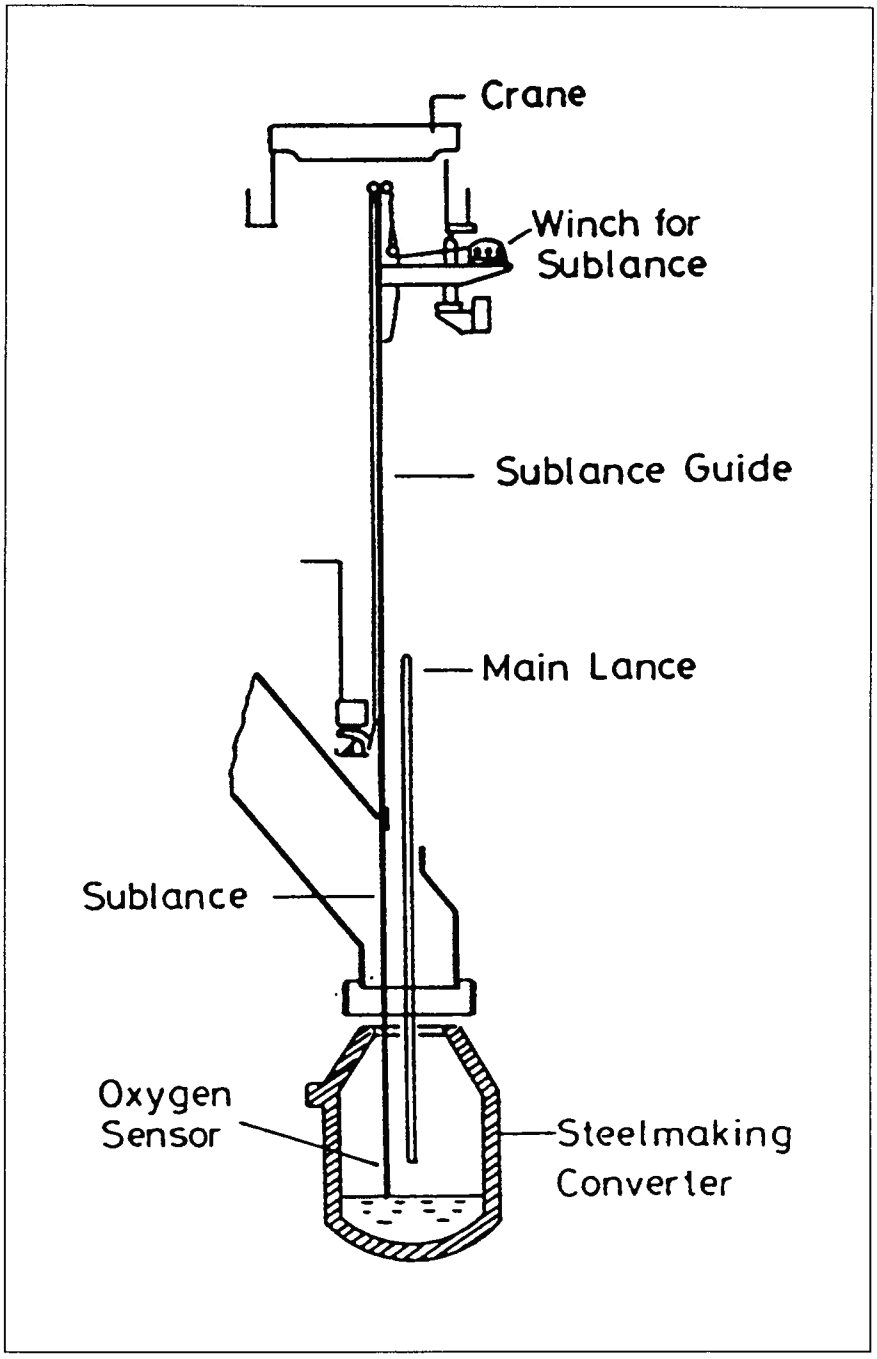

Figure 2.5 - Sublance system for automatic dipping of oxygen sensors into a steelmaking converter (From Goto, 1988, ref. 37, after Ariga and Ogawa, 1977, ref. 35).

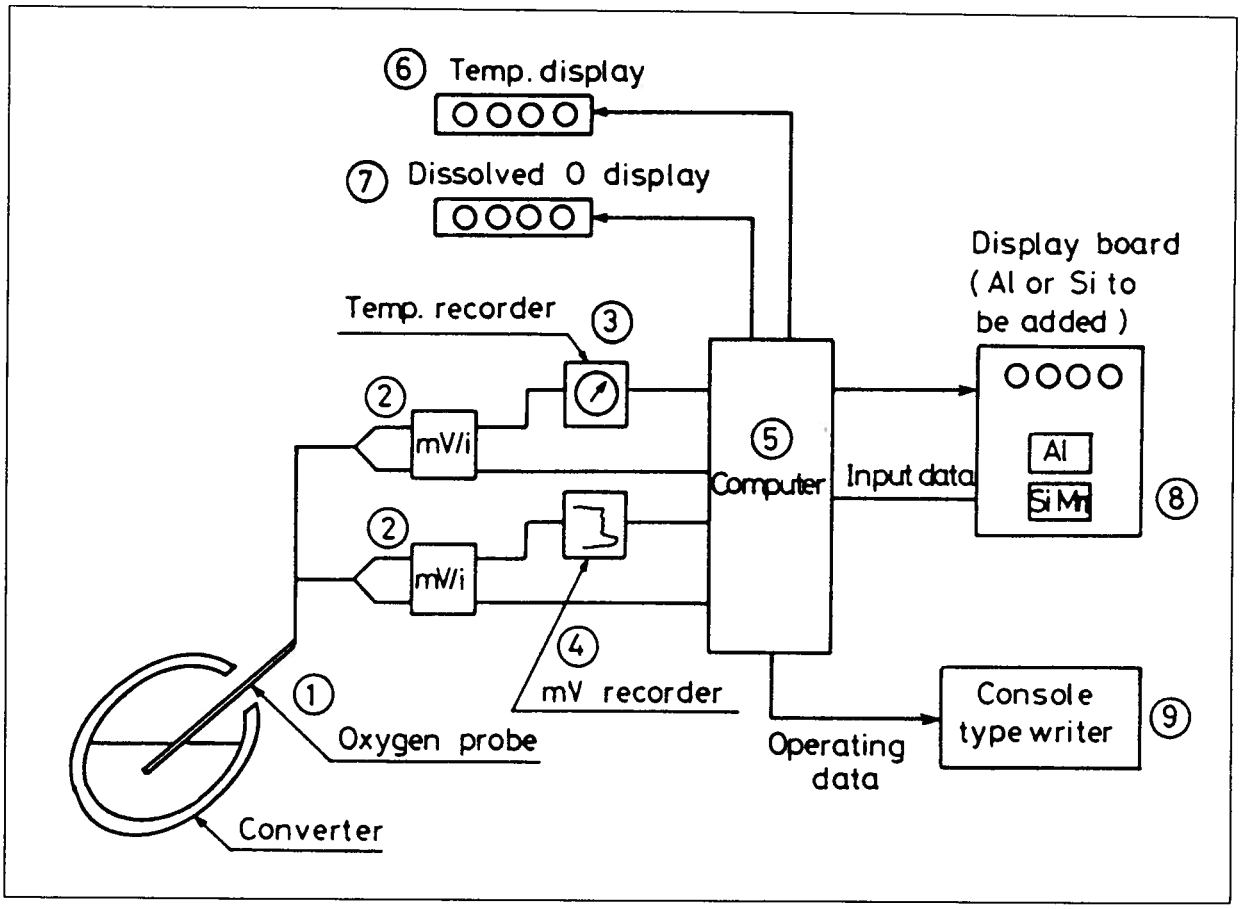

Figure 2.6 - Computing system to control the content of soluble aluminum in Al-Si killed steel and the magnitude of the deoxidation of Si-semi-killed steel (From Goto, 1988, ref. 37, after Hiromoto *et al.*, 1977, ref. 36).

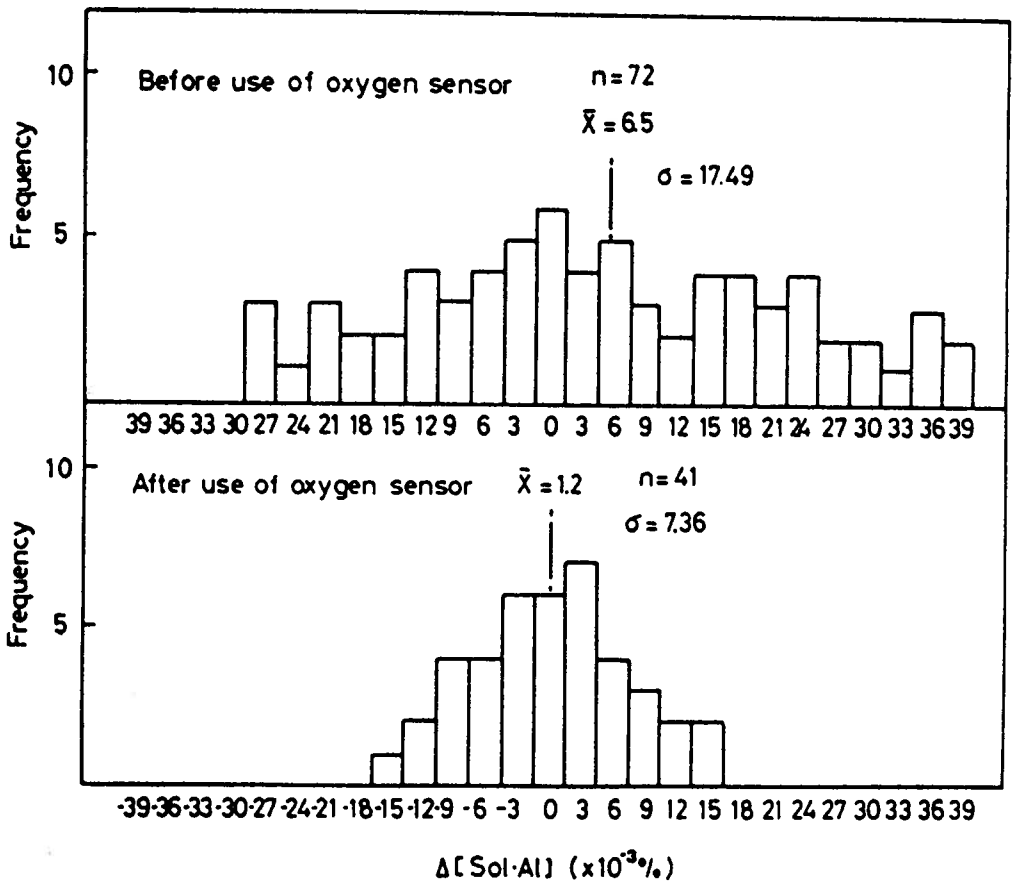

Figure 2.7 - Improvements in deviation from target value of the content of soluble aluminum in Al-killed steels before and after the use of oxygen sensors (From Goto, 1988, ref. 37, after Hiromoto *et al.*, 1977, ref. 36).

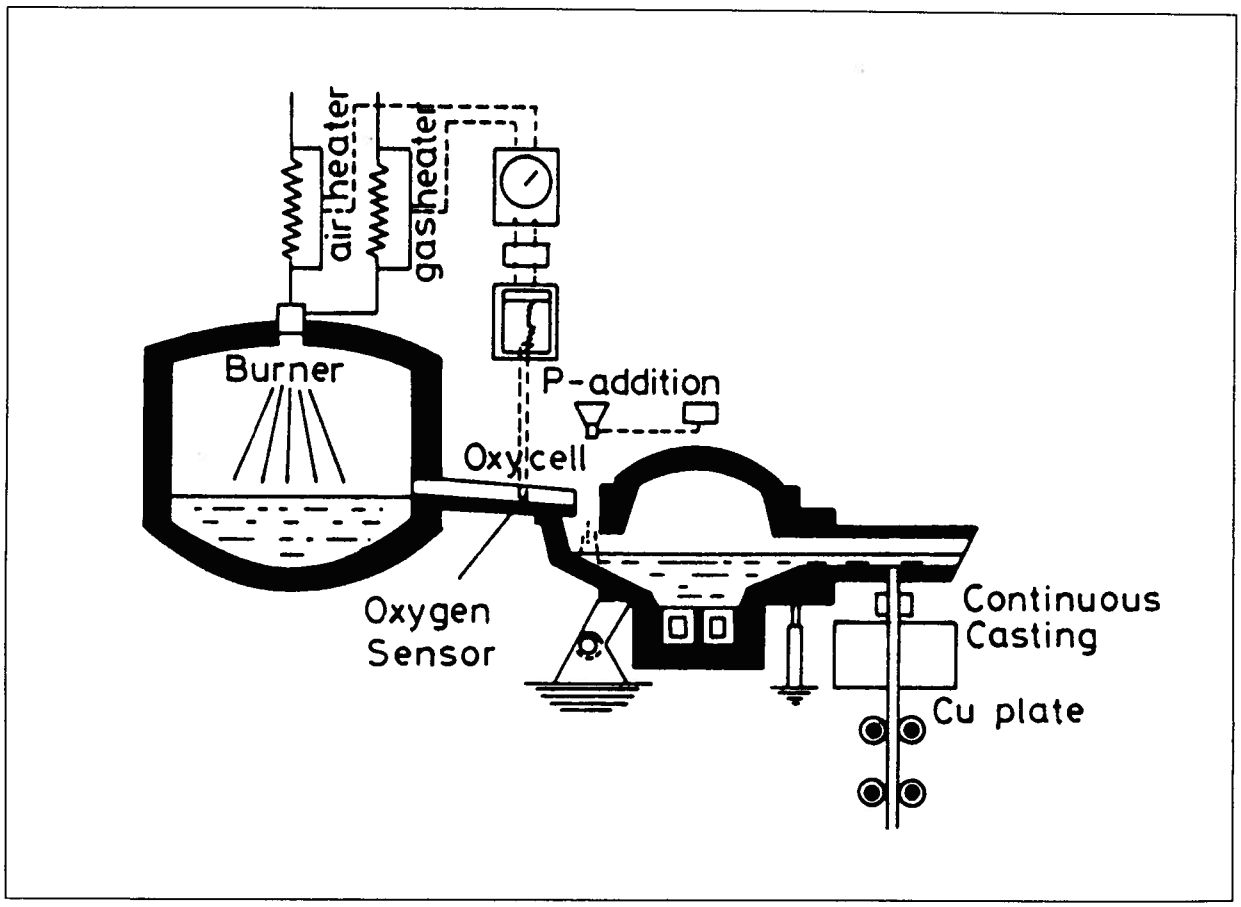

Figure 2.8 - Feed-back control system for continuous casting of tough pitch copper billet using an oxygen probe at the exit of the launder (From Dompas and Lockyer, 1972, ref. 39).

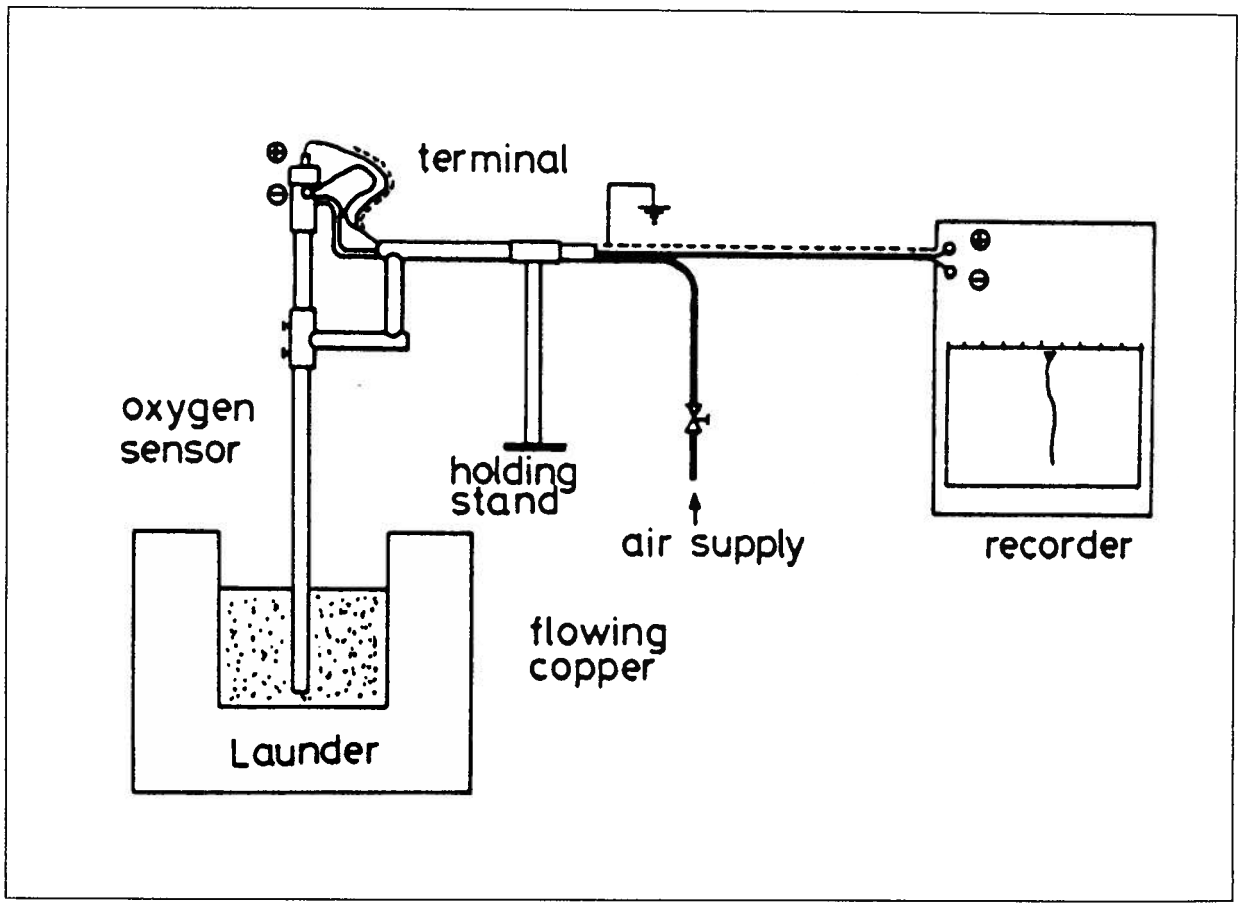

Figure 2.9 - Schematic illustration showing how the oxygen content in flowing molten copper is continuously measured in the launder (From Goto, 1988, ref. 37).

of the slag in the settler below the shaft, at the tap holes and in the electric furnace downstream of the flash furnace were also measured. Even though incomplete, their study suggests that the pyrometallurgical oxidation of the copper concentrate is completed in the shaft or in the settler.

On-line oxygen monitoring for liquid sodium is another application field for oxygen probes. Liquid sodium is used as coolant in nuclear reactors. Dissolved oxygen in liquid sodium has to be monitored to minimize corrosion of the stainless steel piping as well as for early detection of oxygen ingress into sodium circuit to prevent a fire hazard[43]. Due to the low temperature of application, it is customary for a probe to take up to a week before recording a stable emf. Nevertheless, any subsequent change in dissolved oxygen is quickly detected. Such probes can then become part of an on-line warning system.

2.1.3 Oxygen Probe Applications in Liquid Lead

After demonstrating how the use of oxygen probes dramatically improved the production quality of some metallurgical processes, it seems important to investigate the past uses and applications of oxygen probes in such a corrosive environment as molten lead. In the course of this research, a literature survey on electrochemical measurements in lead has been carried out. In an attempt to gather as much information as possible, thermodynamic studies involving electromotive force measurements in lead as well as research oriented towards designing oxygen probes for lead processes were considered.

Electrochemical techniques were successfully used to determined a number of thermodynamic properties in lead systems. Alcock and Belford[44] determined the free energy of formation

of lead oxide, the partial free energy of solution and the solubility of oxygen in lead. Charette and Flengas[45] measured the free energy of formation of various oxide including PbO. Szwarc *et al.*[46] investigated the solubility and diffusivity of oxygen in liquid lead. Bandyopadhyay and Ray[47] evaluated the kinetics of dissolution of oxygen in lead. Jacob and Jeffes[48], and Otsuka and Kozuka[49,50] determined the activity relations of oxygen in lead and lead alloys. Taskinen[51] carried out a comprehensive study on oxygen-metal interactions in dilute molten lead alloys. Temperature dependences of the oxygen self interaction parameter as well as first order interaction parameters of Ag, Au, Bi, Cu, In, Ni, Sb, Sn, and Te were determined.

Contrary to experience in the steel and copper industry, very little attempt has been made to use oxygen probes in lead pyrometallurgy. Fontainas *et al.*[52] report the application of disposable oxygen probes to control the reduction level of lead smelter slags. They claim to reproducibly achieve an accuracy of about ± 10% in the determination of lead content of the slag. The correlation between $\log P_{O_2}$ and wt% Pb in the slag from their industrial measurements in the blast furnace is shown in Figure 2.10. Due to frequent probe failures and occasional out of range readings, the authors stipulate that two probes are routinely necessary for one measurement. Sometimes a third probe is required when the two readings differ by more than 10 mV (20-25% relative error on Pb content). When three probes are used, the cost of one measurement is said to be comparable with the cost of a routine X-ray fluorescence slag analysis.

Continuous oxygen monitoring in liquid lead or liquid lead alloys for process control in the lead smelting or refining industry has not been published in the literature to date. The only reported use of a long-life oxygen probe in liquid lead comes from the nuclear industry, and more precisely from the Center for Nuclear Energy[53-58] in Mol, Belgium. Liquid metal, either pure lithium or the

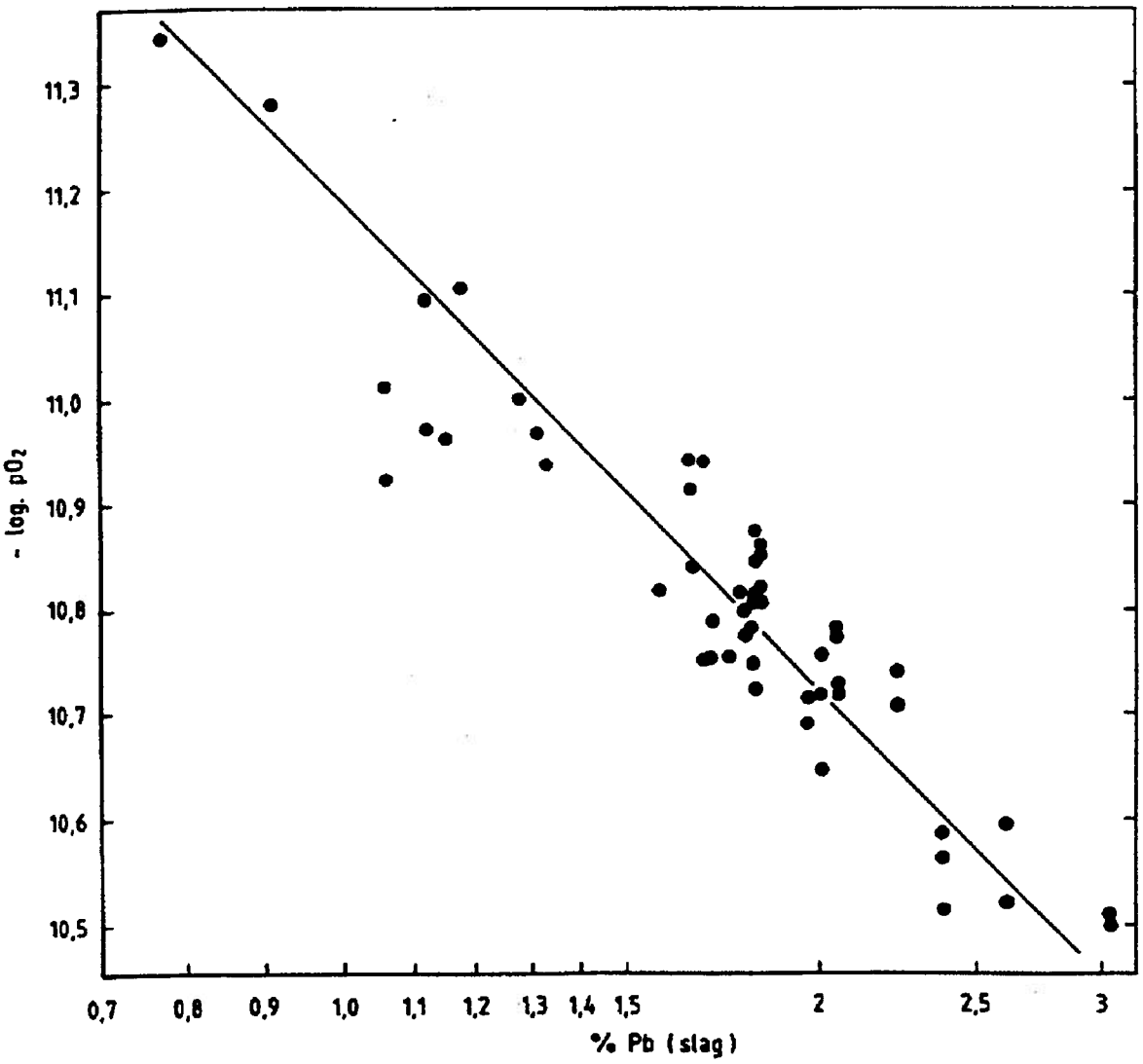

Figure 2.10 - Correlation between oxygen partial pressure in the slag and lead content of the slag (From Fontainas *et al.*, 1985, ref. 52).

eutectic Pb-17Li, has been considered in a number of fusion reactor designs. Liquid metal can be used as coolant for the plasma facing components, or as a protection for the structural materials of a reactor against highly energetic particles and high heat fluxes[58]. Using Pb-17Li as a coolant raises similar problems to the use of liquid sodium: the non-metallic impurities of the coolant, and in particular dissolved oxygen, must be controlled for safety reasons. An oxygen probe was developed to continuously monitor the oxygen content of the liquid Pb-17Li alloy in the temperature range 350°C and 500°C. More than 100 prototype probes were tested amongst which 55% were reliable and could be calibrated. Dekeyser and De Schutter[58] report that the majority of the failures are due to cracks in the solid electrolyte. Cracks can be caused by thermal shock especially at the initial immersion into the liquid alloy. When subject to temperature changes, the probe responds sluggishly, especially upon heating. This behaviour is explained by Dekeyser and De Schutter[58] by assuming slow kinetics of the system Pb-Li and oxygen, i.e. slow restoration of oxygen saturation after a temperature increase. On the other hand, the probe responds quickly to a decrease of temperature (no effect of slow kinetics of the system), but a stable emf is not achieved until after 20 to 50 hours. This behaviour is acceptable when monitoring Pb-Li over long periods of time, i.e. months or years, to detect oxygen pick-up, but would not be acceptable for on-line monitoring of a lead bullion whose composition varies on a daily or even hourly basis.

Kozuka[59] reports the use of an oxygen probe in the forehearth of a lead blast furnace in Sumiko ISP smelter, but cannot confirm that the oxygen concentrations measured correspond to the oxygen potentials in the furnace.

The characteristics of the various oxygen electrochemical cells used in the above works are summarized in Table 2.1. The results of this survey are very encouraging for two major reasons.

Table 2.1 - Characteristics of emf cells used for oxygen measurements in molten lead.

Solid Electrolyte	Reference Electrode System	Conducting Lead (Wire)	Temperature Range (°C)	Applications	Ref.
ZrO_2-14 mol% MgO or ZrO_2-15 mol% ThO_2	Ni-NiO	Ir	440-800	Thermodynamics	44
ZrO_2-10 mol% CaO	Ni-NiO	Pt	500-1100	Thermodynamics	45
ZrO_2-CaO	Air	Chromel (Pt)	740-1080	Thermodynamics	46
ZrO_2-CaO	Ni-NiO	Steel	750	Thermodynamics	47
ZrO_2-7 mol% CaO or ZrO_2-4.5 mol% Y_2O_3	Ni-NiO	Cr-cermet (Pt)	500-1200	Thermodynamics	48
ZrO_2-10.4 mol% CaO	Air	Ir (Pt)	800-1050	Thermodynamics	49-50
ZrO_2-7 mol% CaO	Air	Cr-cermet (Pt)	760-1000	Thermodynamics	51
ZrO_2-CaO	Ni-NiO or Mo-MoO_2	Fe or Pt	1150-1350	Probe (lead slags)	52
ZrO_2-Y_2O_3	In-In_2O_3	Steel	400-600	Probe (liquid Pb-17Li)	53-58
ZrO_2-MgO	Fe-Fe_xO	Steel	1000-1100	Probe (crude lead)	59
ZrO_2-MgO	Cr-Cr_2O_3	Mo	1000-1100	Probe (lead slags)	59

First of all, application of electrochemistry in molten lead has been performed in the past with success, especially in the determination of thermodynamic properties. Solid electrolytes with physical characteristics suitable for molten lead are thus available. Secondly, oxygen potential measurements at temperatures as low as 400°C have been successful even though slow kinetics in the solid electrolyte are expected. The major challenge is then to design a portable probe for continuous measurement that would give satisfactory results when used in the specific conditions of lead softening, i.e. the presence of an oxidic slag, temperature and composition fluctuations on an hourly basis, and a demanding industrial environment.

2.2 Process Modelling

Since the advent of computers process modelling has become an integral part of the metallurgical field. Numerous process models have been developed covering the fields of pyrometallurgy, hydrometallurgy and metal forming. These models cover a wide spectrum of simulation capabilities, from smelting and converting to casting and rolling, with the ability to predict the evolution of process characteristics ranging from chemical composition to microstructure. In particular, thermochemical process models are primarily concerned with the simulation of the chemical composition of the various phases involved in a process. Starting from simple models in the 1950s, they became rather comprehensive in the 1980s. Such models have traditionally been developed in two stages. First, the process is treated as a "black box" operating at thermodynamic equilibrium and a "thermodynamic model" is formulated based on idealized assumptions. Then, the model is expanded to include kinetic factors that have been identified as important. Mass transfer concepts and reaction rates are implemented at this stage. The resulting "kinetics model" then becomes a powerful tool in the elucidation of the rate-limiting steps of the process.

Investigating process fundamentals through modelling avoids the need to carry out extensive and expensive plant tests that would otherwise be required to analyze and optimize a process. In this section, thermodynamic models are discussed first, followed by kinetics models, and finally some conclusions are drawn.

2.2.1 Thermodynamic Models

The fundamental assumption is that the process under consideration runs at thermodynamic equilibrium and consequently, that all reactions involved in that particular process proceed to equilibrium. The main purpose of the model is to determine the equilibrium composition of the chemical system representing the process.

A traditional approach to determining equilibrium compositions of a multiphase system consists in examining the various independent equilibrium reactions at a given temperature, and deriving a set of non-linear simultaneous equations involving the equilibrium constants, the total pressure, and the elemental material balances. Thermodynamic models of slag fuming[60-62], nickel converting[63], and copper converting[64], are all based on this technique. The derived set of equations is solved by means of a nonlinear equation-solving routine. For example, Kyllo and Richards[63] use a Quasi-Newton routine whereas Goto[64] employs a Brinckley-Newton-Raphson routine. This approach can provide good results when reasonable assumptions are made to simplify the system of equations. However, this exercise requires some prior knowledge of the system as well as metallurgical intuition. The technique also presents some difficulties with regard to initial guesses, generality, and convergence.

In the late 1950s, White *et al.*[65] developed a new technique, the Gibbs free energy minimization method, that eliminated the above difficulties. Rather than considering the independent equilibrium reactions involved in the process, this technique considers all possible species representing the process and computes the equilibrium composition by minimizing the Gibbs free energy of the system subject to two constraints: 1) the elemental balances, and 2) the equilibrium composition values determined must be positive. Oliver *et al.*[66] used the two alternative ways to solve the same problem in order to demonstrate the differences between the two methods. Numerous papers on this new method were later published, notably by Eriksson who developed the well-known SOLGASMIX routine[67,68]. Although the underlying principle for all of the programs described in these papers is the same, the mathematical techniques differ. The SOLGASMIX routine, for instance, uses Lagrange's method of undetermined multipliers to set up a system of linear equations that is then solved with a Gaussian elimination technique. The thermodynamic model of the Outokumpu flash smelting furnace of Vartiainen *et al.*[69] is based on this technique and uses a modified version of the SOLGASMIX routine.

Since the slag fuming process provides a very good illustration of the role and purpose of thermodynamic modelling, it was selected for a more detailed review. In 1954, Bell *et al.*[60], who were the first to attempt a quantitative analysis of the process chemistry, assumed that slag fuming was described by the following reactions:

$$C + 1/2\,O_2 \leftrightarrow CO$$

$$C + O_2 \leftrightarrow CO_2$$

$$ZnO_{(slag)} + CO \leftrightarrow Zn_{(g)} + CO_2$$

$$H_2 + 1/2\,O_2 \leftrightarrow H_2O$$

$$ZnO_{(slag)} + H_2 \leftrightarrow Zn_{(g)} + H_2O$$

They developed a model based on mass balances on carbon, hydrogen, oxygen and nitrogen, and on the two equilibria

$$ZnO_{(slag)} + CO \leftrightarrow Zn_{(g)} + CO_2$$

$$H_2O + CO \leftrightarrow H_2 + CO_2$$

The unknown activity of zinc oxide was computed from plant data by the addition of a zinc balance. A system of seven equations was derived and solved for the seven unknowns, P_{CO}, P_{CO_2}, P_{H_2}, P_{H_2O}, P_{N_2}, P_{Zn}, and a_{ZnO}.

With this simple model, Bell *et al.*[60] simulated slag fuming operations and examined the effect of changes in a number of operating parameters. Their model, which accounted fairly well for the furnace heat balance, was successful in predicting the improvements in fuming rates by oxygen enrichment and preheating of the blast. For a simple model, this was quite an achievement even though the model was in variance in predicting the effect of other operating parameters. Further refinements by Kellogg[61], and Grant and Barnett[62], brought the model to such a degree of sophistication, predicting the effect of most variables including the behavior of iron, sulphur, lead, and temperature with time, that it reinforced the belief that slag fuming was operating at thermodynamic equilibrium.

Thermodynamic models usually give realistic results. This is often due to the fact that in

pyrometallurgical processes, reactions are usually relatively rapid and, for the major species in a reactor, advance a considerable way towards the final equilibrium composition in a short time. For that same reason, a thermodynamic model constitutes a useful tool by providing a first step towards the understanding of the working of a process. Paradoxically, a thermodynamic model can also provide evidence against its primary assumption of thermodynamic equilibrium. The nickel converter equilibrium model of Kyllo and Richards[63] corresponds to such an example. From a thermodynamic study, the author show that the nickel converting process is actually governed by kinetics rather than by thermodynamic equilibrium. They conclude that a kinetics model would be more appropriate to investigate the process. The following section presents the background for kinetics models.

2.2.2 Kinetics Models

Contrary to thermodynamic models which assume all reactions to be instantaneous with no specific reaction site, kinetics models take into account both reactions rates and local heat and mass transfer. Instead of being treated as a black box, the process is investigated on a microscopic scale using a mechanistic approach. Reactions are considered to take place at specific locations, such as gas bubble-liquid interfaces or solid particle-liquid interfaces. Although reactions at the various interfaces are usually considered to be instantaneous, this approach still permits the assessment of the rate-limiting steps. These controlling steps often correspond to mass transport to and from the reaction interfaces.

Again, the slag fuming process provides a good illustration of kinetics modelling. The early thermodynamic models of slag fuming, as described in the previous section, all assume that the

injected coal and air react and come to thermal and chemical equilibrium with the slag. Based on an investigation of several industrial zinc slag fuming furnaces, Richards *et al.*[70] suggest that zinc fuming takes place on entrained coal particles in the slag, and that the process is kinetically controlled. They argue that the fuming furnace consists of two reaction zones created by the division of coal between the slag and the tuyere gas stream. The fraction of coal entrained in the slag reduces ZnO and Fe_3O_4, while the fraction of coal remaining in the gas stream combusts and provides the heat for the endothermic reduction reactions and heat losses. A kinetic model was developed by Richards and Brimacombe[71,72], and used to analyze the fuming process. By fitting the model to fuming cycles from five different companies, the fractions of entrained, combusted, and unreacted coal as well as the oxygen utilization were characterized. With the fitted parameters values, the model is able to predict fuming rates with reasonable accuracy. In the light of the kinetic description of the slag fuming, Richards and Brimacombe[71,72] conclude that process improvements should be achieved by increasing the amount of coal entrained in the slag, which in turns increases the amount of reductant available for zinc oxide. Cockcroft *et al.*[73] report on tests carried out with a high-pressure coal injection unit installed on a slag fuming furnace to increase the entrained coal fraction. The results of their tests show that significant improvements in fuming rates (1.5 to 2 times) are obtained. This example demonstrates that kinetics modelling combined with industrial measurements constitutes a very powerful tool to improve the understanding of existing processes. Improved understanding usually leads to process optimization.

2.2.3 Conclusions

BHAS compensated for a limited understanding of process fundamentals of oxygen lead softening by extensive research, including the design and testing of several furnaces, in order to

achieve satisfactory performances from their lead softening process. Although their process is regarded as an example around the world, their task was facilitated by the regularity of concentrate composition.

In the case of a partial softening process, which would also be required to handle bullion composition spikes, a better understanding of process fundamentals are crucial in the success of any control strategy. In view of the previous sections, process modelling is undoubtedly a powerful tool to quantify process chemistry and kinetics. To date, no mathematical model of the oxygen lead softening process has been published. The development of a thermodynamic model is an appropriate first step towards the understanding of the basic reactions involved in the oxygen lead softening process.

CHAPTER 3

SCOPE AND OBJECTIVES

Lead ores generally contain significant amounts of arsenic and antimony. The process of lead softening, corresponding to the removal of these hardening impurities, is therefore of necessity in any pyrometallurgical lead refining circuit. Even in a smelter where electrorefining is used, a partial softening might be required. The treatment of silver bearing concentrates, while providing additional revenues, also introduces additional amounts of arsenic and antimony into the circuit. The efficiency of the Betts electrorefining process depends on the stability of the corroding lead anodes. Anode slime stability is directly related to the antimony and arsenic content of the anodes. Thus, control of bullion quality prior to anode casting is key to optimization of the electrorefining operations, improvement of lead production, and addition of revenues. The (partial) softening stage is the ideal location in a smelter for such a control. When composition spikes are regular occurrences, the batch softening circuit tends to become somewhat complicated to reduce their effects.

The objective of this research work was to explore the option of continuous, single pass softening for the production of bullion of consistent quality. In this case, the softening circuit would appear as in Figure 3.1. Two components are critical to this revision:

- a method of continuously monitoring bullion quality for control purposes, and
- a control strategy based on an understanding of process fundamentals.

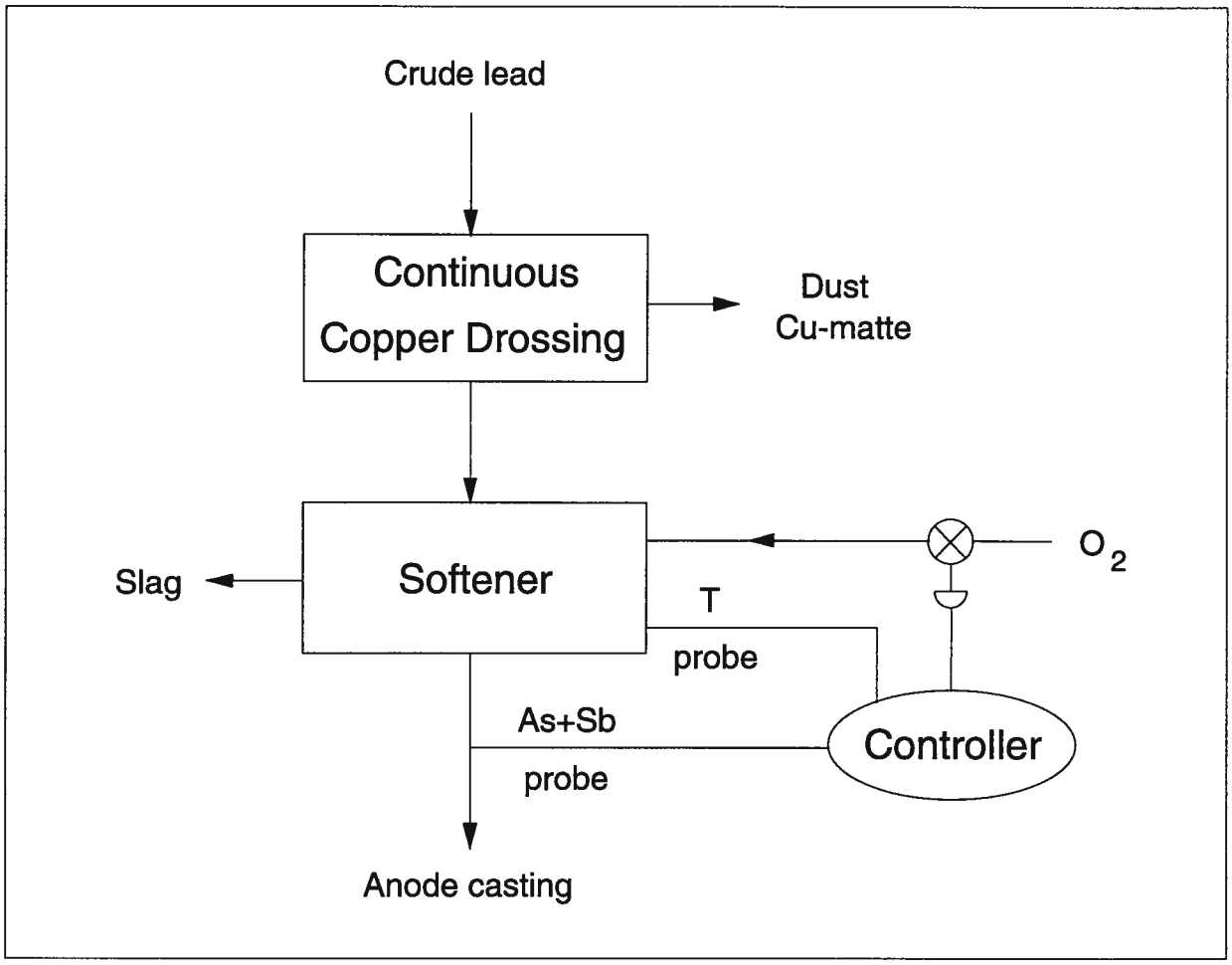

Figure 3.1 - Continuous single pass softening circuit.

3 SCOPE AND OBJECTIVES

The scope of this thesis work was primarily to develop an ***on-line*** sensor for bullion quality control. Continuous monitoring of bullion quality involves a continuous measurement ***in-situ*** of the arsenic and antimony content of the bullion. Solid state sensors, or electrochemical probes, are the most common devices for on-line continuous measurement of liquid metal composition. An antimony (or arsenic) sensor would be most suitable to directly measure the antimony (or arsenic) content of the bullion. No antimony-ion (or arsenic-ion) conducting solid electrolyte is commercially available. The development of such an electrolyte, from fabrication (including setting up the appropriate experimental equipment), to characterization (electrical conductivity, ionic domain, ...), and finally testing in molten lead (stability, corrosion resistance, ...), would by itself represent a PhD research project. Since this project was primarily concerned with oxygen lead softening, including designing a sensor for bullion quality control, rather than developing one single component of a sensor in the form of a new solid electrolyte, an alternate route had to be adopted. The amount of dissolved antimony and arsenic in the bullion is directly related to the amount of dissolved oxygen due to thermodynamic constraints. Thus, measuring the content of dissolved oxygen by means of an oxygen probe would provide an indirect measurement of the antimony and arsenic content, assuming a relationship between dissolved antimony and arsenic and dissolved oxygen is established. Both laboratory and industrial tests were required in the oxygen probe development program, the former to perform all necessary design experimentation on the individual components as well as on the whole assembly, and the latter to test the suitability of the probe in an industrial environment as well as to calibrate the probe.

The second objective was to develop a preliminary control strategy based on a continuous measurement of bullion quality as measured by the combined arsenic and antimony level. Such an assessment required the understanding of process fundamentals, and in particular process chemistry.

3 SCOPE AND OBJECTIVES

As mentioned in Chapter 1, a number of fundamental issues, such as oxygen efficiency, influence of bullion composition, effect of temperature, have not been addressed in the literature. Process modelling, combined with industrial measurements, constitutes a very powerful tool to analyze a process. Since no mathematical model of oxygen lead softening has been published to date, a thermodynamic model of the process has been developed as a first step towards the quantification of softener chemistry. This model was designed to allow the simulation of both batch and continuous operating modes. Once calibrated with plant measurements for the batch mode, the model could be used to analyze the continuous single pass softening option for a variety of conditions in order to demonstrate its ability to meet targets for bullion quality. The acquisition and analysis of industrial data has thus been a major thrust in achieving this objective. Visits to a smelter provided the opportunity to gather data on an industrial softener.

CHAPTER 4

OXYGEN PROBE DESIGN

Designing an oxygen probe for continuous measurements in a lead softening process required the completion of a number of steps. First, the appropriate materials were selected in order to satisfy the requirements of operating in molten lead within a range of temperatures and oxygen partial pressures characteristic of lead softening. Once the materials had been selected, a cell assembly, i.e. the manner in which the various components are assembled together, was adopted taking into account that a number of prerequisite parameters had to be satisfied. The probe needed to be corrosion resistant, robust and portable with a life-span of at least a day. The next step consisted in carrying out laboratory tests in pure molten lead to confirm the adequacy of each component and of the assembly as a whole. The reversibility, thermal resistance and response of the probe were initially the main concerns. The probe was then calibrated to ensure proper oxygen measurements. Finally, the response of the probe to temperature and oxygen partial pressure changes was investigated. The oxygen partial pressure changes were generated by successive additions of antimony into pure lead. At this point, a final laboratory probe design had been achieved. A number of probes could then be constructed for testing in an industrial environment. It was expected that some modifications to the design would probably have to be implemented later to improve the probe characteristics and make it a tool for process control. This chapter is divided in two main parts. In the first section, the selection of materials is discussed. In the second section, the probe design is described and the laboratory tests are presented.

4.1 Selection of Probe Components

Since it is intended to integrate an oxygen probe in a process control system to monitor the lead softening operations at Cominco Ltd plant in Trail, this probe should provide an accurate and continuous measurement of the oxygen content of a lead bullion in the temperature range of 450°C to 750°C, for oxygen pressures in the range of 10^{-10} atm and 10^{-22} atm, and for periods of time of at least several days. One of the critical aspects in the design of such a device consists in selecting the proper materials according to the specific set of operating conditions. In this section, the selection of the probe components such as solid electrolyte, reference system, and conducting lead material, is discussed.

4.1.1 Solid Oxide Electrolyte

The transport properties of solid electrolytes are primarily due to the presence and mobility of lattice defects. In particular, electrical conductivity is determined by the nature and concentration of various ionic and electronic point defects such as vacancies, interstitial or misplaced atoms, impurities, and free electrons or electron holes. All these defects coexist in a solid electrolyte. However, for given temperature and pressure conditions as well as given composition and crystal structure, a particular type of defect predominates due to energy considerations yielding a specific type of conduction. A solid electrolyte will then be either an ionic or an electronic conductor depending on the predominance of either ionic or electronic defects (mixed conduction can also be observed). A knowledge of the defect structure is therefore essential. In the case of solid oxide electrolytes, the generation of lattice defects and the variation of their concentrations are ***temperature*** and ***oxygen partial pressure*** (or oxygen potential, μ_{O_2}) dependent. Consequently, the type

of conduction in a solid oxide electrolyte will also be temperature and oxygen pressure dependent as illustrated in Figure 4.1. A solid oxide electrolyte exhibits ***free electron conduction*** (σ_n, n-type) for low oxygen pressures, ***positive hole conduction*** (σ_p, p-type) for high oxygen pressures, and ***ionic conduction*** (σ_{ion}) for intermediate oxygen pressures as shown in Figure 4.2 (a). Ionic conductivity in solid oxide electrolytes, which occurs only within a limited oxygen pressure range as shown in Figure 4.2 (b), is due to the presence of ***oxygen ion vacancies***. The addition of aliovalent impurities as dopants can increase the number of vacancies to such an extent that these vacancies generate a highly defected structure through which oxygen ions can migrate inside the electrolyte. The most typically used dopants are calcia, CaO, magnesia, MgO, and yttria, Y_2O_3. Figure 4.2 (c) shows the effect of Y_2O_3 addition on ThO_2 conductivity.

The success of the probe depended largely on selecting a material that was an ionic conductor over the range of oxygen partial pressures encountered in the softening process, and that had an adequate ionic conductivity in the temperature range of application. The properties and characteristics of solid oxide electrolytes have been extensively reported in the literature[74-82]. Four principal types of solid oxide electrolyte are available: δ-Bi_2O_3, CeO_2, ThO_2, and ZrO_2 based materials, CaO, MgO, Y_2O_3 being the most commonly used dopants. The relevant characteristics of these electrolytes can be summarized as follows. The δ-Bi_2O_3 based materials cannot be used for oxygen determination in molten metals due to problems caused by their instability at room temperature[82]. The CeO_2 based materials have excellent characteristics at low temperatures, and in particular have a very good conductivity for temperatures below 500°C, but their oxygen pressure range of application is very limited in the temperature range of 500 to 700°C. It extends only down to about 10^{-13} atm at 600°C[77]. The ThO_2 based materials have properties suitable for use as solid oxide electrolytes, but their conductivity is the lowest of the group in the temperature range of

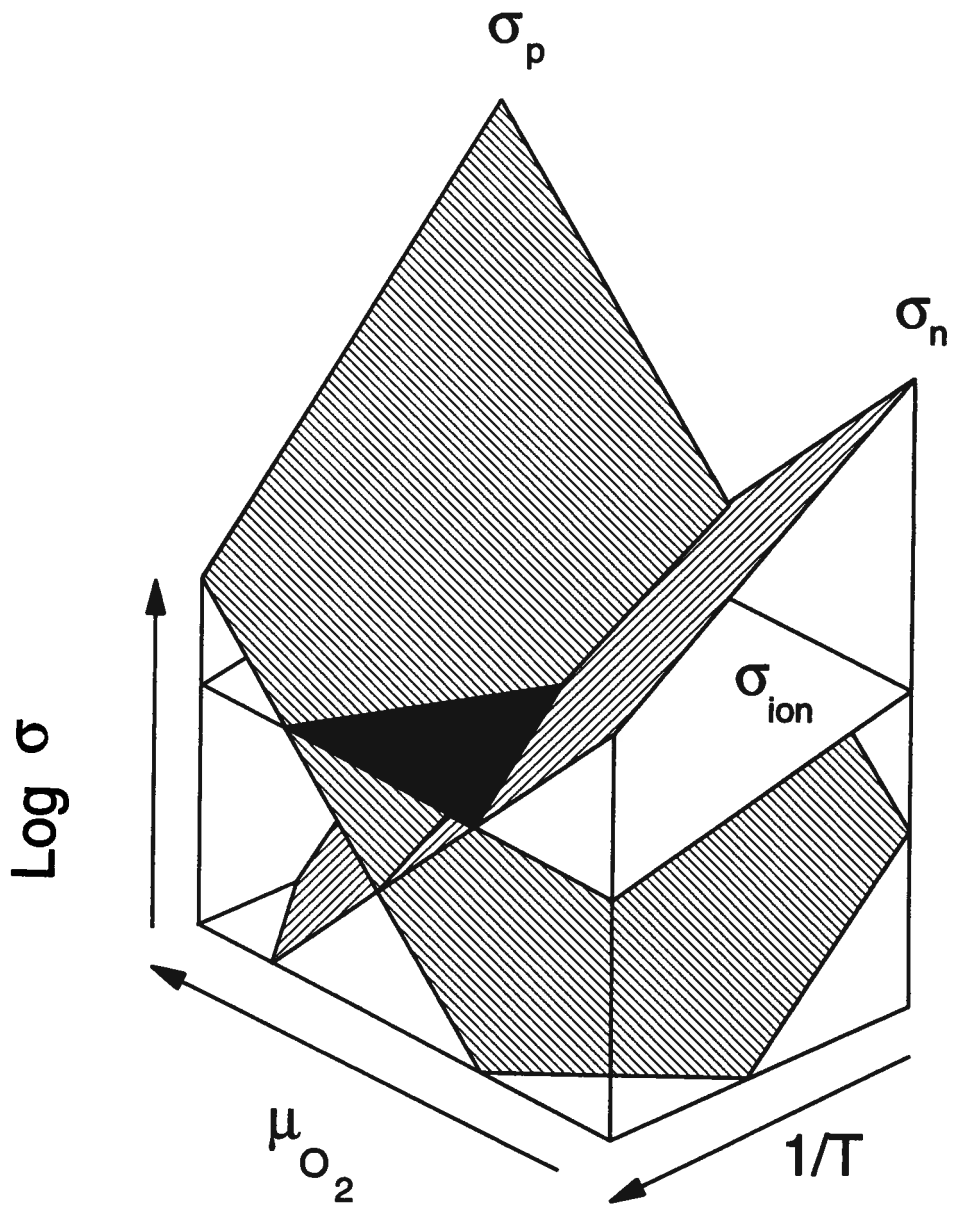

Figure 4.1 - Schematic drawing showing the effect of temperature and oxygen pressure on the conductivity of a solid oxide electrolyte (Adapted from Patterson, 1971, ref. 74).

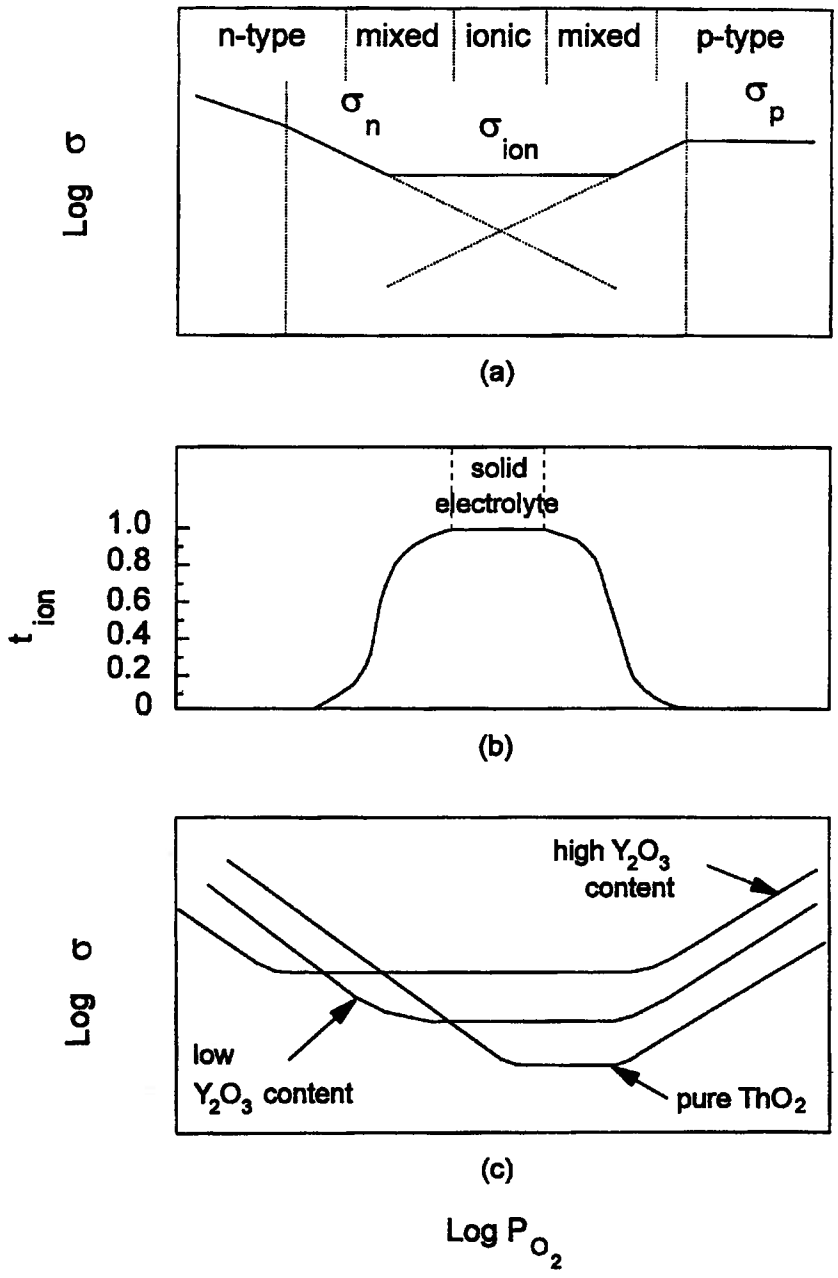

Figure 4.2 - Schematic representation of (a) partial electrical conductivities, (b) ionic transference number in Y_2O_3-doped ThO_2, and (c) effect of dopant concentration on partial conductivities in ThO_2-Y_2O_3 solid solutions (Adapted from Choudhary *et al.*, 1980, ref. 75).

450°C and 750°C (see Figure 4.3). The ZrO_2 based materials have been widely used due to their commercial availability and their wide range of applicability: good electrical conductivity over a large temperature range (see Figure 4.3) and wide electrolytic domain (see Figure 4.4). For these reasons, zirconia based electrolytes were the most appropriate materials for the probe.

From the comparative review of past applications of zirconia electrolytes in molten lead, presented in Chapter 2 and summarized in Table 2.1, and in light of the above restrictions, two materials appeared to have the highest potential for application in lead softening:

- ZrO_2-15 mol% MgO for its corrosion resistance properties and good conductivity at temperatures below 800°C, and
- ZrO_2-6 or 8 mol% Y_2O_3 for its large electrolytic domain and long life span.

Figure 4.5 provides a comparison between the electrical conductivity of commercial zirconia solid electrolytes doped with yttria and magnesia. Yttria stabilized zirconia was chosen since it has a higher conductivity in the temperature range 450°C to 750°C than magnesia stabilized zirconia.

4.1.2 Reference System

When selecting the reference system, two choices were made: first deciding whether to use a gaseous or a solid reference, and secondly deciding which chemical system was best suited. The serious drawback of a gaseous reference system, i.e. diffusion of molecular oxygen through the fine pores and microcracks of the electrolyte, only occurs at a negligible rate at temperatures between 450°C to 700°C. However, a gaseous reference system has the disadvantage of being less convenient

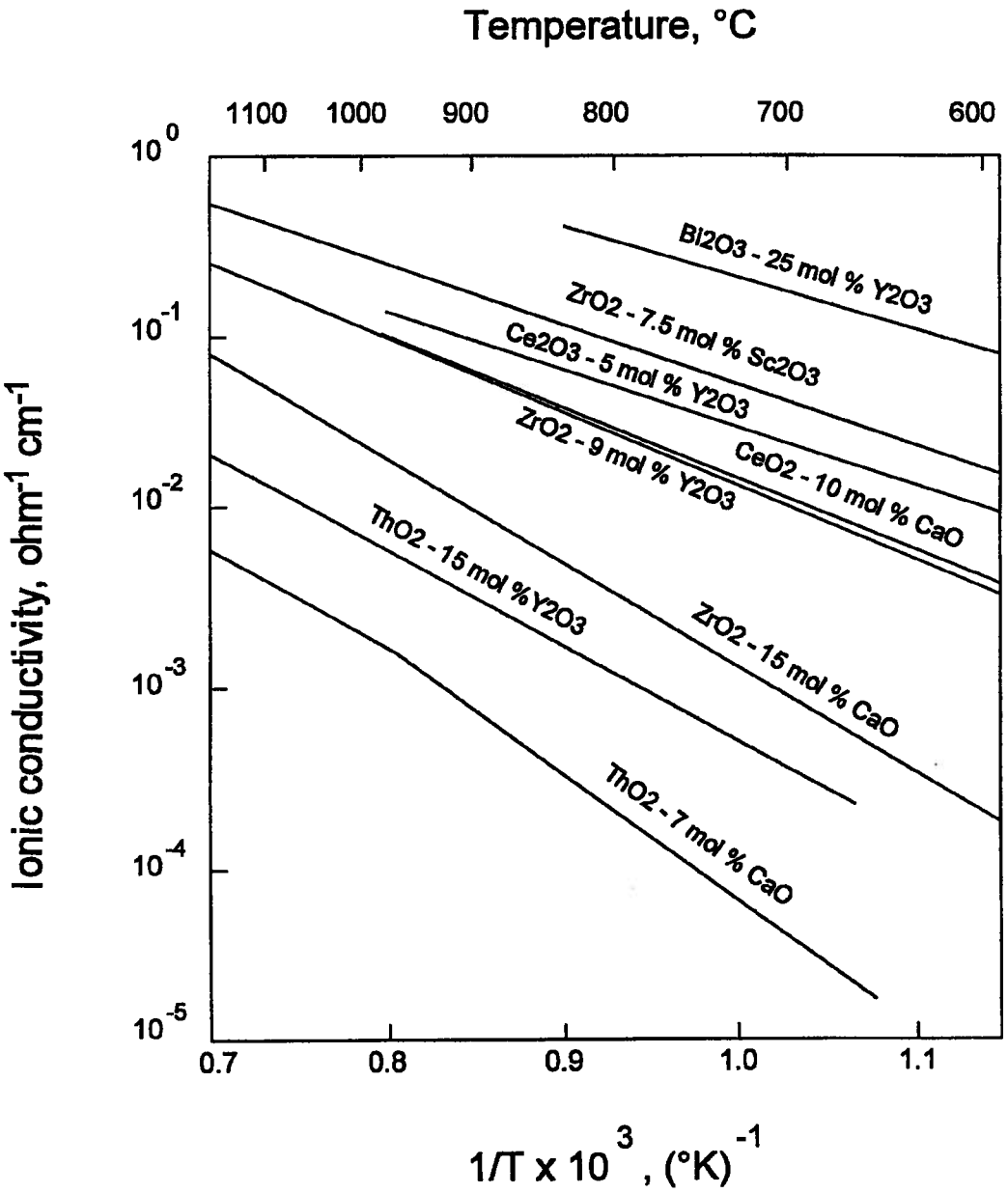

Figure 4.3 - Conductivity of various solid oxide electrolytes as a function of temperature (Adapted from Choudhary *et al.*, 1980, ref. 75).

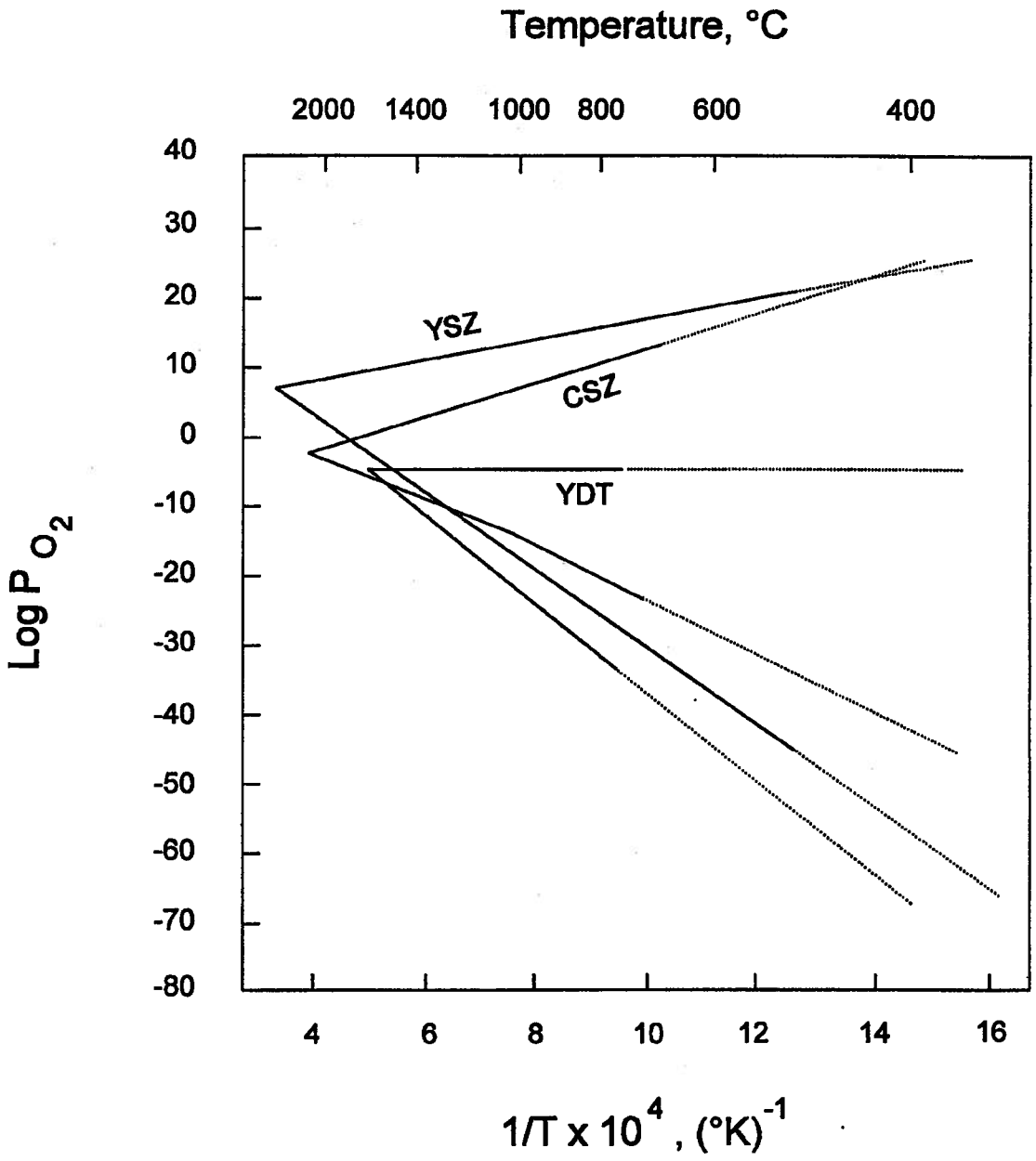

Figure 4.4 - Electrolytic domain of various zirconia solid oxide electrolytes as a function of temperature and oxygen partial pressure. YSZ stands for Yttria Stabilized Zirconia, CSZ for Calcia Stabilized Zirconia, and YDT for Yttria Doped Thoria (Adapted from De Schutter *et al.*, 1991, ref. 57).

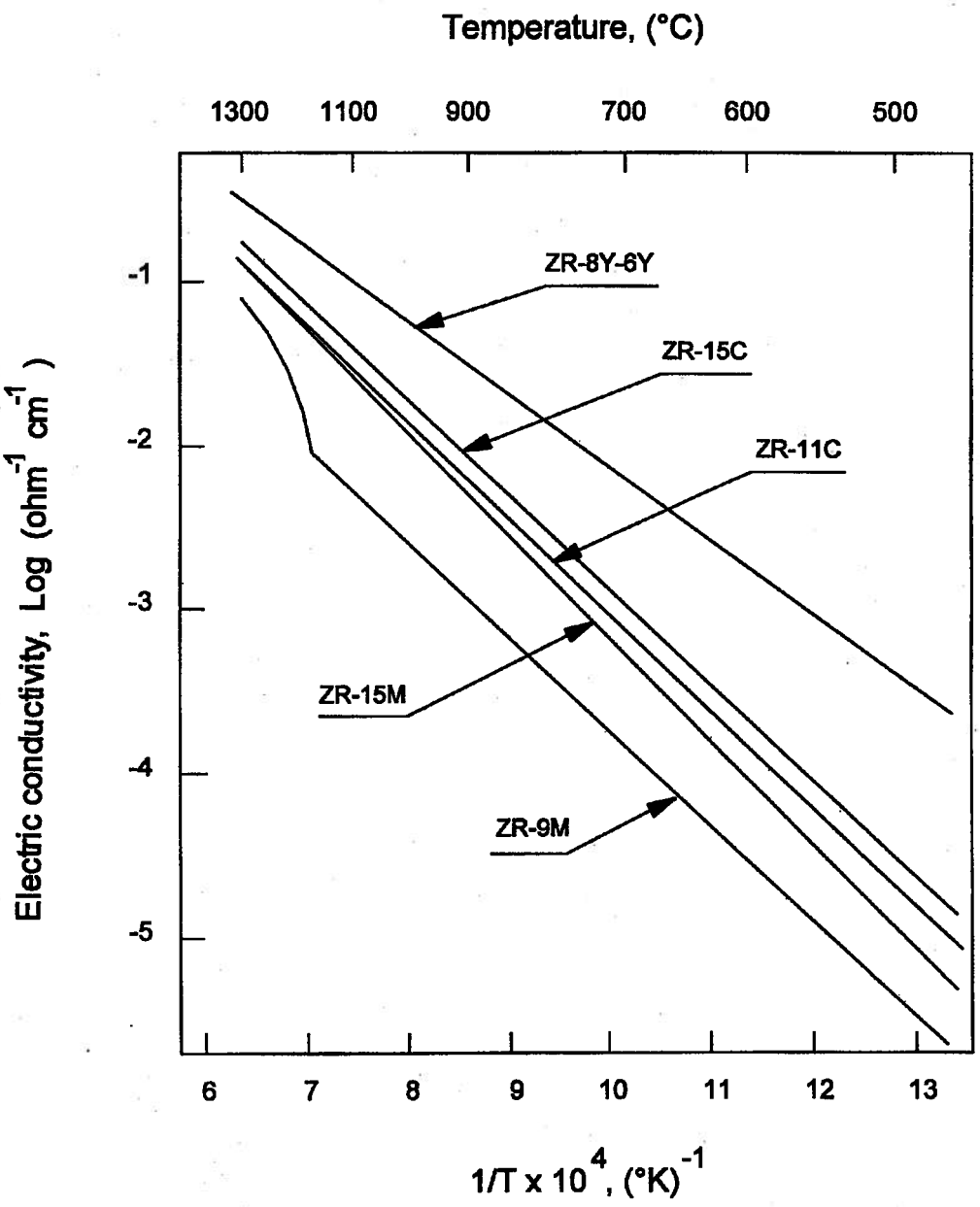

Figure 4.5 - Characteristics of commercial zirconia solid electrolytes. The letters correspond to the type of dopant, with M for magnesia, C for calcia and Y for yttria, and the numbers correspond to the mole percent of dopant. (Adapted from Nippon Kagaku Togyo Co. Ltd. marketing pamphlet, 1991, ref. 83).

than a solid reference system: loss of portability, problem of gas flow rate regulation, and large emf readings resulting in loss of accuracy[23]. On the other hand, a solid reference system seems to be more adapted to the objectives of this project, even though Kozuka[59] suggests that a solid reference might not retain its true oxygen potential for long periods of time. A solid reference system is usually a mixture of fine powders of metal and its oxide. Ni-NiO, Cr-Cr_2O_3, Cu-Cu_2O, and Fe-FeO are some of the commonly used mixtures.

Since solid electrolytes are not fully ionic, $t_{ion} \sim 0.99$, an experimental difficulty may occur when attempting to maintain a desired oxygen potential at the electrode-electrolyte interface. The electronic conductivity contribution of the solid electrolyte, even though very small, $t_{electron} \sim 0.01$, generates a short-circuiting current through the electrolyte, and subsequently a shift in the oxygen potential at the electrode-electrolyte interface from that established by the metal-metal oxide equilibrium to that fixed by the steady state oxygen transfer. This electrode polarization phenomenon is characterized by the generation of an ***overvoltage***. If the short-circuiting current is very small, a stable emf can be obtained which includes an overvoltage contribution. Measurements of overvoltage versus current for symmetrical electrochemical cells of the type

$$\text{Metal, Metal Oxide} \quad | \quad ZrO_2 + CaO \quad | \quad \text{Metal Oxide, Metal}$$

performed by Worrel and Iskoe[84] are reported in Figure 4.6. In order to minimize polarization, the reference system should have an equilibrium oxygen pressure close to that prevailing in the molten lead at the temperature of interest. Values of P_{O_2} for various metal-metal oxide mixtures at temperatures between 500 and 700°C are given in Table 4.1. The equilibrium oxygen pressures were calculated using data from Barin and Knacke[85].

From this review, it appeared that the system Cu-Cu_2O would give the lowest level of polarization as it exhibits an oxygen equilibrium pressure closest to that prevailing in a lead bullion in equilibrium with an oxidic slag. For these reasons, a Cu-Cu_2O mixture was considered the best suited reference for application in lead softening.

Table 4.1 - Equilibrium oxygen pressure of various metal-metal oxide systems at temperatures between 500 and 700°C.

Metal-Metal Oxide System	**Equilibrium Oxygen Pressure (atm.)**		
	500 °C	600 °C	700 °C
$Pb_{(s)} + 1/2\ O_{2(g)} \leftrightarrow PbO_{(s,\ yellow)}$	1.1×10^{-19}	2.7×10^{-16}	1.3×10^{-13}
$Ni_{(s)} + 1/2\ O_{2(g)} \leftrightarrow NiO_{(s)}$	1.1×10^{-23}	5.3×10^{-20}	4.3×10^{-17}
$Fe_{(s)} + 1/2\ O_{2(g)} \leftrightarrow FeO_{(s)}$	1.3×10^{-30}	1.9×10^{-26}	3.7×10^{-23}
$2\ Cr_{(s)} + 3/2\ O_{2(g)} \leftrightarrow Cr_2O_{3(s)}$	2.8×10^{-42}	1.7×10^{-36}	6.7×10^{-32}
$2\ Cu_{(s)} + 1/2\ O_{2(g)} \leftrightarrow Cu_2O_{(s)}$	7.0×10^{-16}	2.8×10^{-13}	3.1×10^{-11}

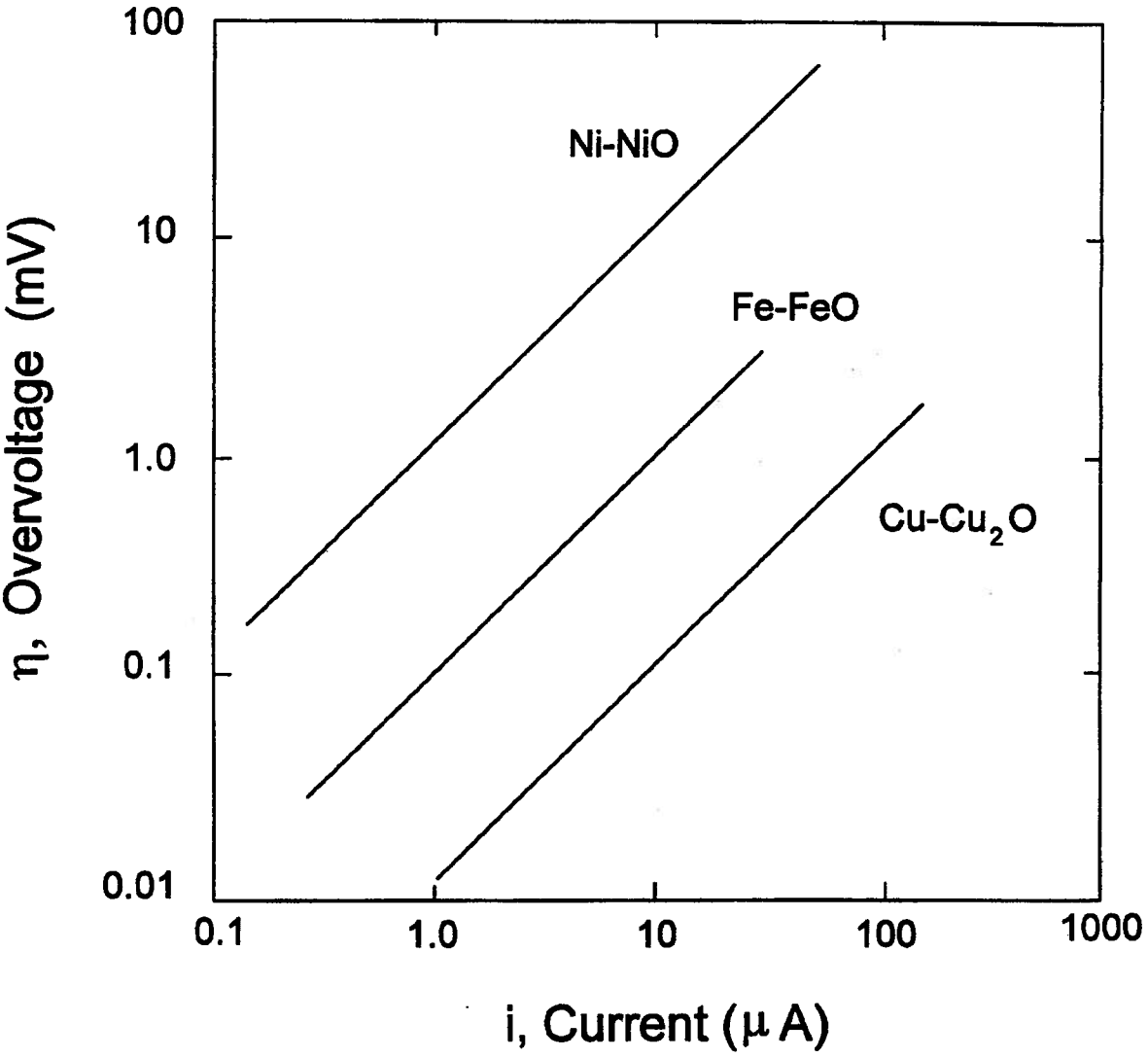

Figure 4.6 - Overvoltage versus current for various metal-metal oxide systems at 900°C (Adapted from Worrel and Iskoe, 1973, ref. 84).

4.1.3 Lead Wire and Conducting Lead

A lead wire is a metallic wire that connects the reference electrode to a measuring device such as an electrometer. Platinum is the most commonly used material for lead wires in laboratory oxygen sensors. A conducting lead corresponds to a rod or tube of conducting material that is dipped into a molten metal in order to provide electrical contact with the melt. The conducting lead actually corresponds to the counter electrode of the probe. Since the conducting lead is in continuous contact with the melt, one of its most important characteristics is that it should be corrosion resistant.

Various metals such as platinum, iridium, molybdenum, as well as stainless steel and Cr-cermet have been successfully employed as conducting lead materials (see Table 2.1). Even though platinum has excellent characteristics in terms of chemical stability, electronic conduction and availability, it might not be the most adequate material for temperatures in the order of 500 to 700°C due to its slow response to oxygen exchange reactions at the electrode-electrolyte interface. Moreover, its cost could be prohibitive for an industrial device. Cr-cermet has been reported to dissolve in molten lead for temperature higher than 850°C, whereas iridium does not show any solubility in molten lead[48]. Stainless steel 316 is very appealing due to its commercial availability in various shapes and sizes (wires, rods and tubes) at reasonable cost. Provided it possesses good corrosion resistance characteristics in molten lead and antimonial lead slag, stainless steel 316 is believed to be the best choice for an oxygen probe in lead softening. To avoid the use of dissimilar leads, stainless steel 316 was also chosen as lead wire material.

4.1.4 Conclusions

In view of the above operating requirements inherent to lead softening, the following materials have been selected for the main components of the probe.

- Solid electrolyte: commercially available yttria stabilized zirconia (ZrO_2-6 or 8 mol% Y_2O_3) from **Coors Ceramic Co.** and **Nippon Kagaku Togyo Co.** (see Table 4.2 for properties).
- Reference system: Cu and Cu_2O powders from **Cerac Inc.** (see Table 4.3 for assays).
- Lead wire and conducting lead: 316 stainless steel wire and tubing.

Table 4.2 - Properties of Y_2O_3 fully stabilized zirconia from Coors Ceramic Co.

Properties	Units	Value
Bulk density	g/cc	5.60
Electrical conductivity (Log σ at 650°C)		- 2.5
Coefficient of thermal expansion (25-1000°C)	10^{-6}/°C	10.5
Thermal shock resistance (maximum tolerable temperature difference)	°C	150
Maximum use temperature	°C	2400

Table 4.3 - Assays for Cu and Cu_2O powders from Cerac Inc.

Impurities %	**Cu powder** (-200, +325 mesh)	**Cu_2O powder** (-200 mesh)
Typical purity	99.5 %	99.9 %
Ag	-	0.008
Al	0.001	0.001
Ca	-	0.001
Fe	0.005	0.004
Mg	-	0.005
Mn	-	0.001
Ni	-	0.003
Pb	0.005	-
Si	0.001-0.01	0.005
Sn	0.005	0.05
Zn	0.005	-

4.2 Probe Development in Laboratory

Once the materials had been selected, the various components of the probe were assembled together according to a chosen probe geometry. The cell assembly design was then tested for thermal and corrosion resistance, calibrated to ensure proper oxygen measurements, and eventually modified to improve its characteristics. This section is divided in three parts. First, the experimental apparatus built for this project is described. Then the development of the cell assembly design is discussed. Finally, the laboratory tests of the probe in molten lead are presented and a probe design for industrial tests is discussed.

4.2.1 Experimental Apparatus

The experimental set-up is composed of three main components: a furnace, a temperature controller, and a data acquisition system as shown in Figure 4.7. The furnace, specially designed and constructed for this project, is a vertical unit with a height of 1 metre and a square base of 0.5 metre. The heating element is made of chromel ribbon with variable pitch windings to provide rigorous temperature control of $\pm$ 1°C within a hot zone of about 10 cm. A temperature profile along the vertical axis of the furnace chamber is given in Figure 4.8. This rigorous control is required in order to avoid temperature gradients within the probe, which would otherwise influence the probe readings. A sheet metal shield provides protection around the hot zone to reduce the electrical pick-up as well as electromagnetic effects created by the chromel windings. The chamber is made of a mullite tube with an inside diameter of about 7 cm which allows the use of crucibles with an outer diameter of up to 6.7 cm. This is particularly important since large crucibles allow simultaneous testing of two probes without restricting access to the crucible for other instrumentation

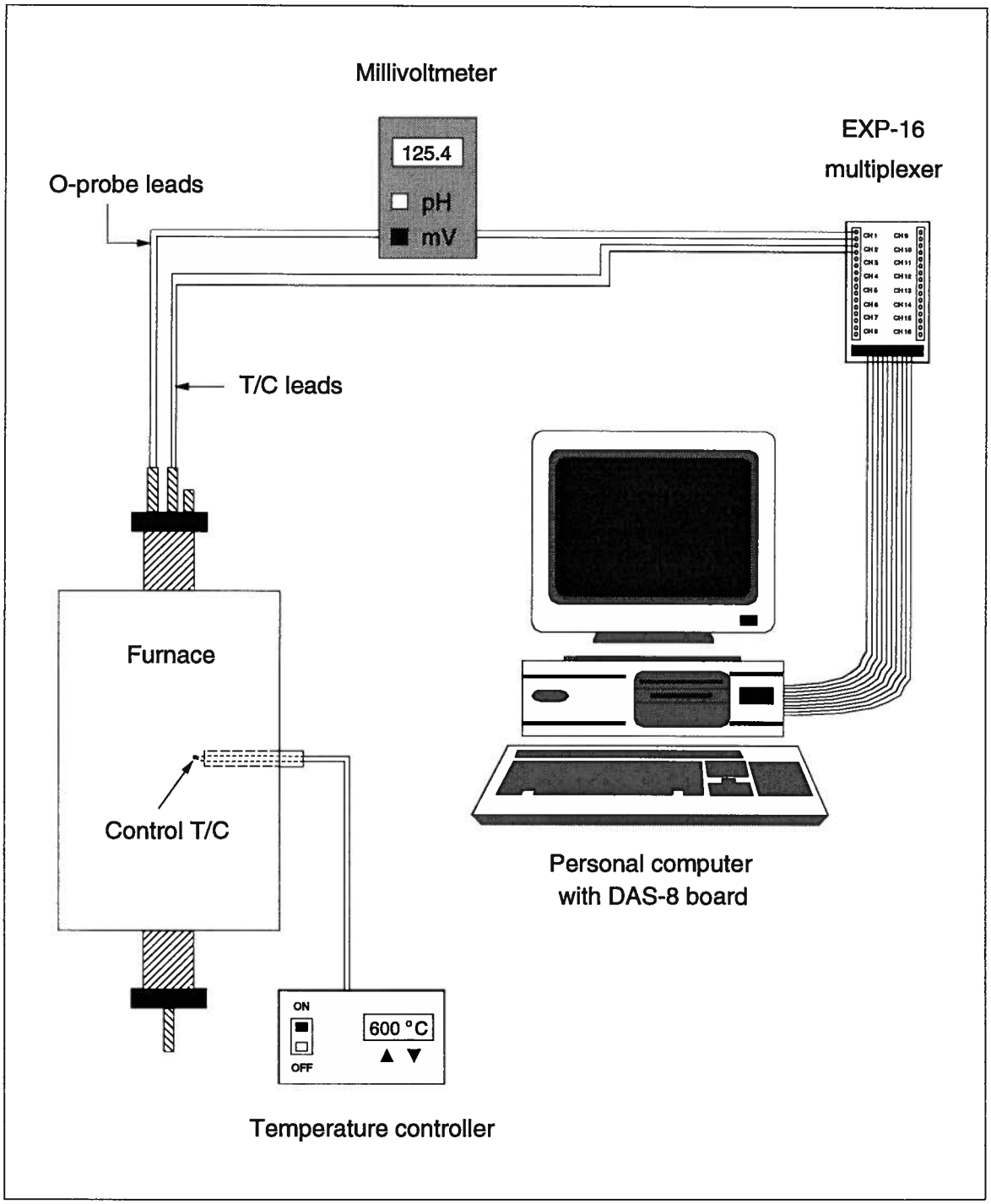

Figure 4.7 - Schematic representation of the experimental set-up for laboratory tests.

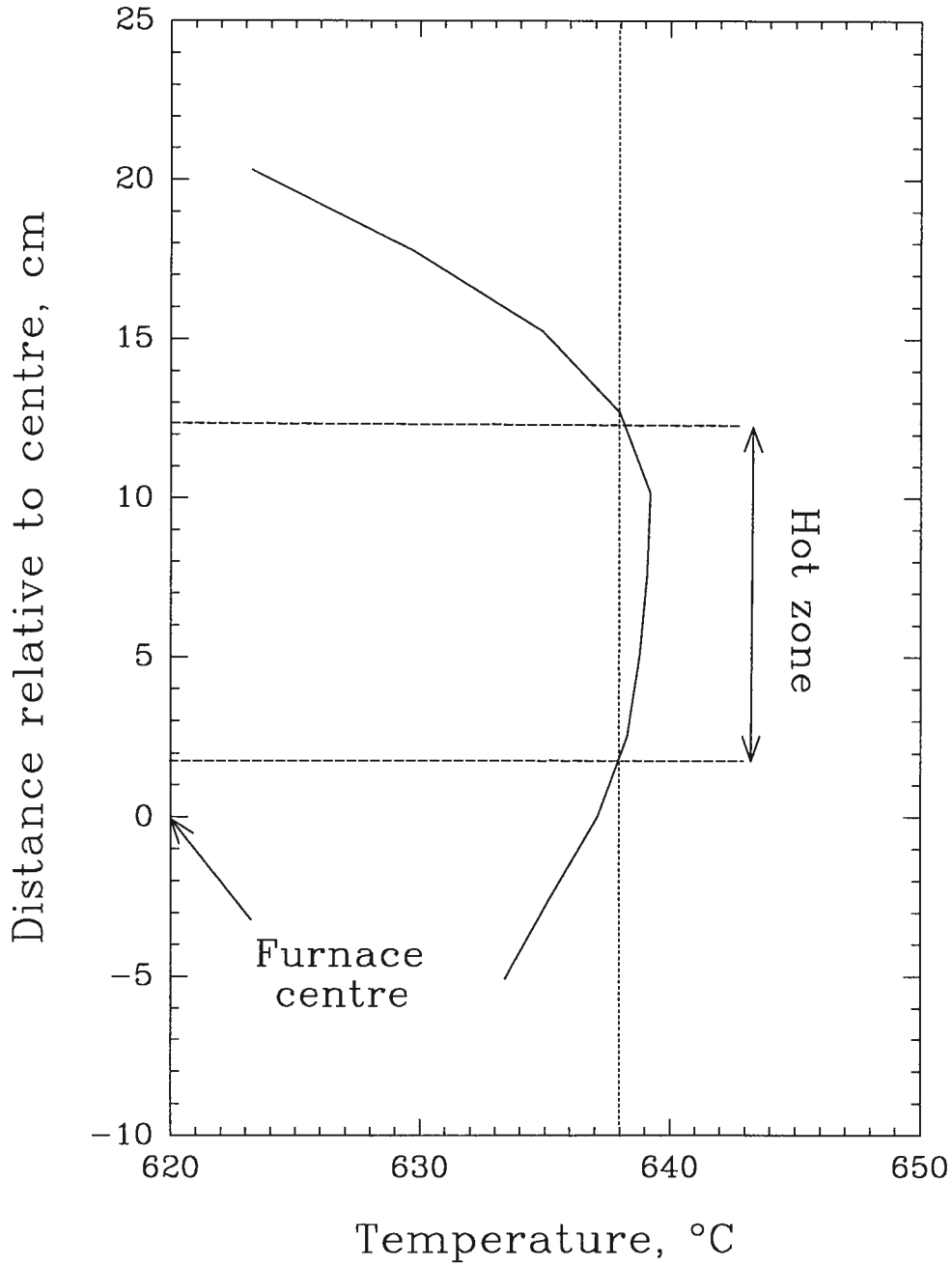

Figure 4.8 - Temperature profile along the vertical axis of the chamber with location and length of the hot zone (± 1°C) for a temperature set point of 610°C using the outer thermocouple (S-type).

such as reagent addition tube, sampling tube, and thermocouple. It also provides some buffering effect for composition control with the use of large volumes of molten lead. The chamber can be closed off with top and bottom gas-tight caps. In these circumstances, all instruments are inserted into the chamber through appropriate gas-tight **Swagelok** tube fittings. Gases can be introduced in the chamber to control the atmosphere when required. For this purpose, a gas purification train, for moisture, oxygen and hydrogen removal using silica gel, phosphorus pentoxide and **BASF catalyst R3-11**, is kept on stand-by. The chamber is schematically represented in Figure 4.9.

Temperature control is achieved by an **Omega CN9000 Series** microprocessor controller which features PID (Proportional-Integral-Derivative), PD (Proportional-Derivative), Proportional, and On/Off control. Two separate thermocouple locations can be used for temperature control: mid-way along the vertical axis of the furnace at the outer periphery of the heating element, or inside the chamber close to the top of the crucible. In both alternatives, a S-type thermocouple (Pt/Pt-Rh) is used. The experimental temperature is measured by means of a K-type thermocouple dipped into the molten lead sample and protected by an alumina sheath closed at one end.

The data acquisition system hardware is composed of a **Keithley EXP-16** multiplexer and a **Keithley DAS-8** board. **Labtech Notebook** is used as data acquisition software. Prior to the multiplexer, the probe leads are connected to a **Corning 130** pH and millivolt meter. Such an instrument has an input impedance greater than 10^{12} ohms, which is required to obtain a reliable reading from an oxygen probe that has a very high resistance.

Further technical details of the furnace, the millivoltmeter, and the data acquisition system are given in Appendix 1.

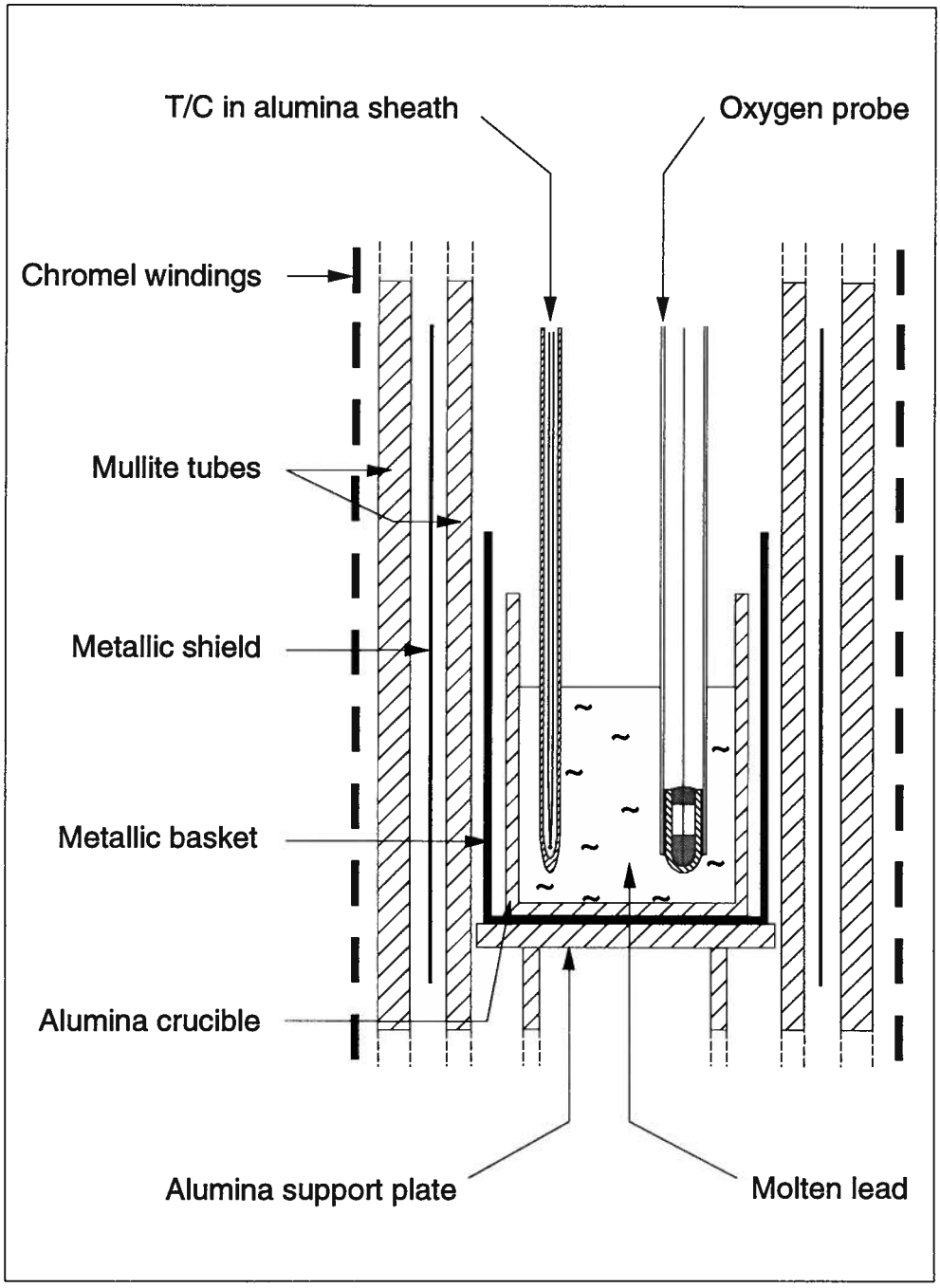

Figure 4.9 - Schematic representation of the chamber with measuring devices in position for laboratory tests.

4.2.2 Cell Assembly

Two cell geometries are possible as illustrated by Figure 4.10. The geometry using a disk cemented at the tip of a silica tube is typical of single reading or disposable probes used in steel-making operations. One of the main advantage of solid electrolyte disks is their low cost compared with thimbles. Problems of leakage at the zirconia-silica joint is however a serious drawback if continuous measurements for long periods of time is desired. For this project, the geometry using a solid electrolyte thimble was the preferred option. Figure 4.11 shows a schematic drawing of a typical probe design for continuous measurements which was adopted to start the experimental work. The dimensions of the zirconia thimbles are: 6 mm OD, 4 mm ID, and 35 mm long.

The behavior of this assembly upon heating was the first concern to be addressed. The component materials have very dissimilar coefficients of thermal expansion: 10.2, 12.7 and 17.4 10^{-6} /°C for the solid electrolyte, the cement and the stainless steel, respectively. Stresses within the assembly and generated during heating or cooling cycles can lead to cracking of the zirconia tube. Two parameters can be adjusted to reduce the risk of cracking due to thermal property differences between the components: the thickness of the stainless steel housing, and the amount of cement used for the metal-ceramic joining. A commercially available, high temperature, magnesia based cement, **Ceramabond 571** from **Aremco Product Ltd.**, was chosen for the metal-ceramic bonding. Experiments demonstrated that the thinner the steel housing and the larger the amount of cement, the better the resistance of the probe to thermal stresses. The success of these experiments, no cracking even after several heating and cooling cycles with the same probe, resulted in the design of a customized steel sleeve to serve as probe tip housing. A scale drawing of this steel sleeve is given in Figure 4.12.

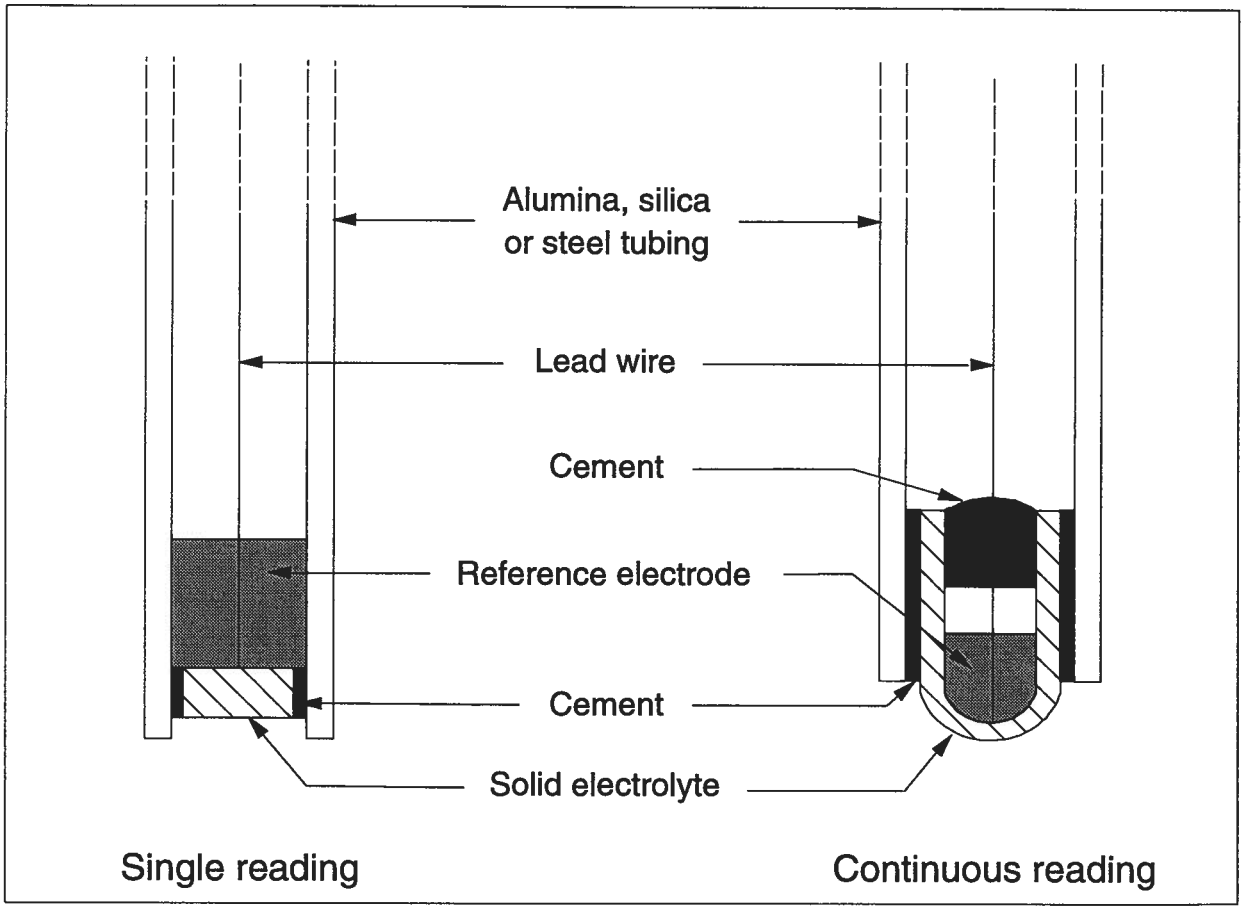

Figure 4.10 - Schematic representation of the possible cell assembly geometries for oxygen probes.

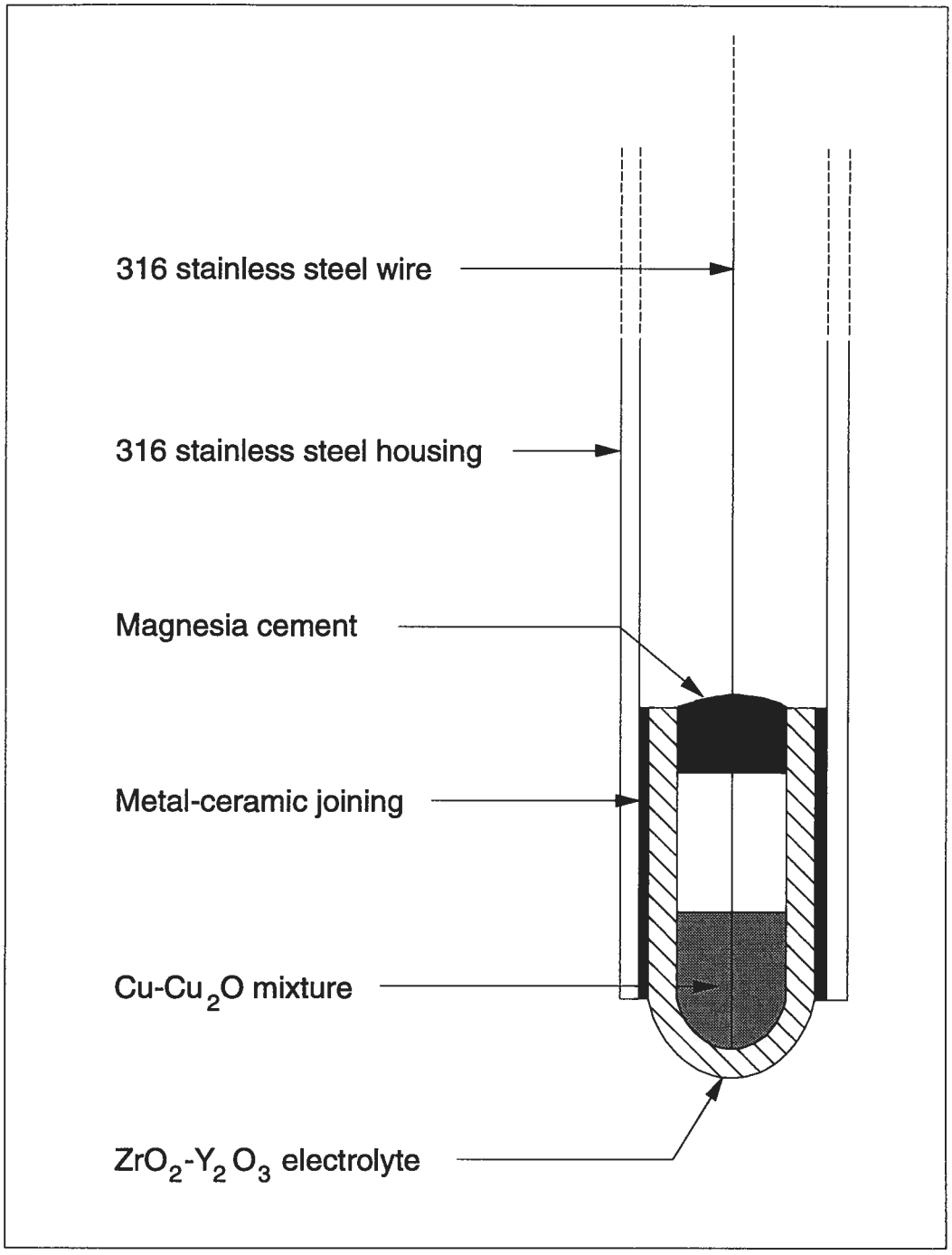

Figure 4.11 - Schematic representation of the first design of cell assembly used in the early experiments.

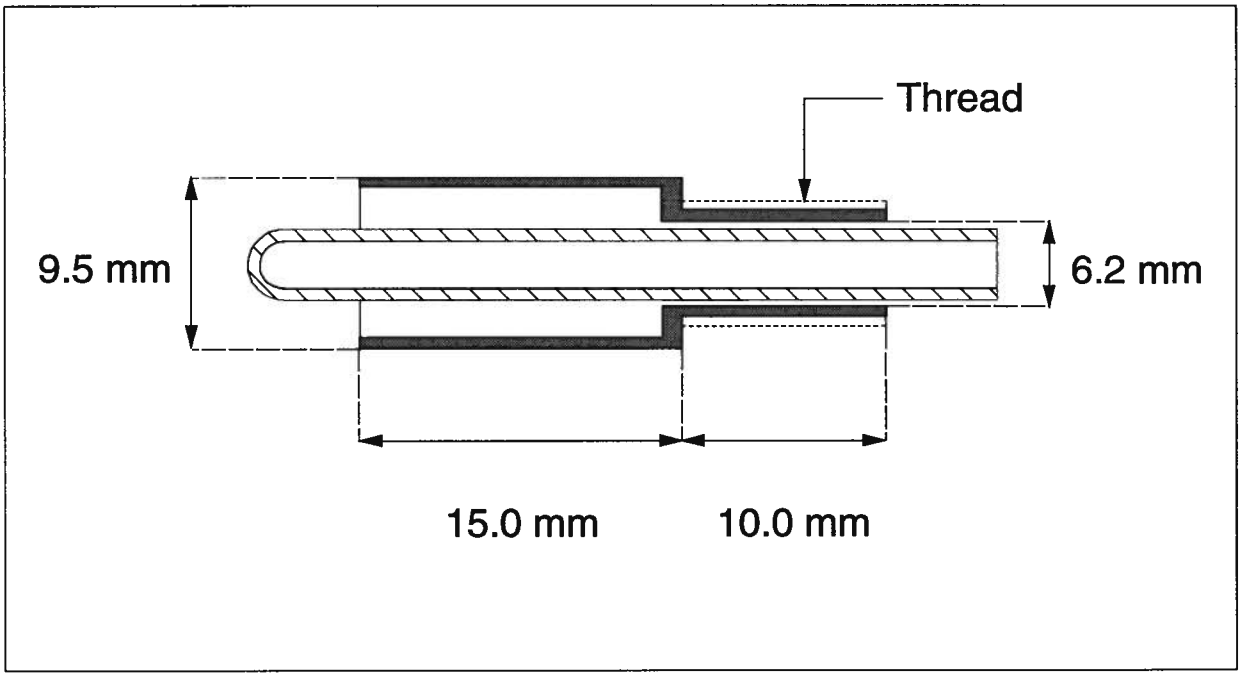

Figure 4.12 - Scale drawing of the steel sleeve used as housing for the probe tip (35 mm long zirconia thimble shown in position).

The next major concern consisted in ensuring that the probe readings were within reasonable accuracy. For this purpose, the probe was immersed in oxygen saturated lead bullion obtained by melting high purity lead in an oxidizing atmosphere and leaving the melt until a layer of yellow lead oxide was formed on the surface. Using oxygen saturated lead provides a solution that exerts an oxygen partial pressure which is temperature dependent only. Monitoring the deviation between the theoretical and measured oxygen partial pressure of the melt permitted the validation of a design or the identification of any problem that needed to be addressed. Using data from Jacob and Jeffes[48], the temperature dependance of the equilibrium oxygen pressure for the formation of lead oxide according to the reaction

$$Pb_{(l)} + 1/2\ O_{2(g)} \leftrightarrow PbO_{(s,\ yellow)}$$

is given by

$$\ln P_{O_2\,(Pb/PbO)} = 23.79 - \frac{52468}{T} \qquad (4.1)$$

where T is the temperature in Kelvin. Similarly, the temperature dependance of the equilibrium oxygen pressure for the formation of copper (I) oxide according to the reaction

$$2\ Cu_{(s)} + 1/2\ O_{2(g)} \leftrightarrow Cu_2O_{(s)}$$

is given by

$$\ln P_{O_2\,(Cu/Cu_2O)} = 17.225 - \frac{40341.2}{T} \qquad (4.2)$$

The oxygen partial pressures $P_{O_2\,(Pb/PbO)}$ and $P_{O_2\,(Cu/Cu_2O)}$ were computed at different temperatures using Equations (4.1) and (4.2). The probe theoretical emf, E_{th}, was then calculated for the same temperatures using Equation (2.8) in which the appropriate oxygen partial pressures were substituted as follows

$$E_{th} = \frac{RT}{4F} \ln \frac{P_{O_2\,(Cu/Cu_2O)}}{P_{O_2\,(Pb/PbO)}} \tag{4.3}$$

The computed oxygen partial pressures as well as the theoretical emf are given in Table 4.4. A regression analysis yielded the following expression of the temperature dependence of E_{th}

$$E_{th}\,(\text{mV}) = 222.6 - 0.1414\,T\,(°\text{C}) \tag{4.4}$$

The standard Gibbs free energies of formation of PbO and Cu_2O from Jacob and Jeffes[48], Alcock and Belford[44], and Charette and Flengas[45], all obtained by an emf technique, yield theoretical emf values in agreement within $\pm$ 2 mV , whereas data from Barin and Knacke[85], and Kubaschewski and Alcock[86] yield theoretical emf values 9 mV and 13 mV lower, respectively. The choice to use data from Jacob and Jeffes[48] was motivated by the fact that among the investigators they were the only ones to use an emf technique and a temperature range which includes the temperatures characteristic of lead softening. In addition, their data is supported by the results of two of the other studies.

Table 4.4 - Computed values of $P_{O_2\,(Pb/PbO)}$, $P_{O_2\,(Cu/Cu_2O)}$, and E_{th}.

Temperature (°C)	$\mathbf{P}_{O_2\,(Pb/PbO)}$ **(atm.)**	$\mathbf{P}_{O_2\,(Cu/Cu_2O)}$ **(atm.)**	$\mathbf{E}_{th}$ **(mV)**
500	7.263×10^{-20}	6.632×10^{-16}	151.9
550	4.479×10^{-18}	1.577×10^{-14}	144.8
600	1.723×10^{-16}	2.610×10^{-13}	137.7
615	4.753×10^{-16}	5.695×10^{-13}	135.6
650	4.462×10^{-15}	3.187×10^{-12}	130.7
700	8.273×10^{-14}	3.008×10^{-11}	123.6
750	1.153×10^{-12}	2.281×10^{-10}	116.5
800	1.257×10^{-11}	1.432×10^{-09}	109.5

A number of probes were built according to the design presented in Figure 4.11, and they recorded an emf out of range while immersed in the molten lead. Figure 4.13 shows typical emf and temperature recordings of such a probe for a test performed at a temperature of 675°C for which the theoretical emf is 127.1 mV. The probe emf reached about 170 mV within one minute after immersion and gradually increased for about one and a half hours until it stabilized around 270 mV. Modifications of parameters such as amount of Cu-Cu_2O mixture, sintering of the Cu-Cu_2O mixture within the thimble, amount of cement, duration and temperature of cement curing, were unsuccessful in attempting to achieve proper emf readings. Even though the stabilization of the measured emf argues against the possibility of cracks in the zirconia tube, carefully cut cross-sections of the probe tips were examined under a microscope for confirmation. No cracks were apparent. Further observations of the same cross-sections revealed that the reference electrode had lost its integrity during the tests. A layer of Copper (II) oxide (CuO) had formed at the reference electrode/solid electrolyte interface indicating that oxygen had reached and contaminated the reference system. Since within the temperature range of the tests, $P_{O_2\,(Cu/Cu_2O)} > P_{O_2\,(Pb/PbO)}$, the hypothesis of oxygen migration from the melt through the zirconia solid electrolyte to oxidize the Cu-Cu_2O mixture is thermodynamically disputed. It was concluded that the oxidation of the Cu-Cu_2O mixture was caused by oxygen ingress from the top of the probe. The oxygen could either come from leftover water contained in the cement or from the oxidizing chamber atmosphere through the porous cement. In either case, this oxygen ingress had to be stopped to maintain reference electrode integrity. The solution was to integrate an oxygen getter between the reference electrode and the cement seal. A plug of copper powder appeared to be well adapted for the purpose. The term "plug" is used because of the property of the copper powder to partially sinter after some exposure to the experimental temperature, becoming more compact and acting as a stopper. Alumina powder was used to separate the copper plug from both the Cu-Cu_2O mixture and the cement. The lead

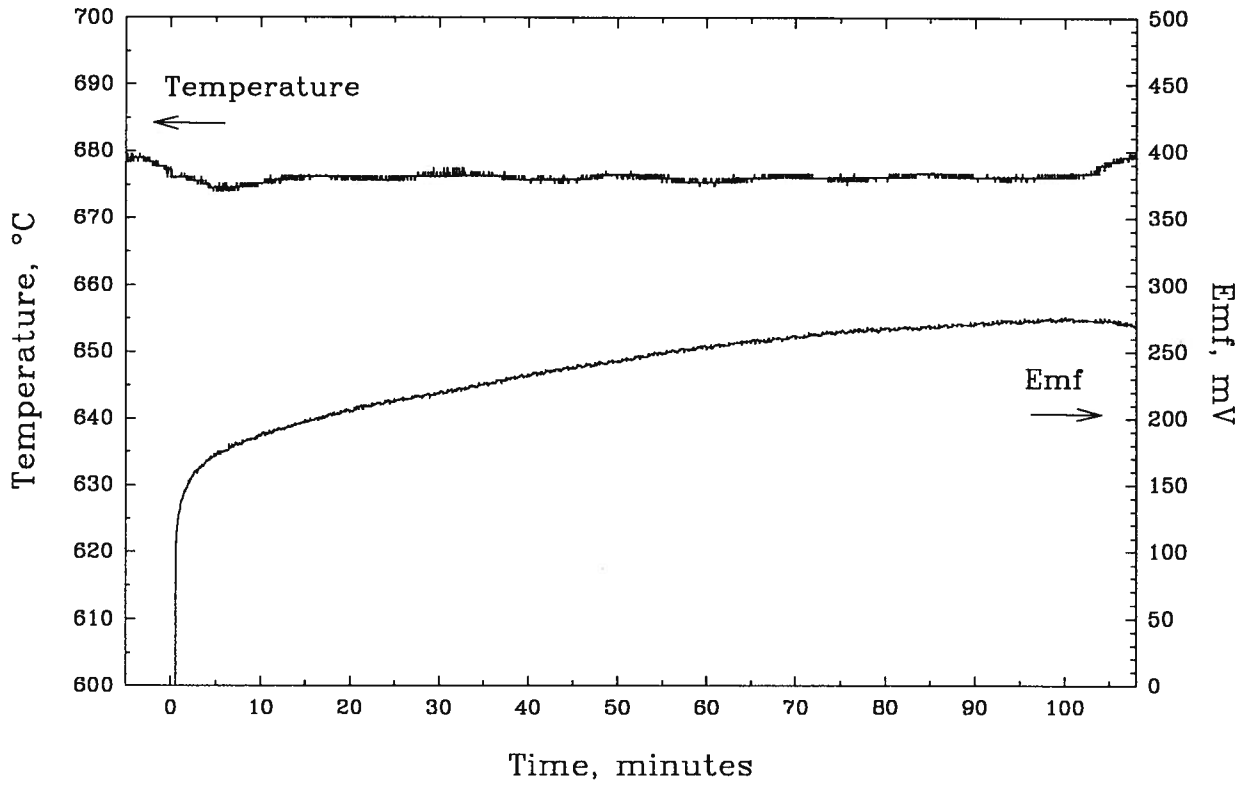

Figure 4.13 - Emf and temperature readings recorded during a test with a probe fabricated according to the design adopted in the early tests.

wire needed to be electrically insulated to avoid any short-circuit by contact with the copper plug. A cement coating was applied on the lead wires for that purpose. To eliminate the risk of oxygen contamination by the water contained in the cement, the cement coating was allowed to completely cure in a drying oven according to the curing treatment recommended by the manufacturer. This improved probe design is schematically represented in Figure 4.14. In order to provide room for the additional alumina and copper powders, longer zirconia thimbles were used. Their dimensions are as follows: 6 mm OD, 4 mm ID, and 70 mm long.

4.2.3 Measurements in Molten Lead

A probe tip, as represented in Figure 4.14, was assembled to a holding device in order to be inserted into the vertical furnace for measurement in molten lead. A probe holder, serving as conducting lead as well, was designed using 316-stainless steel tubing so that a probe tip could be screwed on at one end. A quartz tube was used to insulate the lead wire from the conducting lead in order to prevent electrical contact which would otherwise short-circuit the probe. Pre-purified argon could be introduced through the quartz tube, flush the probe holder and exit at the top of the assembly. Flushing the probe holder provided extra protection for the reference system against oxygen ingress from the atmosphere. Figure 4.15 gives a schematic representation of the probe and its holding device.

A number of experiments were carried out to investigate the characteristics of the probe such as response time and accuracy, cell reversibility, life-span, and reproducibility. All the required tests initially involved molten lead saturated with oxygen obtained as previously described by melting lead in an oxidizing atmosphere and leaving the melt until a layer of yellow lead oxide was

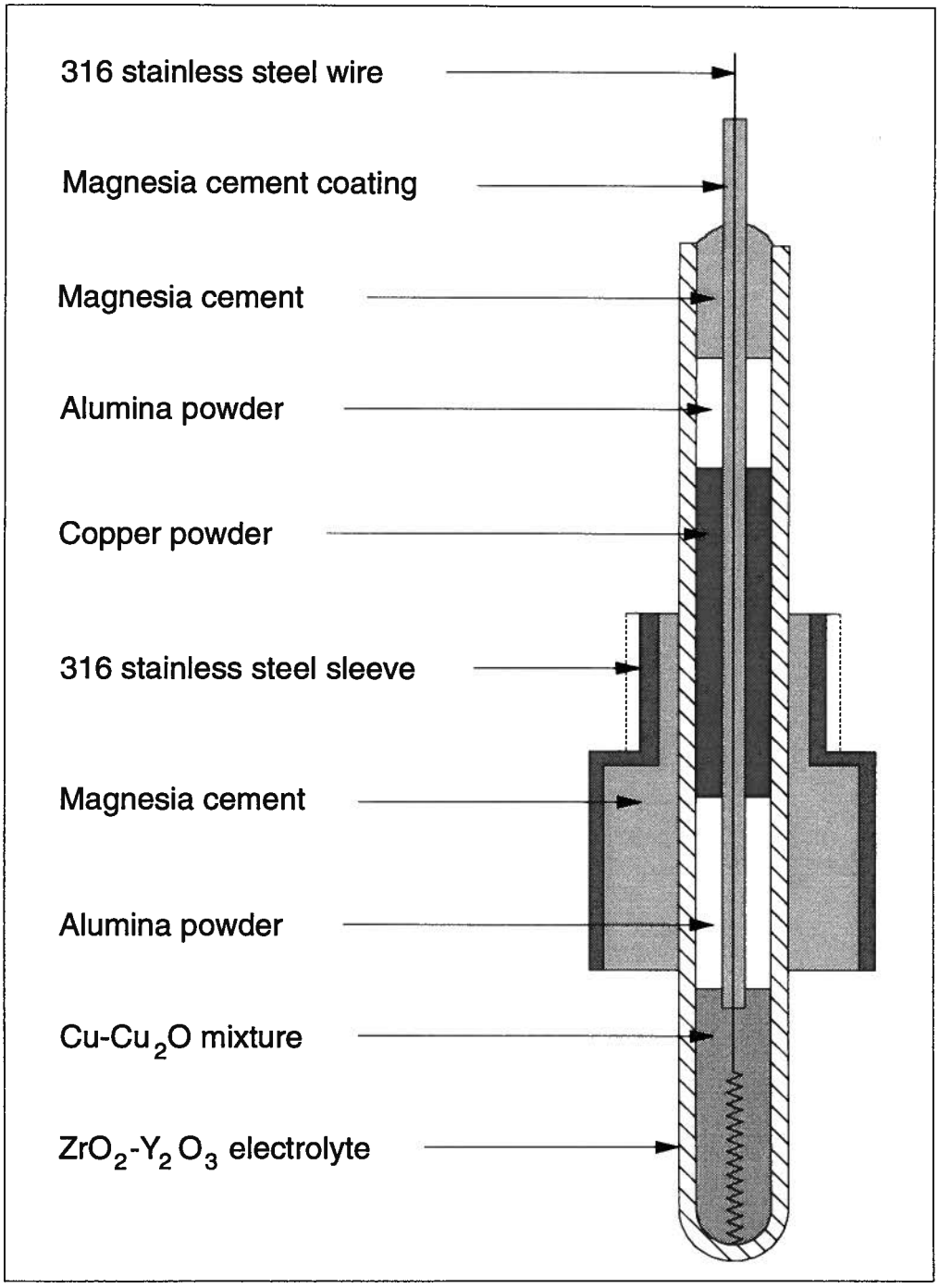

Figure 4.14 - Schematic representation of the improved design of cell assembly.

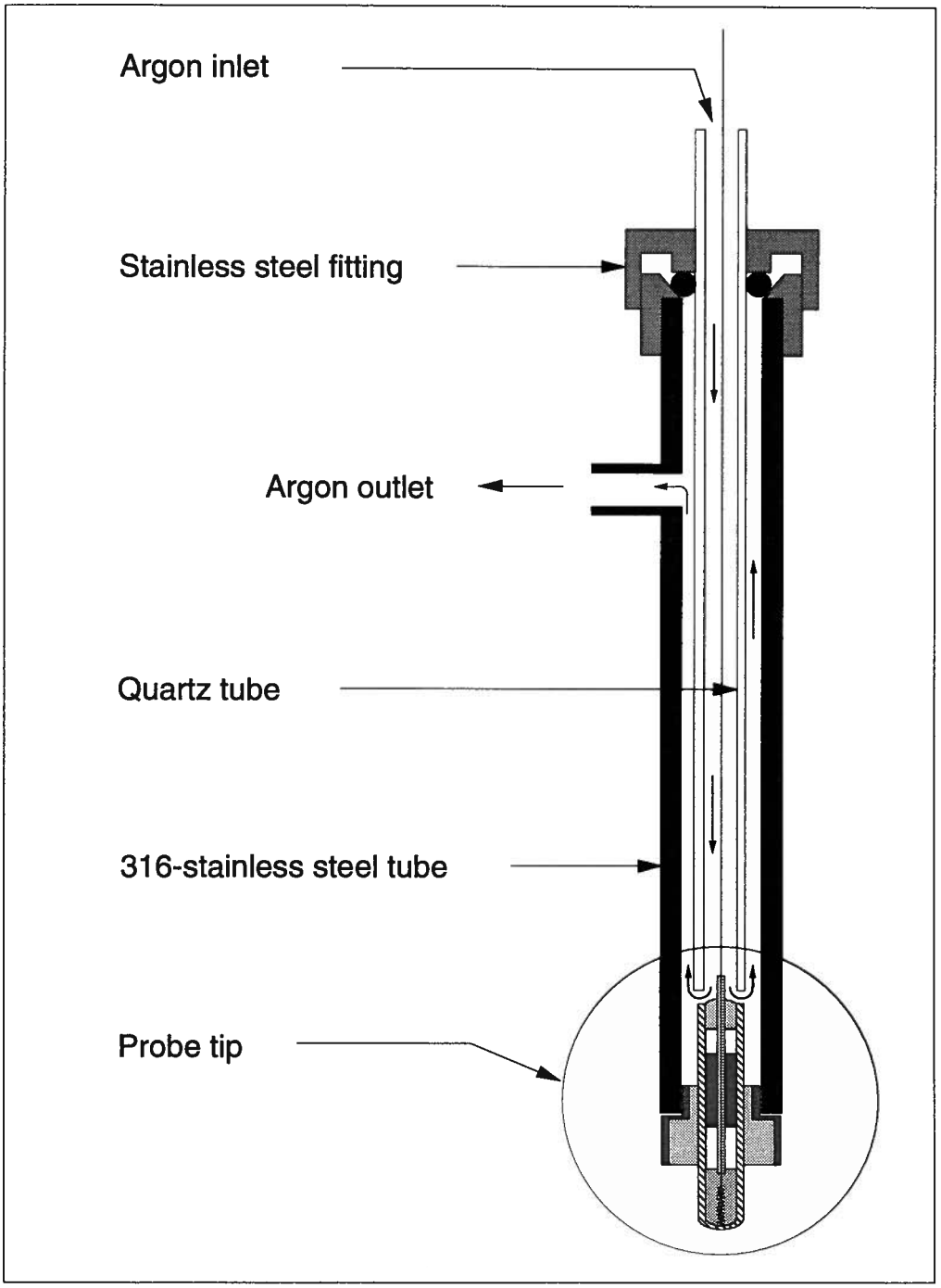

Figure 4.15 - Schematic representation of the probe and the probe holding device.

formed on the surface. Ten probes were built and used for laboratory testing, and only two were dysfunctional (out of range emf). Figure 4.16 shows a typical probe response upon immersion in oxygen saturated molten lead. It can be seen that the probe responded immediately and a stable emf of 125 mV ± 1 mV was obtained in less than fifteen minutes at a temperature of 697°C ± 1°C. The theoretical emf value calculated from Equation (4.4) is 124.0 mV. All the successful probes gave emf readings in very good agreement with the theoretical emf value when immersed in oxygen saturated molten lead (see Table 4.5). Each probe was tested in molten lead obtained by melting pieces of solid lead from the same lot of ingots. Any discrepancy between measured and theoretical emf could be caused by three main factors: 1) uncertainty in the data from which the theoretical emf was calculated, 2) the polarization of the Cu-Cu_2O reference electrode which would decrease the measured emf, and 3) the presence of impurities in the Cu-Cu_2O reference, such as CuO, which would increase the equilibrium oxygen pressure of the reference system, and consequently increase the measured emf. The choice of the standard Gibbs free energies of formation of PbO and Cu_2O from Jacob and Jeffes[48] has been discussed previously. The Cu-Cu_2O reference electrode was specifically chosen to provide, if any, the minimum polarization overvoltage. The Cu and Cu_2O powders, although not of the highest purity (see Table 4.3), seem to provide a reasonably good reference. Since differences ranging from 0.2 to 3.0 mV between measured and theoretical emf were observed, which is within an acceptable error, it was concluded that in the laboratory the probe provides an accurate and reproducible measurement of oxygen dissolved in molten lead.

During some of the above tests in oxygen saturated molten lead, the probe was positioned at various vertical levels within the melt to assess the effect of any potential temperature gradient. The measured emf remained constant which indicated an absence of oxygen potential gradient within the molten lead, and consequently an absence of temperature and composition gradients.

Table 4.5 - Comparison of theoretical and measured emf for various probes immersed in oxygen saturated molten lead.

Probe #	Temperature (°C)	E_{th} (mV)	E_{meas} (mV)	$E_{meas} - E_{th}$ (mV)
1	697.5	124.0	124.4	0.4
2	698.7	123.8	127.0	0.2
3	678.6	126.6	127.0	0.4
4	679.9	126.5	128.0	1.5
5	682.0	126.2	127.6	1.2
6	680.4	126.4	128.0	1.6
7	697.0	124.0	127.0	3.0
8	663.0	128.8	130.0	1.2

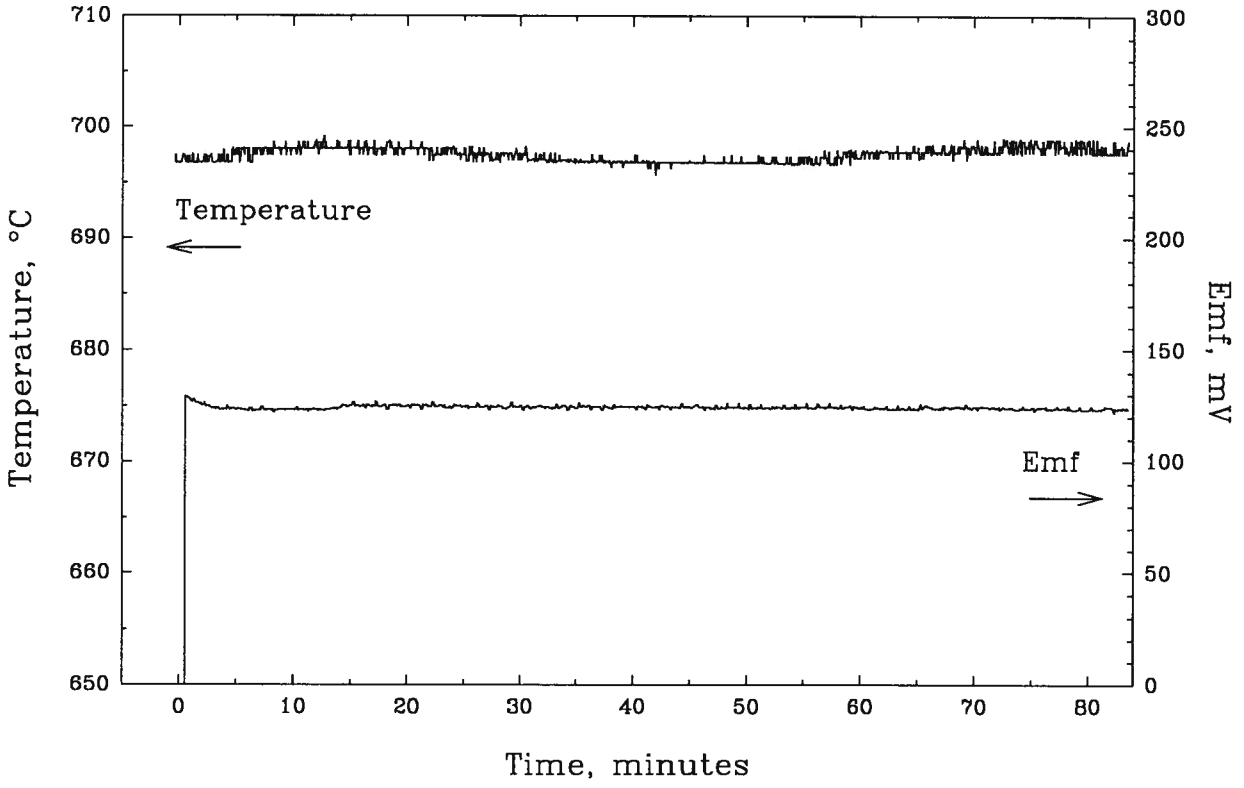

Figure 4.16 - Typical probe response upon immersion into an oxygen saturated lead melt at 697°C ± 1°C.

Once it was established that the probe gives a satisfactory response, it was necessary to ensure that the probe was reproducible. For this purpose, the probe was subject to a temperature change. Increasing the temperature from 683 °C to 730 °C in two steps, as shown in Figure 4.17, generated a decrease of emf from 128 mV to 122 mV. This emf decrease with a temperature increase is consistent with Equation (4.4). Once the temperature was set back to 683 °C, the emf increased back to 127.5 mV proving the reproducibility of the probe.

The life-span of a probe depends on the amount of copper powder used in the probe construction. Below a critical amount, the probe would last only a couple of hours after which the emf would start deviating. With copper powder in excess of the critical amount, the probes lasted for longer periods of time, up to several days. The amount of copper powder is measured as the length of the zirconia thimble that is filled with powder, and the critical amount corresponds to a length of about two centimetres.

The next step consisted in testing the probe response to changes of oxygen partial pressure. For this purpose, solid antimony was added to the melt, where it reacted with the dissolved oxygen to form $SbO_{1.5}$, and a new oxygen partial pressure was established. Figure 4.18 shows the changes in the probe emf in response to successive additions of solid antimony. The probe response was very rapid which was very encouraging since the objective is to use the probe to monitor the oxygen levels in a vessel running in a 30-minute cycle mode. It should be mentioned that the temperature fluctuations observed during the experiment were not large enough and not in the right direction to be responsible for the emf changes. The introduction in the chamber near the controlling thermocouple of a "cold" reagent addition tube for antimony addition created the drop in temperature to which the controller responded by a slight overshoot. As a result, an overall temperature increase

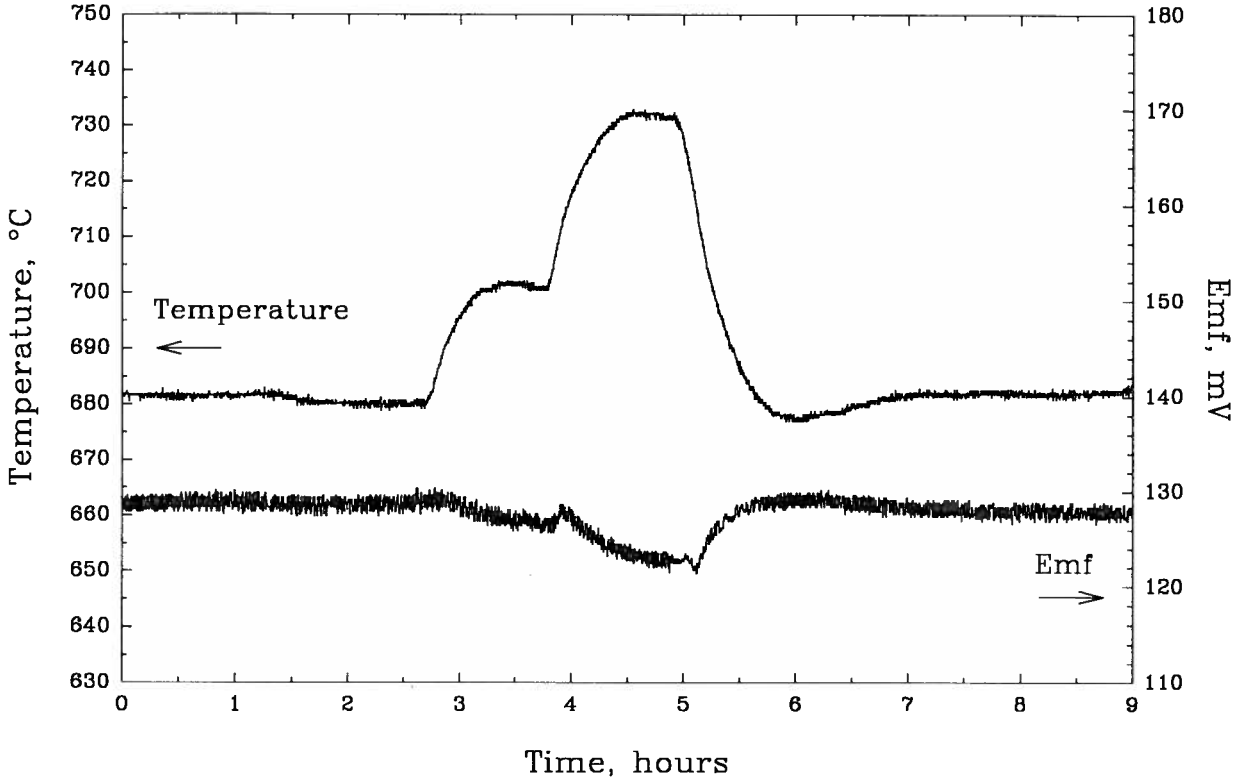

Figure 4.17 - Probe response to a temperature change. Initial temperature 683°C, intermediate temperature 730°C, and final temperature back to 683°C.

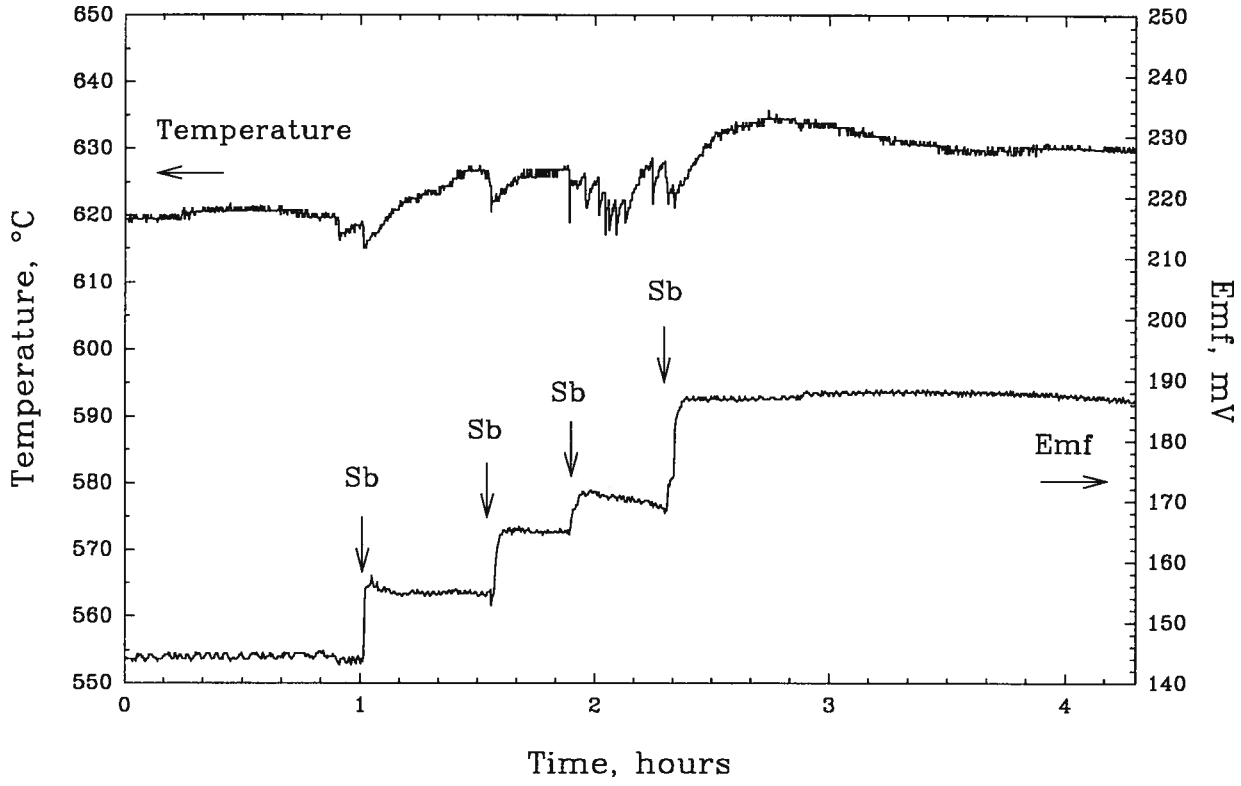

Figure 4.18 - Probe response to additions of antimony at temperatures around 625°C.

of about 10°C was measured between the start and end of the experiment. A number of tests with antimony additions were carried out and samples of molten lead taken. The measured emf and corresponding lead assays are summarized in Table 4.6.

Following the success of the probe in the laboratory, ten probes were built according to the design given in Figure 4.14 in order to carry out a plant testing campaign. The results of this campaign are discussed in the following Chapter.

Table 4.6 - Measured emf in laboratory tests and corresponding lead bullion assays.

Measured Emf (mV)	**Temperature (°C)**	**As + Sb (wt%)**	**Total Impurity (wt%)**	**$\frac{\text{As + Sb}}{\text{Total Impurity}}$**
147	615	0.22	0.22	1.00
143	620	0.24	0.24	1.00
170	621	0.35	0.35	1.00
151	620	0.26	0.26	1.00
182	615	0.61	0.64	0.95
168	615	0.37	0.61	0.61

CHAPTER 5

INDUSTRIAL TRIALS

In order to elucidate the chemistry of the softener unit, as well as to complete the research program on the oxygen probe, time was spent in the plant. For this purpose, visits to the smelter in Trail were planned with three major objectives in mind: investigation of softening process parameters, collection of specific data for process modelling, and testing of the oxygen probe in an industrial environment. Three visits of up to several weeks took place in March, June, and October 1994. Daily plant sampling at various locations in the circuit is routinely done and the subsequent X-ray assays constitute an important source of information to comprehend the overall chemistry of the softening circuit. Monthly tabulations of these plant assays were collected and constituted the original source of data for a mathematical model of the process. The details of the model together with the data analysis are presented in Chapter 6. A number of short visits, of one or two days, were also paid to the smelter throughout the duration of the project. These short visits maintained contact with Cominco personnel, provided information about the modifications made to the softening process, and provided an opportunity to present the progress made in the project. In this Chapter, the first section covers the investigation of the softening process, including the data collection, while the second section reports on the oxygen probe testing program in the softener unit. In the last section, a thermal arrest technique that provides an instantaneous measurement of the impurity level of a lead bullion is described.

5.1 Softening Process Investigations

Investigating the chemistry of a softening cycle consisted in assessing the composition of the bullion in the softener vessel at the beginning and end of the cycle, the composition and amount of slag generated during the cycle, and the amount of oxygen injected during the cycle. A number of preliminary samples were collected in advance to establish the best approach to the monitoring of a softening cycle. These tests, then, also provided the information required to find the most appropriate timing and method for taking the various samples.

5.1.1 Preliminary Sampling Campaign

As described in Chapter 1, during a pumping action, unsoftened lead bullion at 450°C is drawn from the north pot into the softener, while partially softened lead bullion at about 630°C overflows out of the softener back into the north pot. Simultaneously, slag is discharged onto a vibrating cooling launder and collects in a 5-ton pot. A close-up of the softening circuit is given in Figure 5.1 on which the various material flows in and out of the softener unit are indicated. Samples of input and output bullions could easily be obtained by scooping some bullion and quenching it in water. Slag samples were simply collected on the vibrating cooling launder. Since no difficulty arose in sampling the above material streams, their compositional evolution during a pumping action was thoroughly examined. For this purpose, input and output bullion samples, as well as slag samples, were taken every minute over the entire length of a pumping action which lasts from 5 to 10 minutes under normal operating conditions. In an effort to obtain meaningful data, the sampling was repeated several times and carried out only on days when the softener was running under normal operating conditions. The following observations were made.

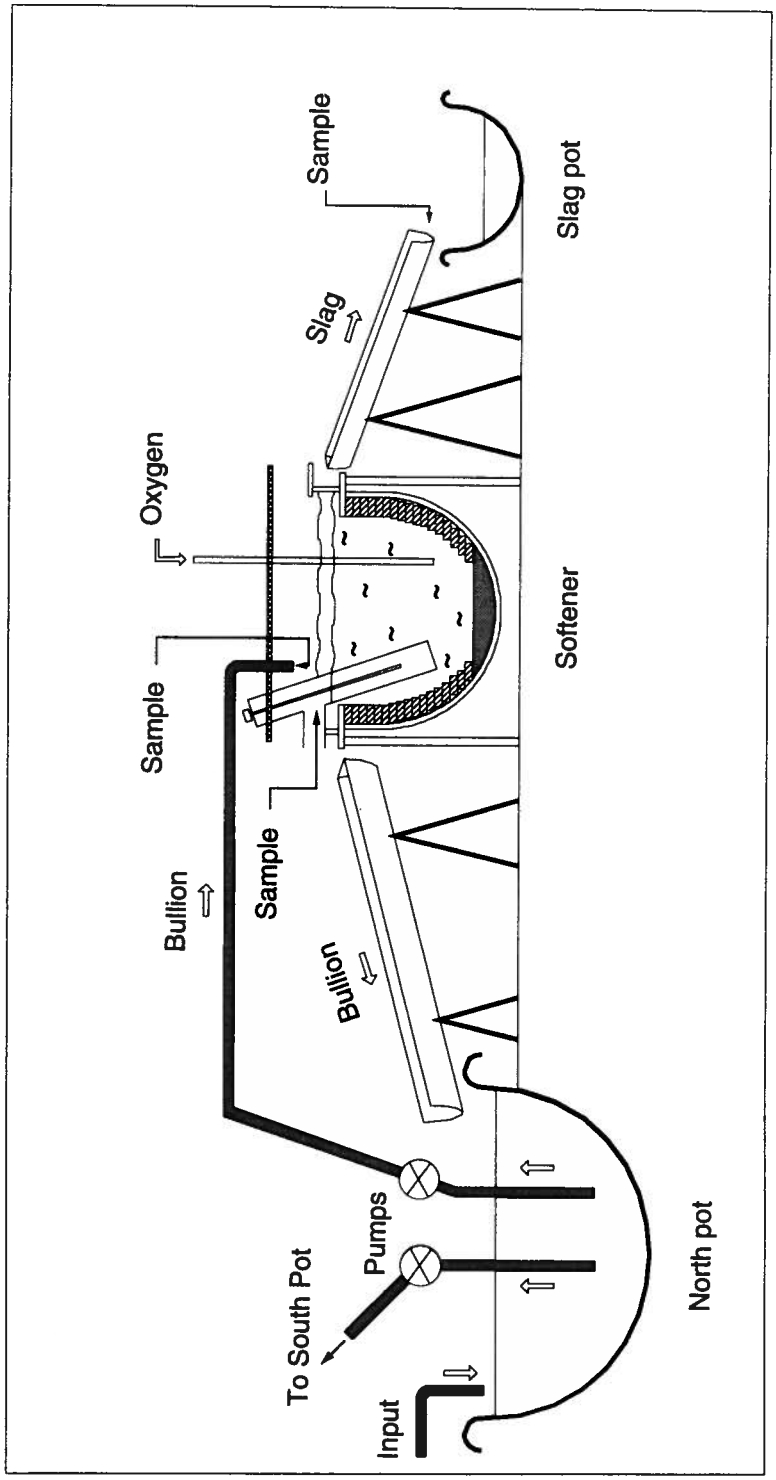

Figure 5.1 - Close-up of softener circuit.

- Characterization of input bullion

The As+Sb content of the input bullion from the north pot remains constant during the pumping action. This suggests that the north pot bullion is fairly homogeneous, or that any vertical composition gradient in the north pot does not affect the softener chemistry within the time frame of a cycle. One input bullion sample should suffice to provide the composition of the unsoftened bullion.

- Characterization of output bullion

The As+Sb content of the output bullion gradually increases by only about 0.1 wt% during a pumping action, typically from 0.7 wt% up to 0.8 wt%. This corresponds to the effect of mixing unsoftened bullion from the north pot into the softener vessel. From this observation, it was concluded that very strict timing should be followed when taking the bullion samples at the beginning and end of a pumping action. Any delay would result in meaningless data.

- Characterization of overflowing slag

The slag composition also remains constant during the period in which it is overflowing. A sample taken at any time during the slag overflow will provide the slag composition corresponding to the preceding cycle, assuming that the slag produced during a cycle has the same composition as the overflowing slag. This hypothesis can be considered valid only when the softener has reached a steady state regime, that is to say, the cycles have been regular for at least 3 to 4 hours.

The characteristics of the bullion and slag within the softener were also examined. In particular, the possibility that composition and temperature gradients develop within the vessel, both horizontally and vertically, has been explored. The dimensions of the softener vessel as of June

1994 are given in Figure 5.2 to provide for a scale of the required sampling equipment. The vessel has an inner diameter of 2.70 m for a depth of 1.80 m. The bath reaches a level of about 1.50 m, including a slag layer of 15 to 25 cm thick.

- Composition gradient in molten lead

Assessing the presence of a compositional gradient along the depth of the vessel required that five or six samples be taken simultaneous along the vertical axis of the furnace. This apparently simple concept proved to be a rather challenging sampling exercise. However, a sampling device was designed and fabricated with materials from the maintenance shop. It consisted of a 4 metre long steel pipe made of tubing material normally used to fabricate the oxygen lances. A series of iron sample tubes, about 10 cm long, were clamped on the pipe at various levels. The opening of each sampling tube was closed off with several layers of masking tape. Tests were performed to determine the number of layers required to provide a 30 seconds delay before lead bullion would collect in the tubes. Such a delay was indispensable to permit the positioning of the device inside the vessel. Measurements were laboriously performed, the weight and length of the device involved combined with its high temperature making it difficult to handle, especially in times of high fume emissions. Two measurements were carried out on separate days. The assays of the first measurement did not reveal the existence of any composition gradient within the depth of the lead bath (see Table 5.1). A relative antimony depletion 75 cm below the slag surface, or 25 cm above the oxygen lances tip, and a copper and arsenic enrichment at about the same level were the only noticeable facts. This surprising discovery was confirmed by the second measurement. Even though the assays were not as consistent as in the case of the first measurement, no pronounced gradient was, however, detected (see Table 5.2). Two additional series of samples collected in the top 50 cm of the lead bullion again confirmed the absence of a gradient (see Table 5.3).

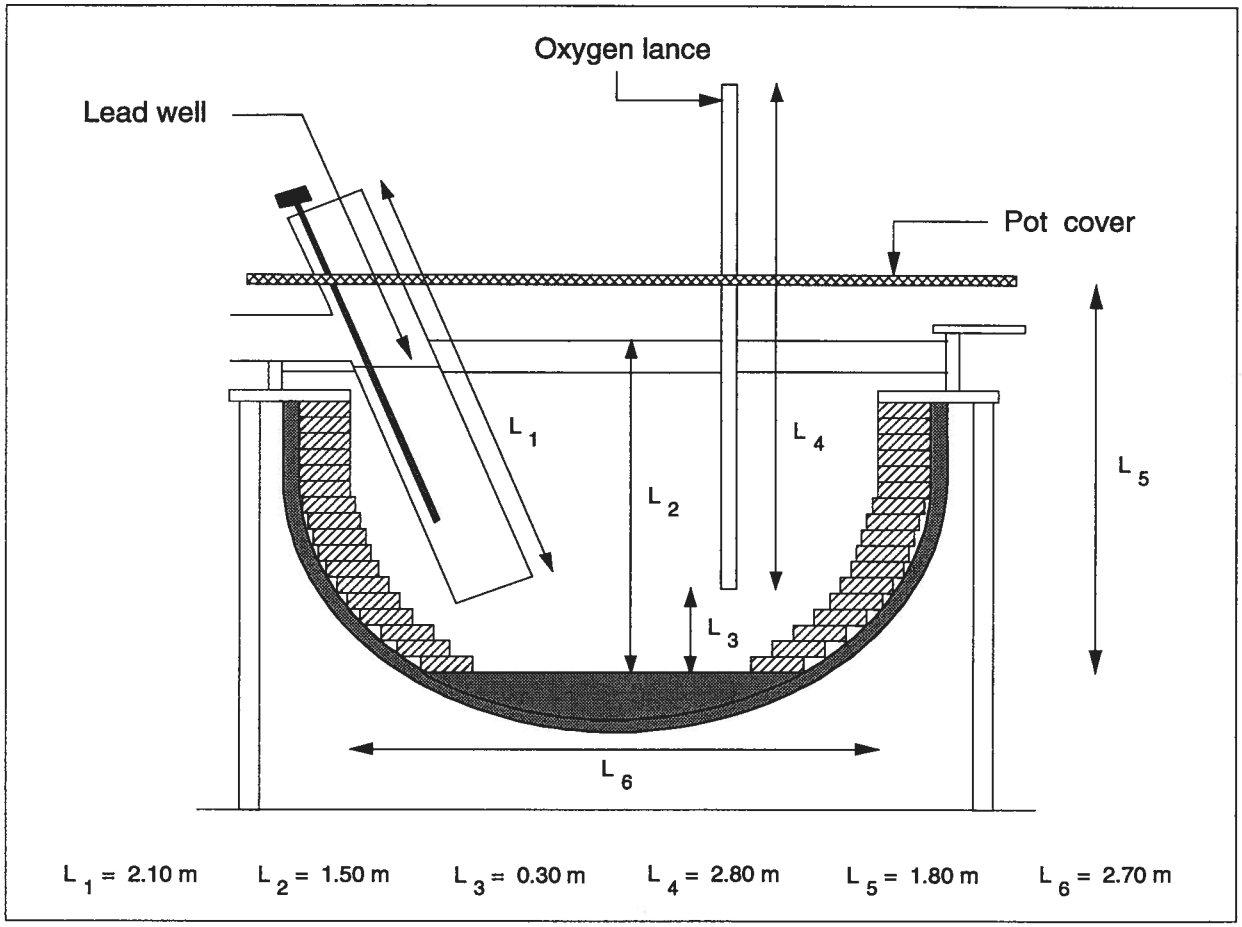

Figure 5.2 - Dimensions of the softener unit as of June 1994.

- Composition gradient in molten slag

Slag samples were taken simultaneously or within 10 second intervals near the slag surface and close to the slag-bullion interface at various locations in the vessel. Extreme care was put into taking the samples, and it is assumed that no local mixing took place during the sampling. The assays did not reveal any composition difference, indicating that the slag was homogeneous in composition over the entire vessel. Assays of slag samples taken at opposite sides of the vessel are given in Table 5.4.

Table 5.1 - Assays of softener bullion for vertical gradient assessment (measurement #1).

Distance below slag surface (cm)	**Sb (wt%)**	**As (wt%)**	**Bi (wt%)**	**Cu (wt%)**
15	0.79	0.09	0.23	0.04
25	0.80	0.10	0.23	0.05
50	0.81	0.23	0.20	0.27
75	0.63	0.10	0.21	0.13
100	0.79	0.08	0.23	0.05
125	0.80	0.08	0.23	0.05
Softener output bullion	0.73	0.08	0.23	0.06
Slag sample	7.2	22.4	-	-

Table 5.2 - Assays of softener bullion for vertical gradient assessment (measurement #2).

Distance below slag surface (cm)	Sb (wt%)	As (wt%)	Bi (wt%)	Cu (wt%)
25	0.90	0.27	0.44	0.07
50	0.90	0.10	0.49	0.06
75	0.85	0.20	0.45	0.44
100	0.91	0.17	0.47	0.36
125	0.99	0.25	0.48	0.52
135	0.92	0.10	0.47	0.06
Softener output bullion	0.92	0.11	0.48	0.08
Slag sample	7.8	22.6	-	-

Table 5.3 - Assays of softener bullion for vertical gradient assessment (measurements #3 and #4).

Distance below slag surface (cm)	Sb (wt%)	As (wt%)	Bi (wt%)	Cu (wt%)
25	0.73	0.09	0.21	0.10
35	0.73	0.09	0.20	0.09
45	0.76	0.09	0.18	0.09
25	0.72	0.10	0.20	0.09
35	0.70	0.08	0.19	0.08
45	0.70	0.09	0.20	0.08

Table 5.4 - Assays of softener slag from opposite sides of the vessel for vertical gradient assessment (measurements #5 and #6).

Distance below slag surface (cm)	Sb (wt%)	As (wt%)	Pb (wt%)
0	19.9	9.3	59
10	20.1	9.3	59
15	20.1	9.2	59
0	20.0	9.3	59
15	19.8	9.0	58

- Temperature gradient in the bath (slag and bullion)

Similar to the composition gradient measurement, assessing the presence of a temperature gradient within the depth of the vessel required the fabrication of a special device to measure the temperature at six different levels simultaneously. A "temperature probe" was made by Cominco's workshop and consisted of six K-type thermocouples inserted in and making contact with a steel pipe closed at one end. Numerous problems were encountered when attempting to use the device in the softener bath. After several trials, a recording was performed over more than 2 hours with only one thermocouple functioning improperly. The remaining five thermocouples recorded temperatures within 5 to 10°C of each other, indicating that no pronounced thermal gradient was established in the bath. When other measurements were carried out on following days, none of the thermocouples seemed to function properly any longer. It has been suggested that the thermocouples were no longer in contact with the pipe giving a meaningless measurement.

- Monitoring of slag-bullion interface temperature

A thermocouple similar to the type used to control the softener, was immersed in the bath to measure the slag-bullion interface temperature during a cycle. The measurements showed that the interface temperature was very close to the controlling temperature, which is measured deeper in the vessel, confirming that no temperature gradient is established during normal operation, at least in the top half of the bath.

No precise data on the amount of oxygen injected in the lead bath was available at the time of the short visits, and only an estimate of the "average normal injection rate" was obtained. Determining the amount of oxygen injected in the lead bath constituted one of the key measurements to be performed during the extended trials. Two alternatives were possible: the use of rotameters that normally equip each lance, or a vortex meter installed on the main oxygen line. The first alternative was hindered by the fact that some lances had defective rotameters and long delays were expected before they could be replaced. The second alternative benefited from the availability of vortex meters on site. The advantage of a vortex meter is that it provides a total oxygen injection rate instantaneously. Its dependence on the gas pressure in the main delivery pipe is, however, a major drawback. Any deviation of the gas pressure from the calibration pressure results in an erroneous oxygen measurement.

5.1.2 Softening Chemistry and Oxygen Efficiency

Whether the injected oxygen equilibrates with the bath or kinetic processes control the softening rate is a critical question to answer in understanding softener chemistry. Important

information on this issue can be obtained by assessing the efficiency with which oxygen is utilized in the process. First, a sampling procedure for investigating the softening process chemistry was devised from the information provided by all preliminary tests. The procedure, which corresponds to a succession of steps carried out during each pumping action for the entire length of the test, is given below in chronological order.

- first sample of output bullion taken 1 minute after the pump is turned on (provides the final composition of the previous cycle)
- sample of input bullion
- sample of slag
- second sample of output bullion taken 1 minute after the pump is turned off (provides the initial composition of the following cycle)

The total oxygen injection rate and the slag-bullion interface temperature were continuously measured for the entire duration of the test by a vortex meter and a thermocouple respectively.

A first test was carried out in June 1994 using this sampling procedure for a duration of six cycles at a time when the softener had been operating at three cycles per hour for more than four consecutive hours. In such circumstances, the slag collected on the launder could be considered representative of the slag generated during a cycle. Unfortunately fume generation was unusually high during this period. The oxygen injection rate was measured by a vortex meter at an average of 73.0 Nm^3/hour. The slag-bullion interface temperature was monitored and evolved in a cyclic mode between 602°C and 626°C. The slag pot was weighed by means of a crane scale prior to and after the sampling test. The slag produced during the test amounted to a total of 1451 kg, corre-

sponding to an average of about 242 kg per cycle. Expressed in terms of oxides, the average slag composition was the following: 29.1 wt% $SbO_{1.5}$, 9.1 wt% $AsO_{1.5}$, 61.2 wt% PbO and 0.5 wt% SnO_2, with $SbO_{1.5}$, $AsO_{1.5}$, PbO and SnO_2 totaling 99.9 % of the slag weight. The oxygen efficiency, calculated as the amount of oxygen utilized in slag formation divided by the total amount of oxygen injected, was found to be about 80%. Fuming, unusually high, should be accounted for in order to provide a proper calculation of the oxygen consumption. Unfortunately, the amount and composition could not be assessed. The process parameters and average assays of slag and bullion samples are given in Table 5.5. The complete assays for all six cycles are given in Appendix 2.

Using a crane scale and weighing the large slag pot was not, in retrospect, the most appropriate method to accurately determine the amount of slag produced during the test. Any large inaccuracy in the slag weight measurement could lead to a substantial uncertainty in the oxygen efficiency calculation. Moreover, it is difficult to determine the effect of fuming on the calculation of oxygen efficiency. A second test, three days later, was unfortunately aborted after sampling three cycles due to operating trouble in the circuit.

A new test was not performed until October 1994 when certain improvements were made in the sampling procedure. All lances were, by then, equipped with brand new rotameters, providing a better measurement of the oxygen injection rate than the vortex meter alone. Due to the variations from day to day in the oxygen pressure in the main delivery line the vortex meter was reliable only on days when the delivery pressure was identical to the calibration pressure. The slag was collected in barrels during the test rather than into the usual 5-ton pot. In this manner, the barrels could be handled without the need for a plant operator to maneuver the crane, and also be weighed with a calibrated plate scale. This method is believed to provide better accuracy in measuring the amount

of slag produced. A total of three tests were attempted, only the third one was carried to completion without any problems. A steady state regime had prevailed for more than 5 hours. The test was limited to three cycles rather than six, to minimize the chances of interruption, and lasted 54 minutes. The oxygen injection rate was set at 74.8 Nm^3/hour. The temperature recorded by the controlling thermocouple varied between 592°C and 614°C, which is about 10 degrees lower than in the test performed in June. A total of 784 kg of slag, corresponding to an average of 261 kg per cycle, was collected with the following average composition: 22.5 wt% $SbO_{1.5}$, 11.2 wt% $AsO_{1.5}$, 64.6 wt% PbO, and 0.9 wt% SnO_2, the sum of $SbO_{1.5}$, $AsO_{1.5}$, PbO and SnO_2 totaling 99.2% of the slag weight. The oxygen efficiency was calculated to be about 92%. Fuming, which did not appear to be any higher than "normal", was not accounted for in the calculation. The process parameters and average assays of slag and bullion samples are summarized in Table 5.6. Complete assays for all three cycles are given in Appendix 2.

5.1.3 Conclusions

The main purpose of the preliminary sampling campaign was to characterize the various softener streams and develop a procedure to investigate the process. The major outcome can be summarized as follows:

- No composition gradient (both vertical and horizontal) has been observed in the slag.
- No composition gradient has been observed within the depth of the bullion.
- No vertical temperature gradient has been observed in the bullion (up to the slag-bullion interface) under normal operating conditions.

Another important result from this preliminary campaign was to define so called "normal operating conditions" as follows: 3 to 4 cycles per hour, regular temperature cycle within the control range,

bullion composition within the desired target range, minimum lance consumption, and minimum fuming. When the process is running under the normal operating conditions as described above, very few bubbles break the surface, suggesting a high oxygen efficiency is achieved. The major result from the softener investigations is the confirmation that the oxygen efficiency is high, in the order of 90%. It can then be assumed that under these operating conditions, kinetic constraints have only a limited influence on the process. To summarize the major findings of the investigations, the softening process chemistry is characterized by the following parameters:

- initial bullion composition: 0.75 to 0.85 wt% As+Sb
- final bullion composition: 0.65 to 0.75 wt% As+Sb
- slag composition: 35 to 40 wt% $AsO_{1.5}$+$SbO_{1.5}$
- slag production: about 250 kg/cycle
- slag layer thickness: 20 to 25 cm
- oxygen injection rate: 68 to 76 Nm^3/h
- oxygen efficiency: about 90% (fume formation not included)
- temperature cycle: within the range 600 to 630°C

To maintain the steady state regime as described above, good maintenance is essential. However, good maintenance does not provide control over input bullion composition, and dramatic alterations in the process regime are mainly due to composition changes. Such changes need to be detected in order to adjust the process parameters accordingly. Continuous monitoring of the bullion impurity content is a potential solution that would give a warning of any deviation from "normal operating conditions". The following section reports on industrial tests with oxygen probes to determine whether composition control could be achieved by monitoring the oxygen potential of softener bullion.

Table 5.5 - Process parameters and assays of softener slag and bullion for softener chemistry assessment (test #1, June 1994).

Process Parameters	**Values**
Number of cycles sampled	6
Total sampling time	120 min
Oxygen injection rate	73 Nm^3/h
Temperature cycle	602°C - 626°C
Total slag weight	1451 kg
Average slag amount per cycle	242 kg
Average initial bullion composition	0.76 wt% Sb 0.07 wt% As 0.31 wt% Bi 0.11 wt% Cu 0.01 wt% Sn
Average final bullion composition	0.69 wt% Sb 0.06 wt% As 0.31 wt% Bi 0.11 wt% Cu 0.01 wt% Sn
Average slag composition	29.1 wt% $SbO_{1.5}$ 9.1 wt% $AsO_{1.5}$ 61.2 wt% PbO 0.5 wt% SnO_2
Oxygen utilization	80% (calculated)

Table 5.6 - Process parameters and assays of softener slag and bullion for softener chemistry assessment (test #2, October 1994).

Process Parameters	**Values**
Number of cycles sampled	3
Total sampling time	54 min
Oxygen injection rate	74.8 Nm^3/h
Temperature cycle	592°C - 614°C
Total slag weight	784 kg
Average slag amount per cycle	261 kg
Average initial bullion composition	0.67 wt% Sb 0.09 wt% As 0.25 wt% Bi 0.07 wt% Cu 0.01 wt% Sn
Average final bullion composition	0.61 wt% Sb 0.08 wt% As 0.26 wt% Bi 0.08 wt% Cu 0.01 wt% Sn
Average slag composition	22.5 wt% $SbO_{1.5}$ 11.2 wt% $AsO_{1.5}$ 64.6 wt% PbO 0.9 wt% SnO_2
Oxygen utilization	92% (calculated)

5.2 Oxygen Probe Plant Tests

A number of oxygen probes were tested in the plant during the October 1994 visit to the smelter in Trail. At that time, a number of operating problems occurred and perturbed the normal operation of the softener in such a way that the combined arsenic and antimony level in the vessel varied from as low as 0.4 wt% to as high as 1.9 wt%. These peculiar operating conditions had mixed repercussions on the oxygen probe testing program. On one hand, this situation was beneficial since it permitted investigating the probe response to a wide range of lead bullion compositions. On the other hand, at times of low antimony and arsenic concentrations, oxidation by contact with the atmosphere was very fast, and large amounts of oxide sludge were generated on the surface of the bullion inside the lead well (bullion outlet as shown in Figure 5.2). Obtaining proper measurements was difficult because of sludge adhesion onto the probe within an hour after immersion. This section covers the various aspects of the oxygen probe testing program, describing the difficulties encountered and the solutions used to overcome them. The results are discussed and a calibration curve of the measured emf as a function of the combined As+Sb content is given. To conclude, some recommendations for improving the probe design to better suit the industrial environment are discussed.

5.2.1 Oxygen Potential Measurements

The oxygen potential measurements were done in the lead well at the lead bullion outlet. Simultaneous temperature measurements were performed with a K-type thermocouple inserted into a closed end alumina tube. The oxygen probe was connected to a **Corning 125** millivolt and pH meter similar to the instrument used in the laboratory. Both emf and temperature were recorded with a chart recorder with a digital panel for quick reading.

Breakage of the zirconia tube upon immersion and molten lead infiltration through the probe thread were the two major problems encountered in the early stages of the testing campaign. The temperature difference between the atmosphere just above the bath surface and the lead bullion was measured to be about 300°C, a differential twice as large as the maximum tolerable by zirconia. Slowly lowering the probe close to the bath surface and leaving it there for a few minutes to allow thermal equilibration would therefore not be sufficient to avoid breakage upon immersion due to thermal shock. To remedy this problem, a piece of steel tube about 10 cm long was attached to the tip of the probe holding tubing. The role of this "extension tube" was to make contact with the lead bullion before the probe itself so that the temperature of the probe tip would slowly increase by heat conduction. This worked on all but two occasions. Ineffective conduction due to poor metal contact is the most likely reason for the failures rather than the possible presence of defects in the zirconia tubes. Once a probe had survived immersion, the possibility of a zero millivolt reading was the next problem. Such a reading is typically due to molten lead infiltration through the probe thread and short-circuiting of the lead wire and conducting lead. The only way to avoid this problem was to make sure that the probe tip was not immersed too deep into the lead bullion thus avoiding high pressures in the liquid lead.

Another factor that determined the length of time that a probe would last in the bullion was the problem of a "sludge" coating. As mentioned earlier, at times of low antimony and arsenic content, an oxidic sludge formed on the surface of the lead bullion and gathered around any instrument present in the lead well. This sludge, accumulating with time and slowly creeping down to the probe tip, ended up covering the probe completely. As a result, a constant emf reading was obtained which corresponded to the oxygen potential of the sludge layer directly in contact with the zirconia. This phenomenon could take place within an hour after immersion thus considerably

limiting the duration of a meaningful test. Even though the probe was still functioning and could be removed, cleaned, and reused, it did not fulfill its role of a continuous measuring device. It is worth mentioning that such operating conditions are not normal but merely the results of operating troubles that might easily be avoided if a probe was used to control the system.

5.2.2 Results and Discussion

The emf measurements successfully obtained with five different probes on various days during the trials and for which a bullion assay is available are given in Table 5.7. The corresponding lead bullion temperatures and assays are also given in the same Table. The range of measured emf, between 178 mV and 312 mV, corresponded to a total impurity content ranging from 0.97 wt% to 2.41 wt%. As seen in Table 5.7, the measurements were not carried out at constant temperature, but actually within the range 600°C to 623°C. These relatively small temperature differences do not have a large influence on the measured emf. In the laboratory experiments with oxygen saturated lead bullion, a temperature change of 10°C corresponded to an emf change of 1.4 mV. A typical recording of emf and temperature is given in Figure 5.3. The probe response was qualitatively consistent with the Nernst equation: an increase of temperature and/or a decrease in impurity content generated an emf decrease. However, a quantitative analysis of the probe response would require the measurement of both temperature and bullion composition changes as well as an understanding of the fluid flow and mixing in the vessel. The velocity of the output bullion stream, which varied from very high at the start of a softening cycle to almost nil at the end, appeared to have a temporary effect on the emf readings as marked by the discontinuity of the emf trace on Figure 5.3. The measured emf given in Table 5.7 correspond to the stable emf obtained at low bullion velocity towards the end of a cycle and read on Figure 5.3 just prior to the discontinuities.

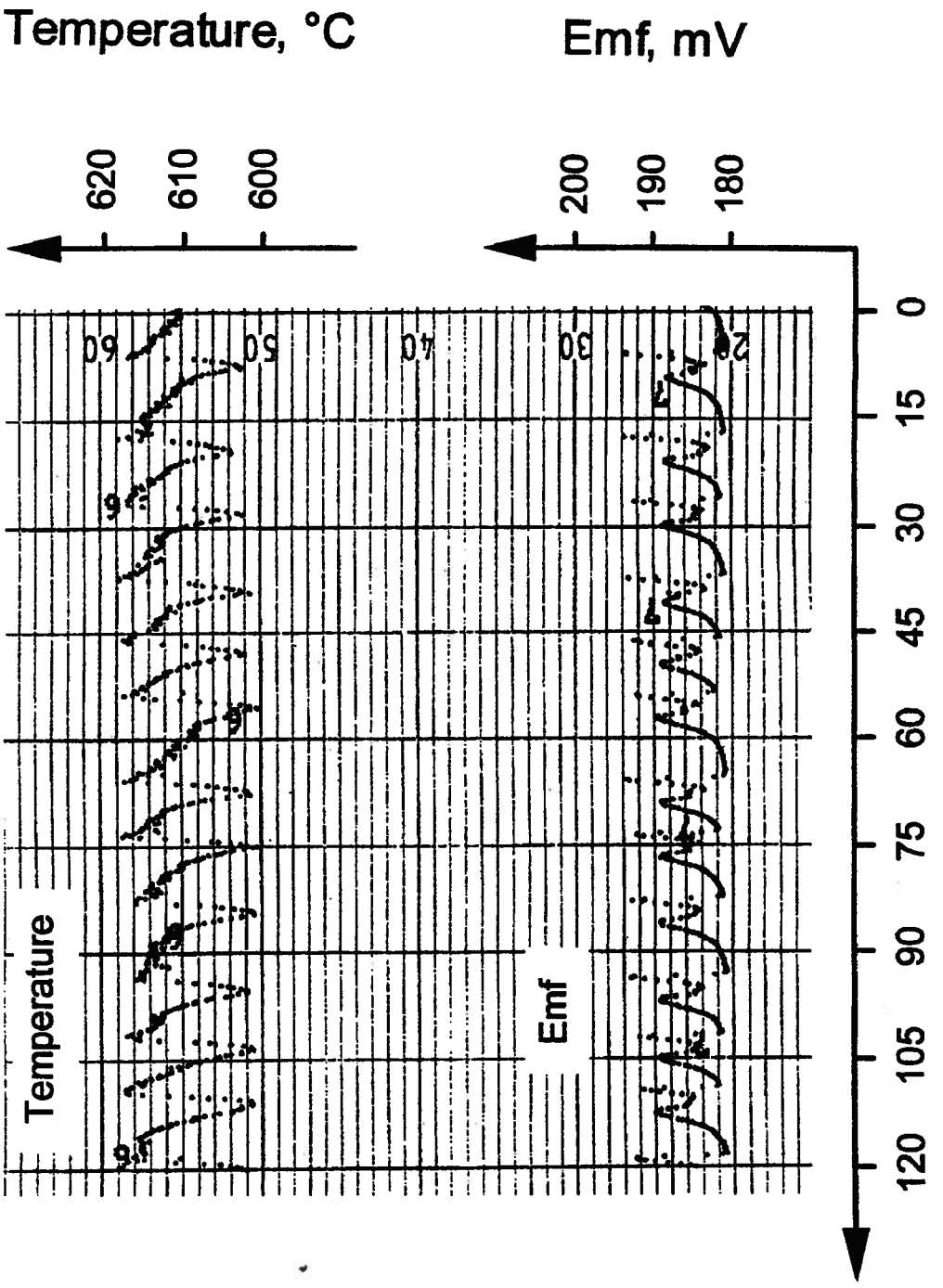

Figure 5.3 - Typical recording of emf and temperature measured in the softener vessel.

The emf data from both plant and laboratory tests (see Tables 5.7 and 4.6 respectively) were plotted versus the total impurity content. As can be seen in Figure 5.4, these data show noticeable scatter. On the other hand, when the measured emf was plotted versus the combined As+Sb, a better correlation was obtained as shown in Figure 5.5. This demonstrates that the impurities other than arsenic and antimony, i.e. bismuth, tin, silver, and copper, do not participate in the oxygen equilibria. Thus, the emf reading is almost solely dependent on the As+Sb content of the bullion. The correlation between measured emf and As+Sb content was determined by a least-square regression analysis as follows

$$(mV)_{meas} = 133.5 + 95.65\,(wt\%)_{As+Sb} \qquad (5.1)$$

where $(mV)_{meas}$ is the measured emf in mV, and $(wt\%)_{As+Sb}$ is the combined As+Sb content in wt% obtained from the bullion samples assays. The intercept of the above equation gives an emf value for the "zero impurity content" of 133.5 mV. This value compares well with the theoretical value of 135.9 mV calculated with Equation (4.4) at 613°C, the average measured temperature from Table 5.7. The good correlation between measured emf and As+Sb content given by Equation (5.1) can be rearranged as follows

$$(wt\%)_{As+Sb} = -1.396 + 10.45 \times 10^{-3}\,(mV)_{meas} \qquad \pm 0.05\,(wt\%) \qquad (5.2)$$

This relationship provides the necessary calibration curve that will permit the use of the probe in the plant.

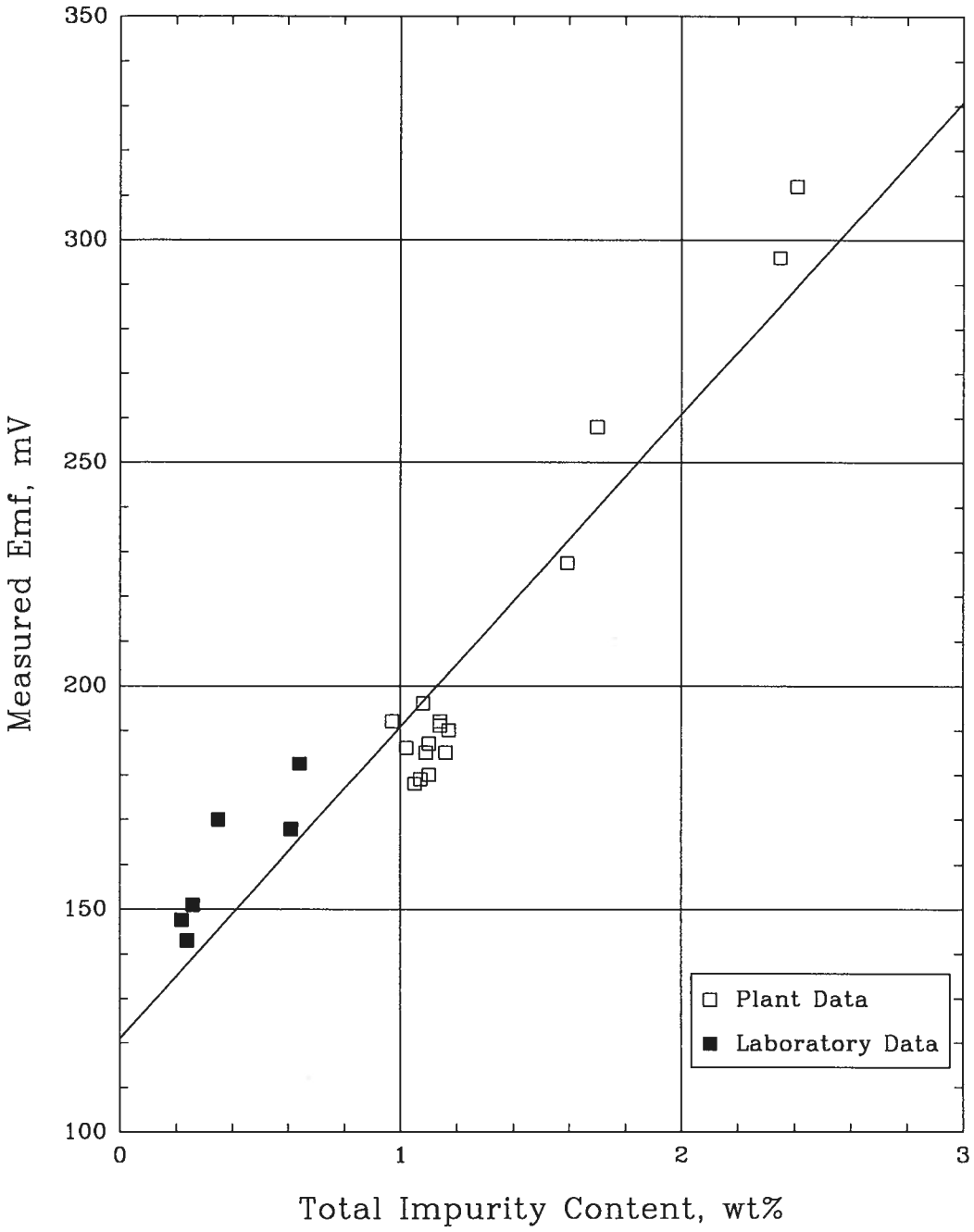

Figure 5.4 - Plot of plant and laboratory emf measurements versus total impurity content of lead bullion. The solid line corresponds to a least-square analysis.

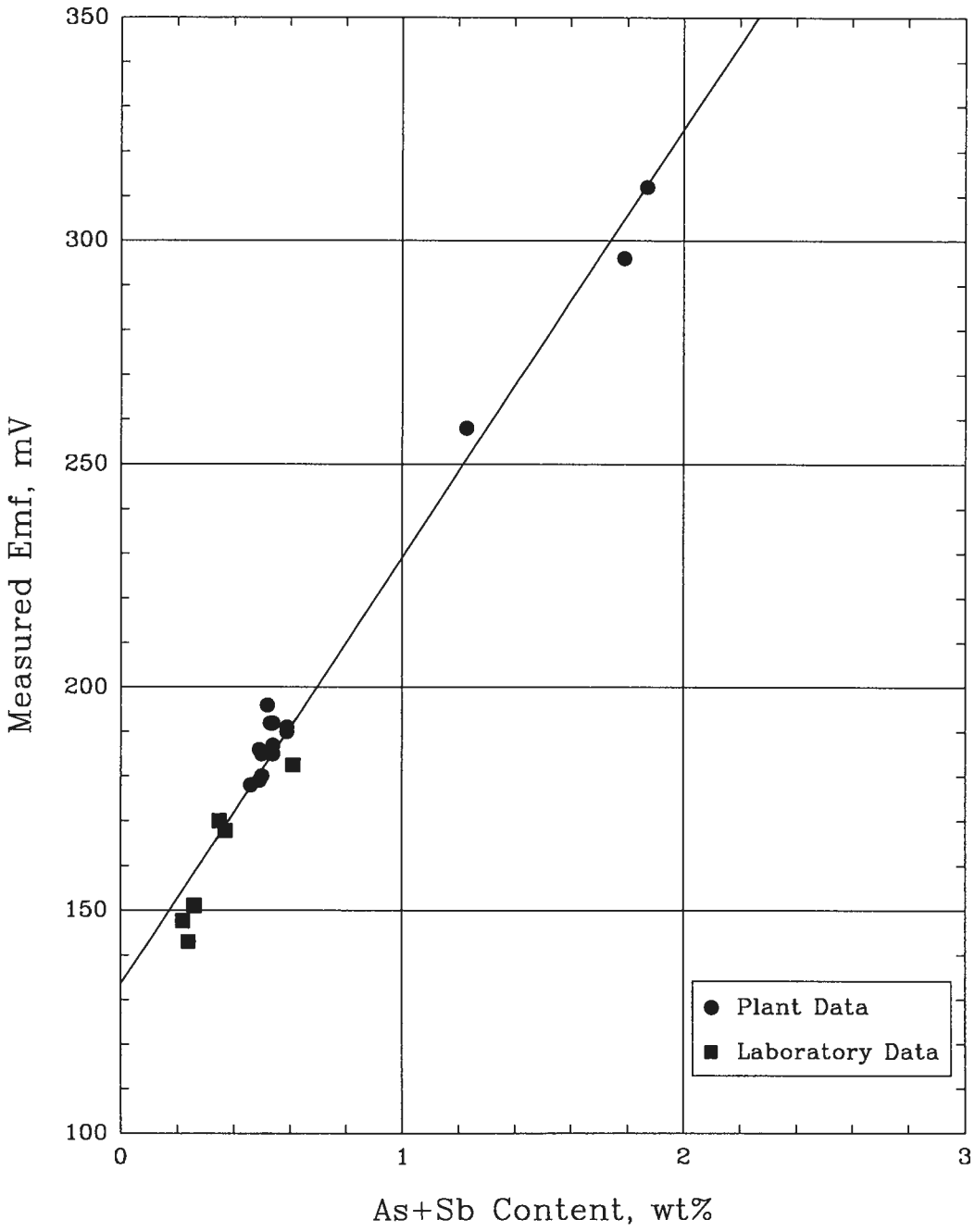

Figure 5.5 - Plot of plant and laboratory emf measurements versus As+Sb content of lead bullion. The solid line corresponds to a least-square analysis.

Table 5.7 - Measured emf in softener vessel and corresponding lead bullion assays.

Measured emf (mV)	Temperature (°C)	As + Sb (wt%)	Total impurity (wt%)	$\frac{\text{As + Sb}}{\text{Total impurity}}$
196	623	0.52	1.08	0.48
186	620	0.49	1.02	0.48
187	617	0.54	1.10	0.49
190	620	0.59	1.17	0.50
191	617	0.59	1.14	0.52
185	600	0.50	1.09	0.46
178	614	0.46	1.05	0.44
179	614	0.49	1.07	0.46
180	614	0.50	1.10	0.45
185	612	0.54	1.16	0.46
192	612	0.54	1.14	0.47
192	600	0.53	0.97	0.55
296	618	1.79	2.35	0.76
312	608	1.87	2.41	0.78
258	610	1.23	1.70	0.72

5.2.3 Conclusions

The oxygen probe, which was designed and tested in laboratory, was successfully used in an industrial environment. One of the key achievements of the program was determining a correlation between measured emf and combined As+Sb content of the softener bullion. Out of ten probes built for the industrial tests, five provided satisfactory measurements for various length of time depending on the conditions prevailing in the vessel. Two probes continuously monitored the oxygen potential of the bullion for more than a day, thus proving the potential of the design. In most cases, the reason for interrupting a test was the fact that the tip of the probe was coated with an oxidic sludge. However, a probe with such a coating could possibly be removed from the melt, cooled down, cleaned, and reused immediately or later. The fact that a number of probes failed upon immersion or shortly after suggest that some improvements in the "laboratory design" of the probe should be implemented in order to upgrade the probe to an "industrial design". In particular, failure due to thermal shock is the most critical issue. Completely eliminating the problem is not realistic since zirconia tubes can have defects that become points of weakness upon heating. However, the failures can be reduced by ensuring that the probe is preheated to a temperature close to that prevailing in the bath. This could be achieved by integrating the "extension tube" concept used in the plant into the probe design. An alternative would be to slowly preheat the probe to the desired temperature by means of a small furnace prior to immersion. Slag and sludge protection is another critical issue to be dealt with. The probe tip could be enclosed in a protective steel cup that would stop the sludge from creeping down along the probe holding tube and prevent it from coating the zirconia (see Figure 5.6). As for the lead infiltration problem, the attachment between the probe tip and the probe holder could be modified in such a way that the thread would not be below the liquid surface, therefore eliminating the risk of infiltrations.

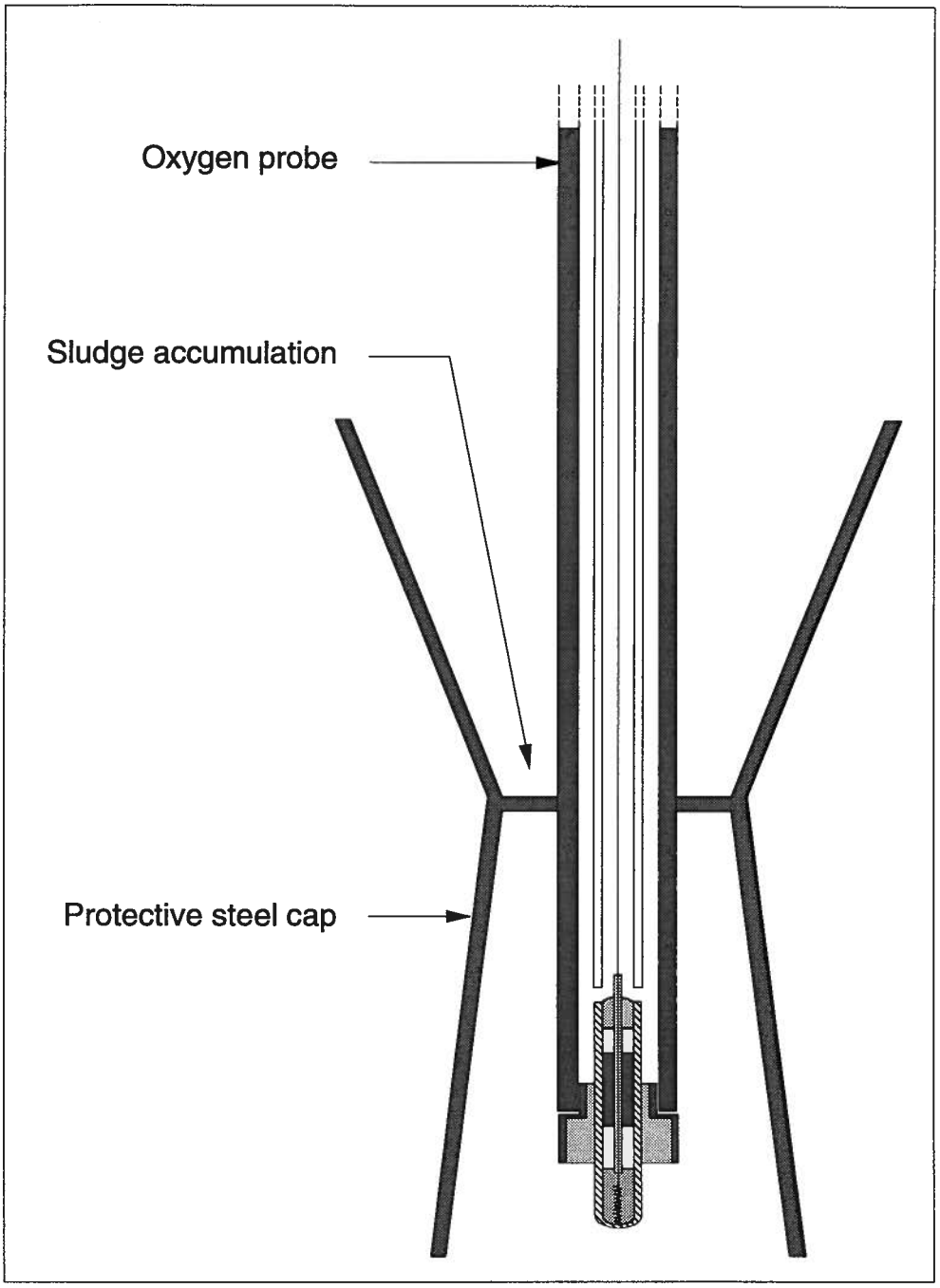

Figure 5.6 - Schematic representation of a probe tip with a steel cup for sludge protection.

5.3 Thermal Arrest Technique

One of the major concerns about the use of an oxygen probe to continuously monitor the bullion composition is the possibility of erroneous emf readings. In a situation where the probe has failed, unless its reading is suddenly strongly off-range, the malfunction would not be detected until routine assay results were available, which can take several hours. A quicker assessment of the state of the probe would be extremely valuable. The thermal arrest technique provides such an instantaneous check. The **Quick-Cup** system from **Heraeus Electro-Nite** was chosen, tested and calibrated for that purpose. A schematic description of the apparatus is given in Figure 5.7. The principle of the technique is based on the fact that the liquidus temperature of a metallic alloy is composition dependent, the higher the alloying element(s) content, the lower the liquidus temperature. Thus, the plotting of the temperature versus the time of cooling yields a time-temperature cooling curve. Quenched bullion samples of various composition from the plant were remelted in the laboratory and their cooling curves recorded. The change of slope in the curve indicates the liquidus temperature of the sample. For pure lead, a well defined plateau is obtained, as shown in Figure 5.8. For samples containing more than 1 wt% impurity, the change of slope in the curve is usually abrupt without a well defined plateau, as shown in Figure 5.9. A plot of liquidus temperature versus total impurity content is given in Figure 5.10. A regression analysis yielded the following relationship

$$(°C)_{\text{Liquidus}} = 324.4 - 8.2\,(wt\%)_{\text{Total impurity}} \qquad (5.3)$$

where $(°C)_{\text{Liquidus}}$ is the liquidus temperature in Celsius, and $(wt\%)_{\text{Total impurity}}$ is the total impurity content of the bullion. The obtained value of 324.4°C instead of 327.2°C for the melting point of pure lead shows that the technique still requires some fine tuning.

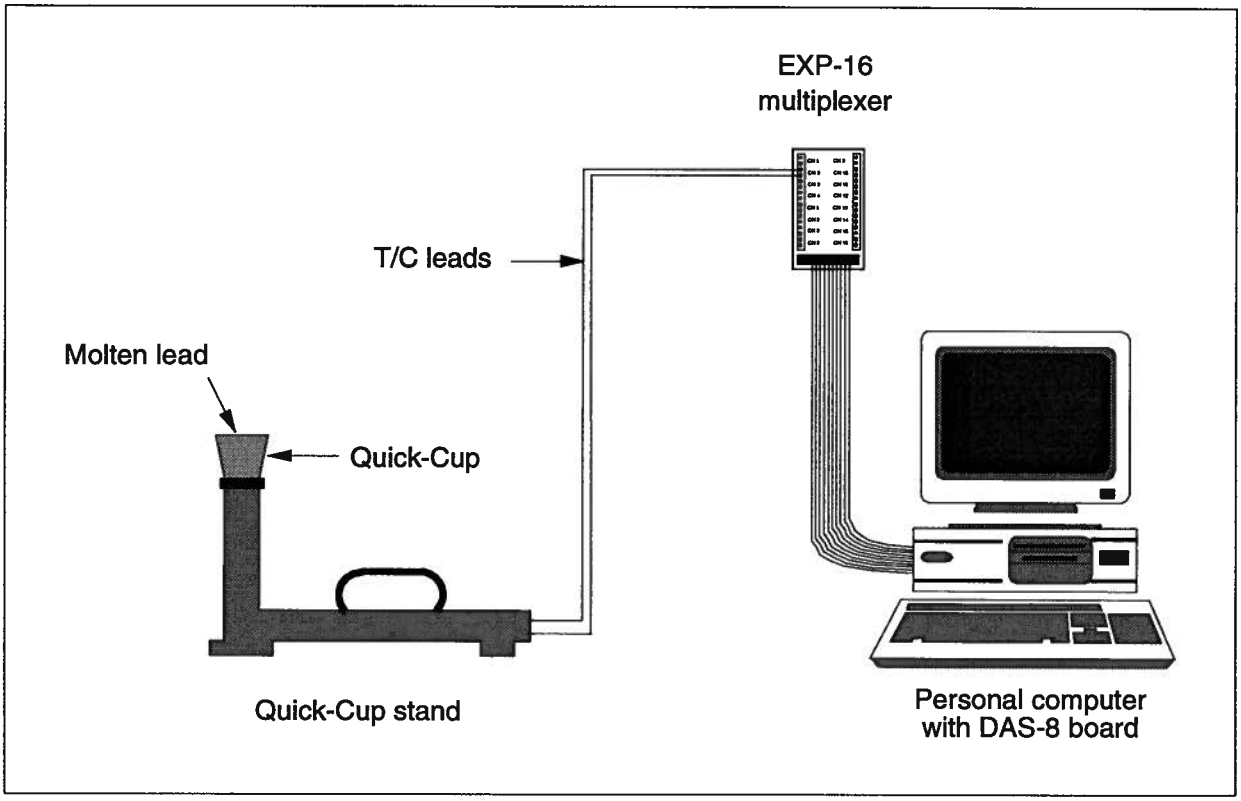

Figure 5.7 - Thermal arrest apparatus.

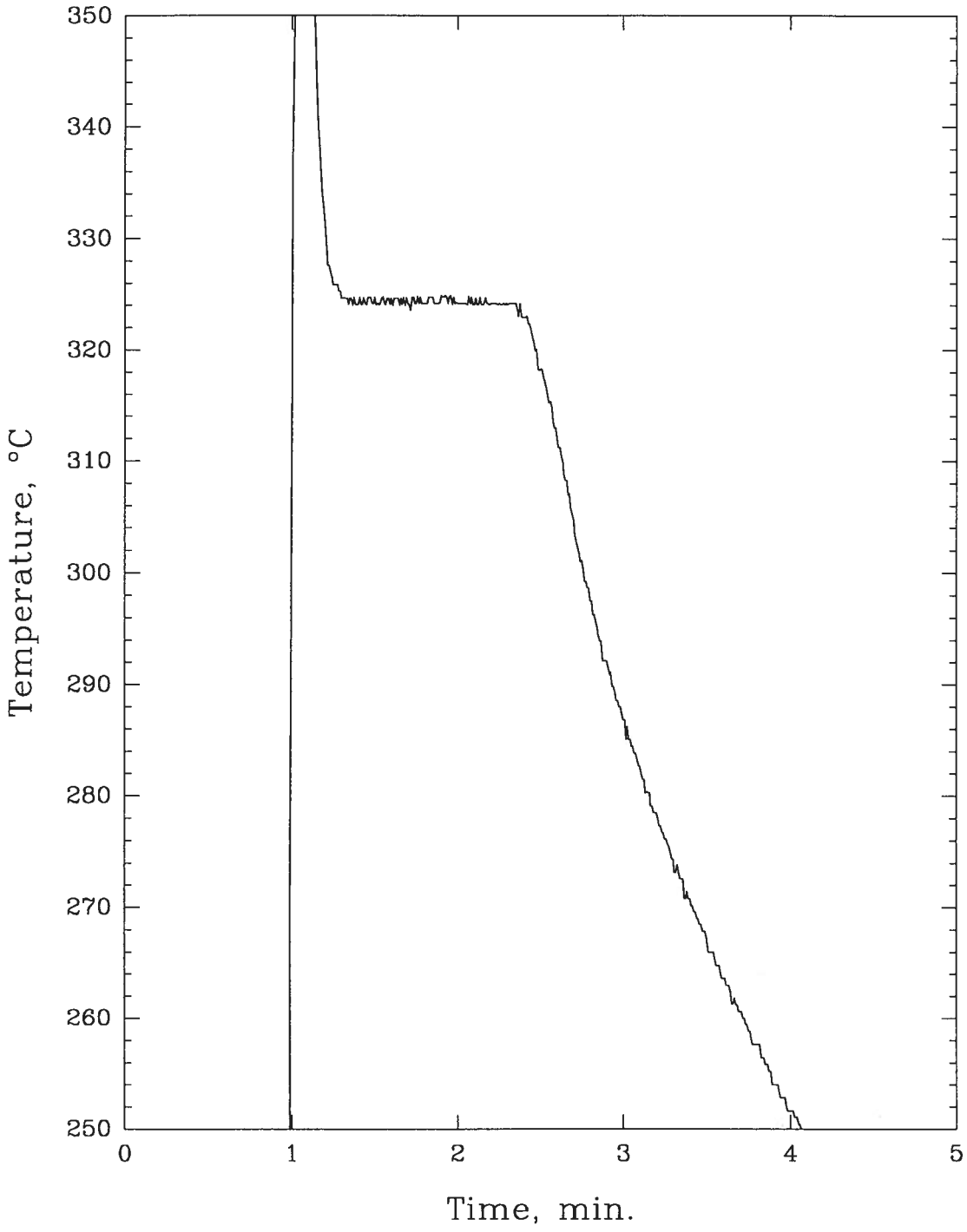

Figure 5.8 - Cooling curve of pure lead.

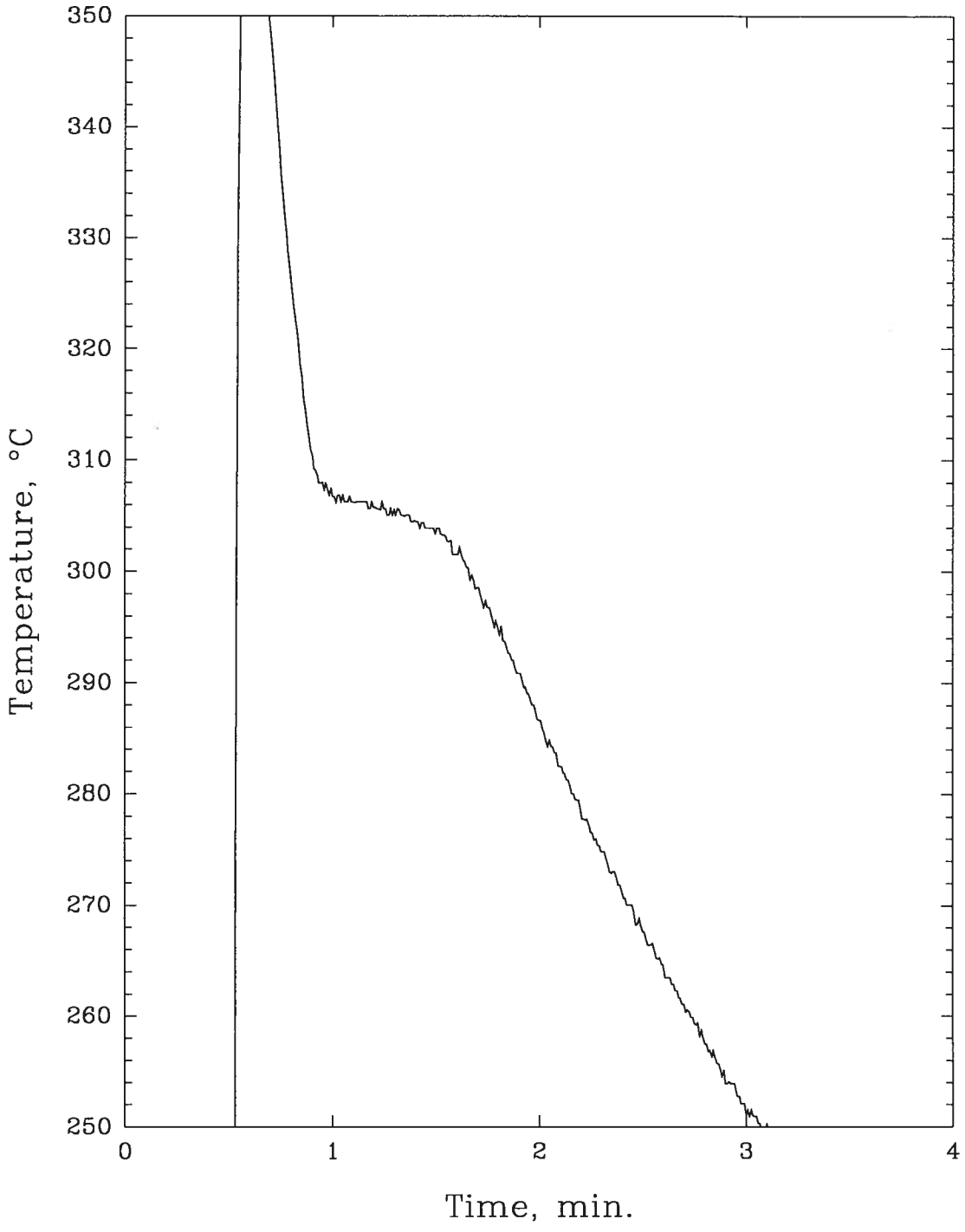

Figure 5.9 - Cooling curve of "North Pot" bullion containing 2 wt% total impurity.

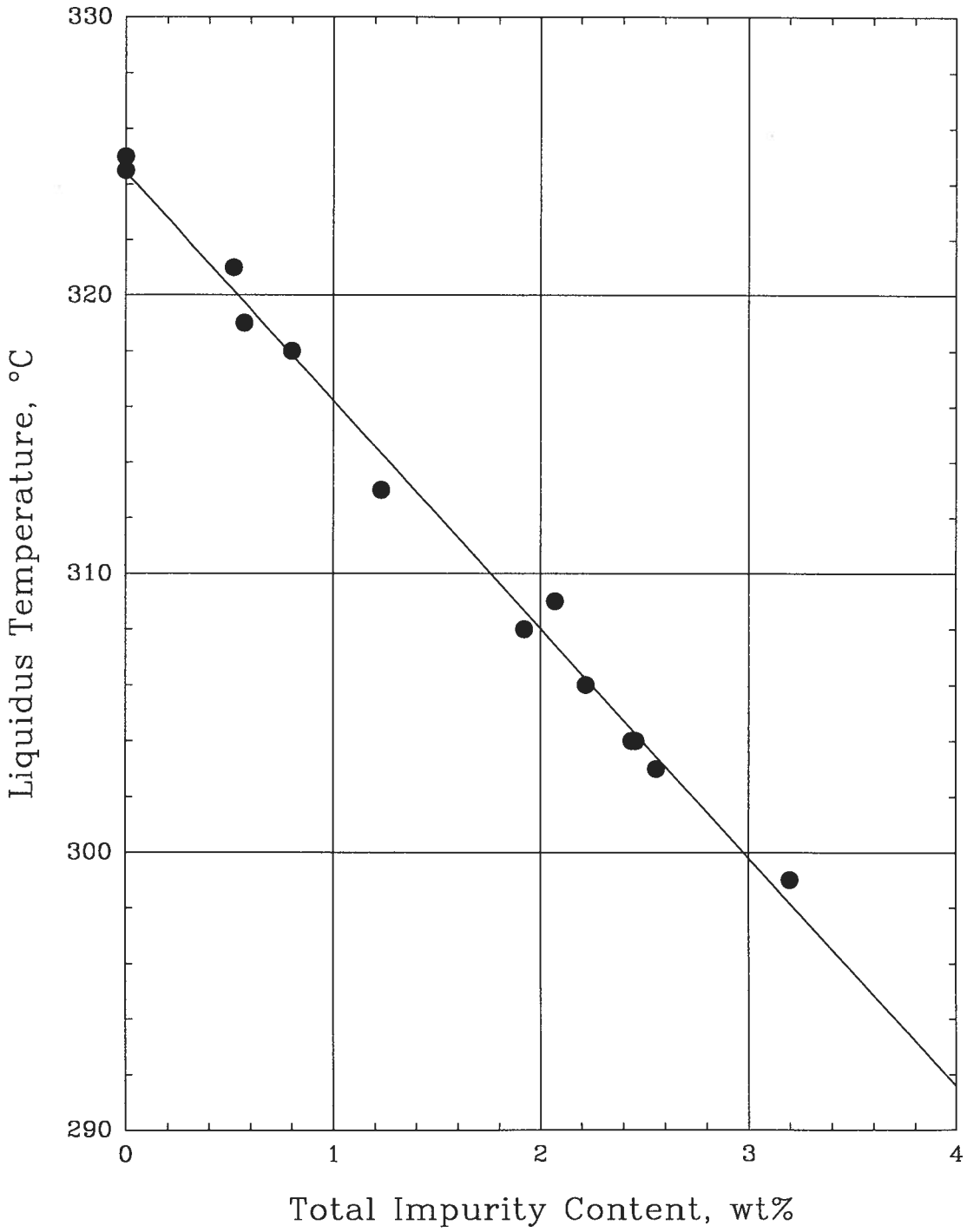

Figure 5.10 - Calibration curve for thermal arrest technique.

As opposed to the insensitivity of dissolved oxygen to impurities other than As and Sb, each impurity element has a non negligible effect on the liquidus temperature drop of the lead bullion. Temperature drops of 6.8°C, 14.0°C, 9.5°C and 3.7°C for each one wt% of Sb, As, Ag, and Bi, respectively, have been estimated from phase diagrams. For that reason, it is not possible to directly assess the As+Sb content of the softener bullion with the thermal arrest technique. However, if a correlation between As+Sb content and total impurity content was established, an indirect assessment would be possible. A total of 130 softener bullion samples were examined and a plot is given in Figure 5.11. A least-square regression analysis yielded the following equation

$$(wt\%)_{As+Sb} = -0.473 + 0.964 \cdot (wt\%)_{Total\ impurity} \quad (5.4)$$

where $(wt\%)_{As+Sb}$ and $(wt\%)_{total\ impurity}$ are the softener bullion As+Sb content in wt%, and the total impurity content in wt%, respectively. By combining Equations (5.2) and (5.3) and rearranging, the following correlation between liquidus temperature and As+Sb level in the softener bullion is obtained

$$(wt\%)_{As+Sb} = 37.57 - 0.117\,(°C)_{Liquidus} \pm 0.15\,(wt\%) \quad (5.5)$$

The characteristics of the softener bullion, that is to say both the absolute and relative amounts of the various impurities, have evolved since the start of this research project. For example, the relative amount of bismuth has regularly increased since 1992. In order to consider the long term changes in the feed bullion composition, the relationship corresponding to Equation (5.4) should be updated on a regular basis by analyzing the current daily assays of the softener bullion.

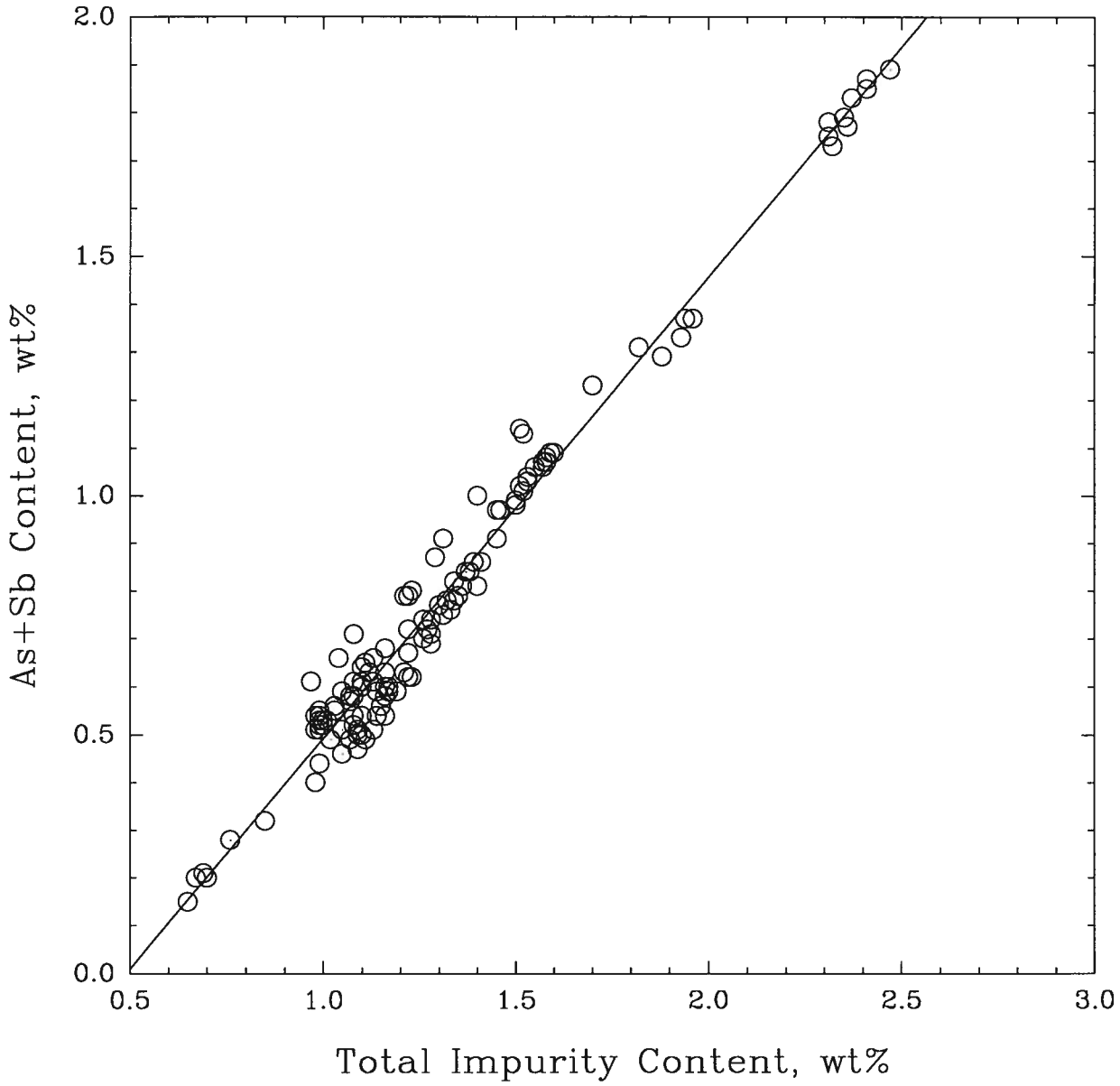

Figure 5.11 - Plot of As+Sb content of output bullion versus total impurity content.

CHAPTER 6

PROCESS MODELLING
AND
CONTROL STRATEGY

Assessing a control strategy for an improved softening process required the understanding of the process fundamentals, and, in particular, the process chemistry. The collection of industrial data on Cominco's current softener, as reported in Chapter 5, provided the necessary basis to carry out an analysis of the process. A thermodynamic model was developed to serve as a process investigation tool. This model was validated by performing an analysis of operating plant data. Once it was ascertained that the thermodynamic model gave a reasonably good representation of the batch process operation, and that an equilibrium analysis gave a good fit of operating data, the model was modified to simulate continuous softening. In this manner, the option of a continuous, single pass process could be examined, and a preliminary control strategy assessed. First, all aspects of the model formulation, and in particular the assumptions and the solution modelling, are covered. Then, the model validation and calibration is presented. Finally, the continuous single pass softening alternative is discussed, and a number of conclusions are drawn.

6.1 Model Formulation

To determine the equilibrium composition of the multiphase system representing the softening process, it was decided to develop a simpler version of the free energy minimization algorithm than the previously mentioned SOLGASMIX routine. In this manner, changing and adapting the model to perform various process simulations, i.e. batch, semi-batch or continuous modes for example, would be easily and quickly done. In this Section, the model assumptions are first presented, then a description of the mathematical algorithm is given, and finally, the solution modelling of the chemical system representing the lead softening process is discussed.

6.1.1 Assumptions

As a first step in the analysis of the softening process it was assumed that the process operates at thermodynamic equilibrium. Although this is not strictly correct because the oxygen efficiency was measured in the plant to be about 90%, it still provides a basis on which to understand the basic reactions taking place in the process. A thermodynamic process model essentially assumes that all reactions are instantaneous and that the degree of reaction is controlled by thermodynamics alone. Daily plant assays of Cominco's softener bullion consider up to seven metallic elements, i.e. lead, antimony, arsenic, bismuth, tin, copper, and silver. In order to simplify the computations, the chemical system chosen to represent the process has been limited to the four elements involved in the main reactions, i.e Pb, Sb, As, and O. Thus, the molar balance considers four species in the bullion, Pb(l) and three dissolved elements, $\underline{Sb}_{(Bullion)}$, $\underline{As}_{(Bullion)}$, and $\underline{O}_{(Bullion)}$, and three species in the slag, PbO, $SbO_{1.5}$, and $AsO_{1.5}$. The equilibrium reactions and molar balance equations which describe the above system are given in Tables 6.1 and 6.2.

Table 6.1 - Equilibrium reactions representing the oxygen softening process.

Equilibrium reactions	$1/2\ O_{2\,(g)} \leftrightarrow \underline{O}_{(Bullion)}$
	$Pb_{(l)} + 1/2\ O_{2\,(g)} \leftrightarrow PbO_{(Slag)}$
	$Sb_{(l)} + 3/4\ O_{2\,(g)} \leftrightarrow SbO_{1.5\,(Slag)}$
	$As_{(l)} + 3/4\ O_{2\,(g)} \leftrightarrow AsO_{1.5\,(Slag)}$

Table 6.2 - Molar balance equations of the chemical system representing the oxygen softening process ("n" stands for the number of moles).

Elemental balances	$n_{Pb,\,Tot} = n_{Pb} + n_{PbO}$
	$n_{Sb,\,Tot} = n_{\underline{Sb}_{(Bullion)}} + n_{SbO_{1.5}}$
	$n_{As,\,Tot} = n_{\underline{As}_{(Bullion)}} + n_{AsO_{1.5}}$
	$n_{O,\,Tot} = n_{\underline{O}_{(Bullion)}} + n_{PbO} + 1.5\,n_{SbO_{1.5}} + 1.5\,n_{AsO_{1.5}}$
Phase balances	$n_{Bullion} = n_{Pb} + n_{\underline{O}_{(Bullion)}} + n_{\underline{Sb}_{(Bullion)}} + n_{\underline{As}_{(Bullion)}}$
	$n_{Slag} = n_{PbO} + n_{SbO_{1.5}} + n_{AsO_{1.5}}$

Oxygen gas does not appear in the balance because the equilibrium partial pressure in the system is well below one atmosphere. As a result, thermodynamics predicts all oxygen is consumed below the bath surface. The model operates by reacting a given amount of oxygen with the bullion and minimizing the free energy of the system by shifting the oxygen between PbO, $SbO_{1.5}$, $AsO_{1.5}$, and $\underline{O}_{(Bullion)}$. The temperature is considered to be constant and equal to the slag-bullion interface temperature. It is also assumed that no fuming and no interactions with the gas phase take place.

6.1.2 Computation of Equilibrium Composition

The Gibbs free energy function of a multiphase system is defined as follows,

$$G_{system} = \sum_{\text{phases}} \sum_{\text{species}} n_{i,j} \left(G^{0}_{i,j} + RT \ln a_{i,j} \right) \tag{6.1}$$

where $n_{i,j}$, $G^{0}_{i,j}$, and $a_{i,j}$ are the number of moles, the standard Gibbs free energy, and the activity of species i in phase j, respectively. Expressed in an expanded form, Equation (6.1) gives

$$G_{system} = \sum_{\text{phases}} \sum_{\text{species}} n_{i,j} \left(G^{0}_{i,j} + RT \ln X_{i,j} + RT \ln \gamma_{i,j} \right) \tag{6.2}$$

where $X_{i,j}$ and $\gamma_{i,j}$ are the mole fraction and activity coefficient of species i in phase j, respectively. Following the assumption that only two phases are considered, the lead bullion and the liquid slag, the Gibbs free energy function for the system becomes

$$\begin{aligned} G_{system} = & \sum_{i} n_{i,\,bullion} \left(G^{0}_{i,\,bullion} + RT \ln X_{i,\,bullion} + RT \ln \gamma_{i,\,bullion} \right) \\ & + \sum_{i} n_{i,\,slag} \left(G^{0}_{i,\,slag} + RT \ln X_{i,\,slag} + RT \ln \gamma_{i,\,slag} \right) \end{aligned} \tag{6.3}$$

The reduced Gibbs free energy of the system, G^{*}_{system}, defined as follows,

$$G^{*}_{system} = \frac{G_{system}}{RT} = \sum_{i} n_{i,\,bullion}\left(\frac{G^{0}_{i,\,bullion}}{RT} + \ln X_{i,\,bullion} + \ln \gamma_{i,\,bullion}\right) + \sum_{i} n_{i,\,slag}\left(\frac{G^{0}_{i,\,slag}}{RT} + \ln X_{i,\,slag} + \ln \gamma_{i,\,slag}\right) \quad (6.4)$$

is minimized subject to two constraints: 1) the elemental balances, and 2) the equilibrium composition values determined must be positive.

In the search for a minimum value of the Gibbs free energy function of a system, subject to the mass balance relations, various mathematical techniques have been used. The SOLGASMIX program, for instance, uses Lagrange's method of undetermined multipliers to set up a system of linear equations that is then solved with a Gaussian elimination technique. The EQUIL program, written in FORTRAN IV and based on a technique presented by Rao[87], uses a Newton-Raphson routine to achieve final convergence. The algorithm developed for this project was inspired by Rao's technique. Simplified flow diagrams of the whole algorithm and the minimization routine are given in Figures 6.1 and 6.2. As in the EQUIL program, an estimate of the minimum that satisfies the mass balance relations is first determined, but the final value of the minimum is then obtained in a manner that only requires the computation of the first derivative of the reduced free energy function. The Newton-Raphson routine of the EQUIL program requires the computation of both first and second order derivatives. The minimum of the G^{*}_{system} function is mathematically defined by

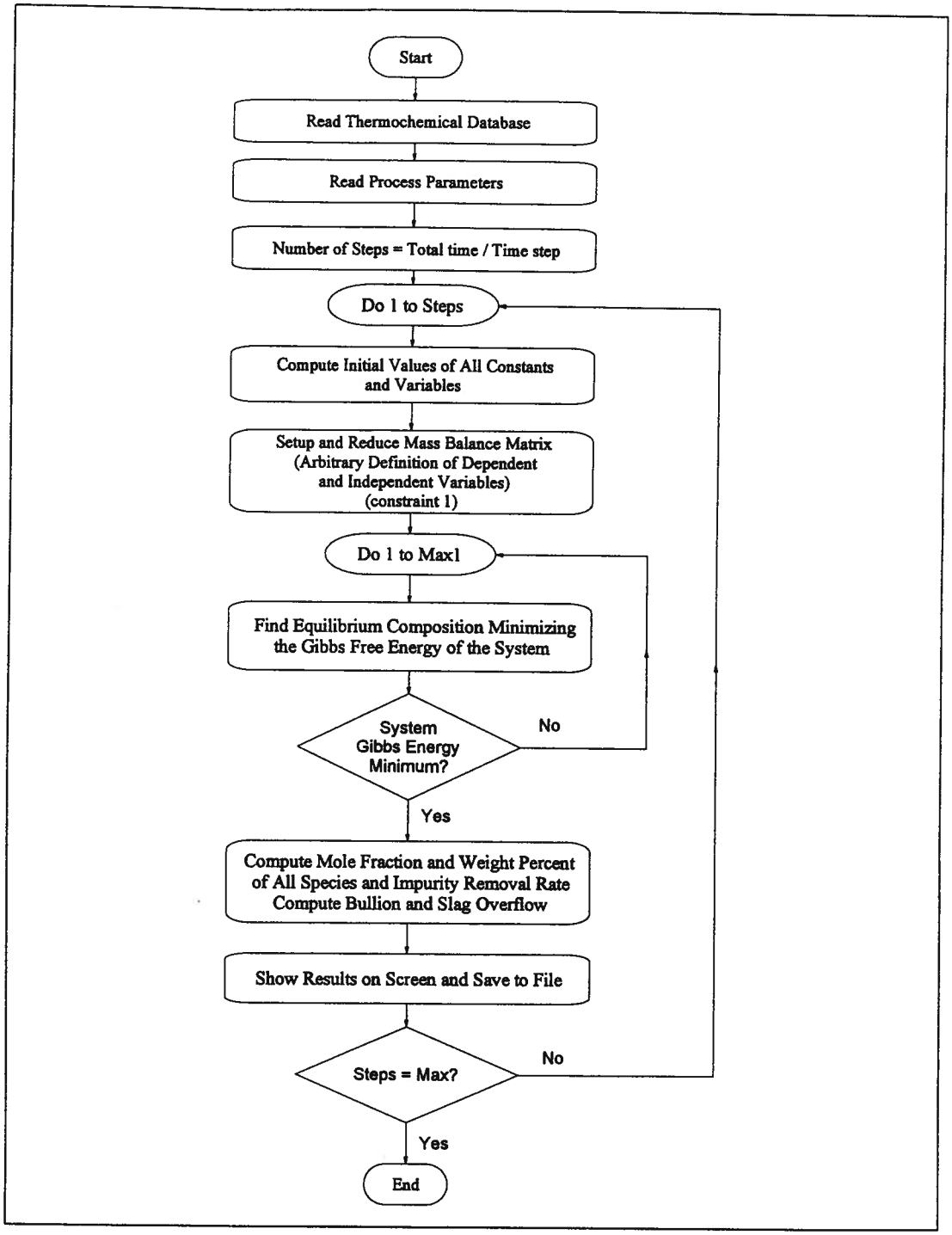

Figure 6.1 - Simplified flow diagram of the whole algorithm.

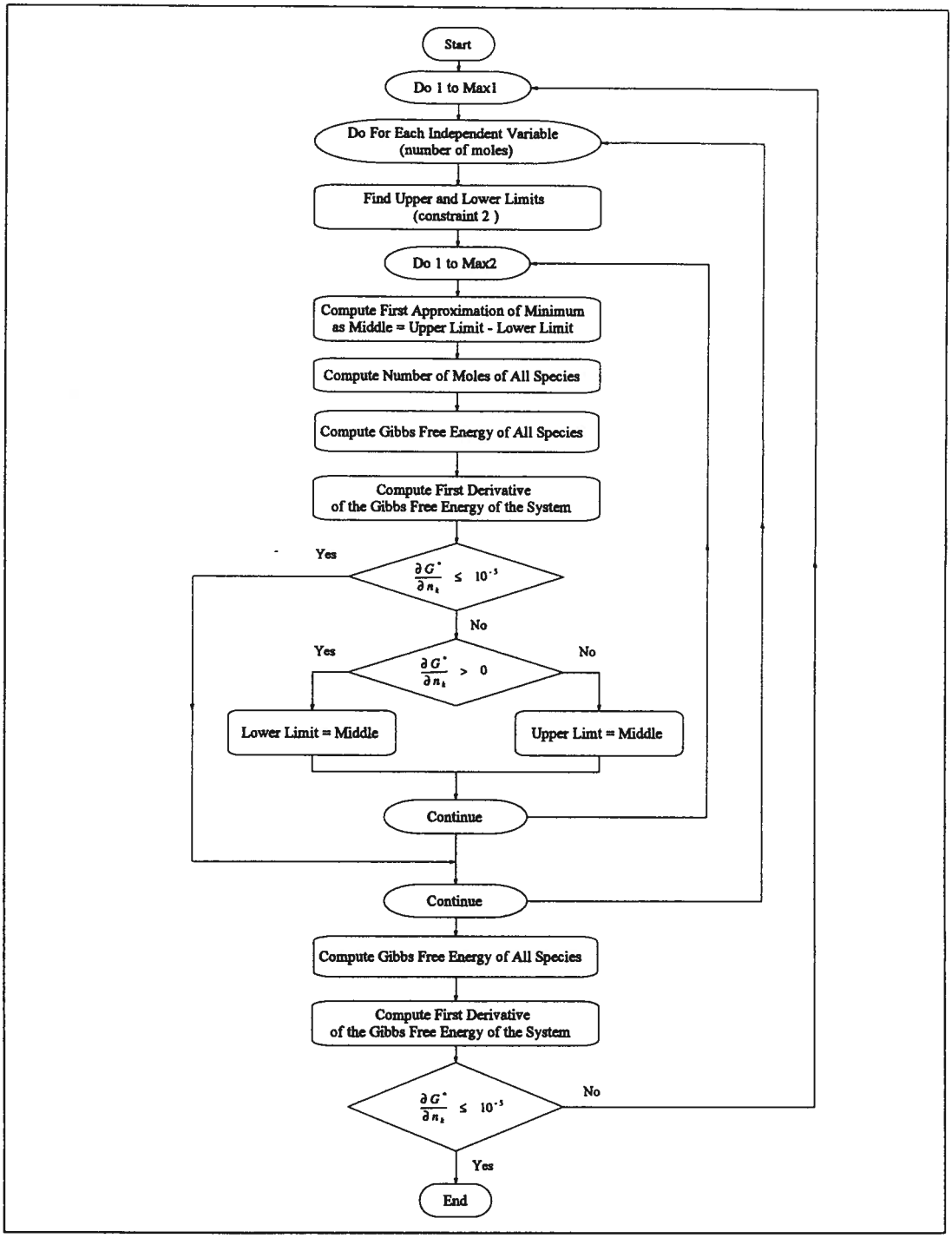

Figure 6.2 - Simplified flow diagram of the minimization routine.

$$\left(\frac{\partial G^{*}_{system}}{\partial n_k}\right)_{k=1,2,\ldots,N} = 0 \qquad (6.5)$$

where N is the total number of species in the system (bullion and slag). Although the derivative of the G^{*}_{system} function must be equal to zero at the minimum, in practice a zero value is very seldom attained. An accuracy limit of 10^{-5} was therefore chosen for the computations.

The algorithm has been designed so that additional elements, species or phases can easily be implemented provided the corresponding thermodynamic data required in the computations are available. However, the molar balance is limited to a maximum of 30 species altogether.

6.1.3 Solution Modelling

It is apparent from Equations (6.2) to (6.4) that the Gibbs free energy minimization algorithm requires the knowledge of two thermodynamic quantities for each species, the standard Gibbs free energy, G_i^0, and the activity coefficient, γ_i. The standard states were chosen as follows: pure liquid for lead, antimony and arsenic, pure gas for oxygen, pure solid for lead oxide and antimony oxide, and pure liquid for arsenic oxide. Expressions for the temperature dependence of the standard Gibbs free energies of all species were derived using data from Barin and Knacke[85], Pankratz[88], and Barin[89]. These expressions are given in Table 6.3.

Table 6.3 - Expressions for the temperature dependence of the standard Gibbs free energies of all species.

Standard Gibbs Free Energy (J / mole)
$G^0_{Pb} = -4251.0 + 125.405\,T - 29.455\,T \ln T$
$G^0_{Sb} = 8054.1 + 147.516\,T - 32.38\,T \ln T$
$G^0_{As} = 11862.9 + 144.823\,T - 29.156\,T \ln T - 0.002\,T^2$
$G^0_{O_2} = -9679.0 - 2.204\,T - 29.956\,T \ln T - 0.002\,T^2 + 83680\,T^{-1}$
$G^0_{PbO} = -233580.9 + 241.37\,T - 44.819\,T \ln T$
$G^0_{SbO_{1.5}} = -364331.2 + 212.573\,T - 39.957\,T \ln T$
$G^0_{AsO_{1.5}} = -344661.7 + 447.448\,T - 76.358\,T \ln T$

The activity coefficients of the bullion species have been derived from published data. Lead is assumed to obey Raoult's law, consequently $\gamma_{Pb} = 1$. The details relevant to the solution modelling of the dissolved elements are given below.

Oxygen

Oxygen is considered to form an infinitely dilute solution in liquid lead. For an infinitely dilute solution, the basic equation for the activity coefficient of a solute is

$$\ln \gamma_i = \ln \gamma_i^0 + \sum_j \varepsilon_i^j X_j \tag{6.6}$$

where γ_i^0 and ε_i^j are the activity coefficient of solute i at infinite dilution, and interaction coefficient of solute j on solute i, respectively. Taskinen[51] measured the oxygen activities in lead and dilute lead alloys in the temperature range from 762°C to 1000°C, and derived expressions for the temperature dependence of the activity coefficient as well as self-interaction coefficient of oxygen at infinite dilution in lead as follows

$$\ln \gamma_O^0 = 6.133 - \frac{14040}{T} \tag{6.7}$$

and

$$\varepsilon_O^O = 52.0 - \frac{70900}{T} \tag{6.8}$$

It is assumed that the above expressions for $\ln \gamma_O^0$ and ε_O^O are valid in the temperature range characteristic of lead softening, i.e. between 600°C and 630°C, and up to saturation. This hypothesis will be discussed in the next section. Due to the scarcity of available and reliable interaction

coefficients for antimony and arsenic, only the two above coefficients are used for the solution modelling of oxygen.

Arsenic

Itagaki *et al.*[90] investigated the liquid Pb-As system in the temperature range between 464°C and 582°C. They showed that a slight positive deviation from Raoult's law is observed for dilute solutions of arsenic in liquid lead when the arsenic atom fraction is less than 0.15 at a temperature of 464°C. However, this deviation becomes so small at 582°C that arsenic is considered to form an ideal solution in liquid lead, as suggested by Davey[1].

Antimony

Antimony is considered to obey Henry's law over the composition range characteristic of lead softening. Extrapolating the data from Hultgren *et al.*[91], and Seltz and De Witt[92], the following expression for the temperature dependence of the activity coefficient of antimony dissolved in lead was derived

$$\ln \gamma^{0}_{Sb} = -0.0027 - \frac{219.1}{T} \tag{6.9}$$

This expression provides data in agreement with results from Zunkel and Larson[93].

The activity relations in the slag constitute the greatest uncertainty due to the scarcity of data in the literature. Values of the activity coefficients of the slag species have been obtained by fitting of the model to industrial data. These values were then compared to the limited data available to check their validity. The procedure is detailed in the next section.

6.2 Model Validation and Calibration

Prior to using the model to investigate the concept of continuous single pass softening, a number of preliminary steps were performed in order to demonstrate that a thermodynamic model can be used to represent process operation. In particular, the validity of the solution modelling was tested, and the batch process currently used at Cominco was analyzed. These two aspects are presented in this section.

6.2.1 Solution Modelling Validation

As a first step towards validating the model, the system Pb(l) - $\underline{O}_{Pb}$ - PbO(s, yellow) was considered, and the oxygen saturation in molten lead was computed with the model in the temperature range from 527°C to 827°C. The results are presented in Table 6.4. The oxygen saturation data computed with the relationship

$$\ln (\text{at\% } \underline{O}) = - \frac{12065.55}{T} + 10.477 \qquad (6.10)$$

from Alcock and Belford[44], are also given in Table 6.4 for comparison. A better agreement between the two sets of values is obtained in the temperature range 577°C to 677°C. Even though the expressions for $\ln \gamma_O^0$ and ε_O^O were determined by Taskinen[51] in the temperature range between 762°C and 1000°C, they appeared to be suitable for the temperature conditions of lead softening, and thus their use in the model is justified.

Table 6.4 - Oxygen saturation in liquid lead at different temperatures. Comparison between the model computations and the relationship from Alcock and Belford (1964, ref. 44).

	Oxygen Saturation (at%)	
Temperature (°C)	**From Equation (6.10)**	**From Model**
527	1.003×10^{-4}	0.957×10^{-4}
577	0.243×10^{-3}	0.239×10^{-3}
615	0.447×10^{-3}	0.448×10^{-3}
627	0.536×10^{-3}	0.540×10^{-3}
677	0.108×10^{-2}	0.113×10^{-2}
727	0.205×10^{-2}	0.220×10^{-2}
777	0.363×10^{-2}	0.408×10^{-2}
827	0.613×10^{-2}	0.723×10^{-2}

6.2.2 Model Calibration

Industrial data collected at the Cominco smelter were used to determine the activity coefficients of the slag species by fitting them to the model. This was achieved by running the simulation for a given amount of oxygen consumed and changing the values of the coefficients until the final amount and composition of the slag generated in the simulation match the industrial data. The plant data collected in June and October 1994, and presented earlier in Tables 5.5 and 5.6, were used as

process parameters in the simulations. The "June test" data were gathered by monitoring 6 softening cycles for a total duration of 2 hours, whereas the "October test" data were obtained by monitoring 3 softening cycles for a total duration of 54 minutes. The slag composition was normalized for the ternary PbO-$SbO_{1.5}$-$AsO_{1.5}$ system. The input (plant data) and output (calculations) process parameters are summarized in Tables 6.5 and 6.6. The activity coefficient of PbO was obtained using data from Sugimoto *et al.*[94] and preliminary results from Chaskar[95]. Sugimoto *et al.* measured the activity of PbO at 800°C for the whole range of composition in the binary system PbO-$SbO_{1.5}$ using an emf technique. Chaskar carried out a study of the ternary system PbO-$SbO_{1.5}$-$AsO_{1.5}$ using a Knudsen cell technique. The activity coefficients of $SbO_{1.5}$ and $AsO_{1.5}$ were then fitted using the above procedure. Their values are presented in Table 6.7.

With the above procedure, from a set of activity coefficients including the two fitted values, the mole fractions of all species are calculated by minimizing the free energy of the system. The activity of each species can subsequently be computed from the knowledge of its mole fraction and activity coefficient. Once the activities are known, the validity of the fitted activity coefficients can be verified in the following manner. The equilibrium constants of the equilibria

$$3/2\ PbO_{(s)} + Sb_{(l)} \leftrightarrow 3/2\ Pb_{(l)} + SbO_{1.5\,(s)} \qquad (I)$$

and

$$3/2\ PbO_{(s)} + As_{(l)} \leftrightarrow 3/2\ Pb_{(l)} + AsO_{1.5\,(l)} \qquad (II)$$

can be calculated through the relationships

$$K_{I} = \frac{a_{SbO_{1.5}} a_{Pb}^{3/2}}{a_{Sb} a_{PbO}^{3/2}} \tag{6.11}$$

and

$$K_{II} = \frac{a_{AsO_{1.5}} a_{Pb}^{3/2}}{a_{As} a_{PbO}^{3/2}} \tag{6.12}$$

using the activities obtained in the simulations. At this point, it should be emphasized again that these activities were not obtained with Equations (6.11) and (6.12) but through the computation of the mole fractions of all species as described above. The simulation results using the "June test" data yield values of 303.8 and 82.9 whereas the results using the "October test" data yield values of 303.5 and 82.9 for K_{I} and K_{II}, respectively.

The equilibrium constants K_{I} and K_{II} can also be computed using standard Gibbs free energy data. This alternative provides values of 303.0 and 80.1 for K_{I} and K_{II}, respectively. This very good agreement between the two sets of values demonstrate that the activity coefficients obtained with the fitting procedure provide self consistent results in the model calculations.

The final bullion composition obtained in the simulations also compares very well to the operation data, as presented in Tables 6.5 and 6.6, demonstrating that the thermodynamic model can give a reasonably good fit of operating data.

Table 6.5 - Batch softening model parameters (June plant data and corresponding model calculations).

Parameters	**Plant Data**	**Model Calculations**
Initial bullion composition		
Sb	0.76 wt%	
As	0.07 wt%	
Final bullion composition		
Sb	0.69 wt%	0.66 wt%
As	0.06 wt%	0.04 wt%
Normalized Slag composition		
PbO	61.5 wt%	61.6 wt%
$SbO_{1.5}$	29.3 wt%	29.3 wt%
$AsO_{1.5}$	9.2 wt%	9.1 wt%
Slag production	242 kg/cycle	239 kg/cycle
Temperature	615°C	
Oxygen injection	73.0 m^3/hour	
Oxygen efficiency	80%	
Vessel capacity	60 tonnes	
Softening cycle length	20 min.	

Table 6.6 - Batch softening model parameters (October plant data and corresponding model calculations).

Parameters	**Plant Data**	**Model Calculations**
Initial bullion composition		
Sb	0.67 wt%	
As	0.09 wt%	
Final bullion composition		
Sb	0.61 wt%	0.59 wt%
As	0.08 wt%	0.06 wt%
Normalized Slag composition		
PbO	65.7 wt%	65.7 wt%
$SbO_{1.5}$	22.9 wt%	22.9 wt%
$AsO_{1.5}$	11.4 wt%	11.4 wt%
Slag production	261 kg/cycle	259 kg/cycle
Temperature	615°C	
Oxygen injection	74.8 m^3/hour	
Oxygen efficiency	92%	
Vessel capacity	60 tonnes	
Softening cycle length	18 min.	

Table 6.7 - Batch softening model parameters.

	Activity Coefficients		Source
	June Data	**October Data**	
Bullion			
Pb	1	1	
Sb	0.78	0.78	91-92
As	1	1	1,90
O	dependent on composition	dependent on composition	51
Slag			
PbO	0.29	0.31	94-95
$SbO_{1.5}$	0.405	0.56	fitted
$AsO_{1.5}$	0.030	0.041	fitted

6.2.3 Analysis of the Batch Process

Once the activity relations in the slag were obtained, the model was used to analyze the mechanism of softening in a fully batch mode and with continuous slag removal. The process parameters from the October test (see Table 6.6) and their corresponding activity coefficients (see Table 6.7) were used in this analysis. In the initial stage of the process, injected oxygen is largely absorbed into the liquid lead with little slag formation. This effect is really only significant when starting with an oxygen free lead bullion, as done in the simulations. In the actual process, this initial stage is much shorter since the bullion is close to oxygen saturation. However, once the bullion is saturated, slag formation begins and relatively high rates of antimony and arsenic removal are achieved (see Figure 6.3). With time, as the concentration of antimony and arsenic in the bullion

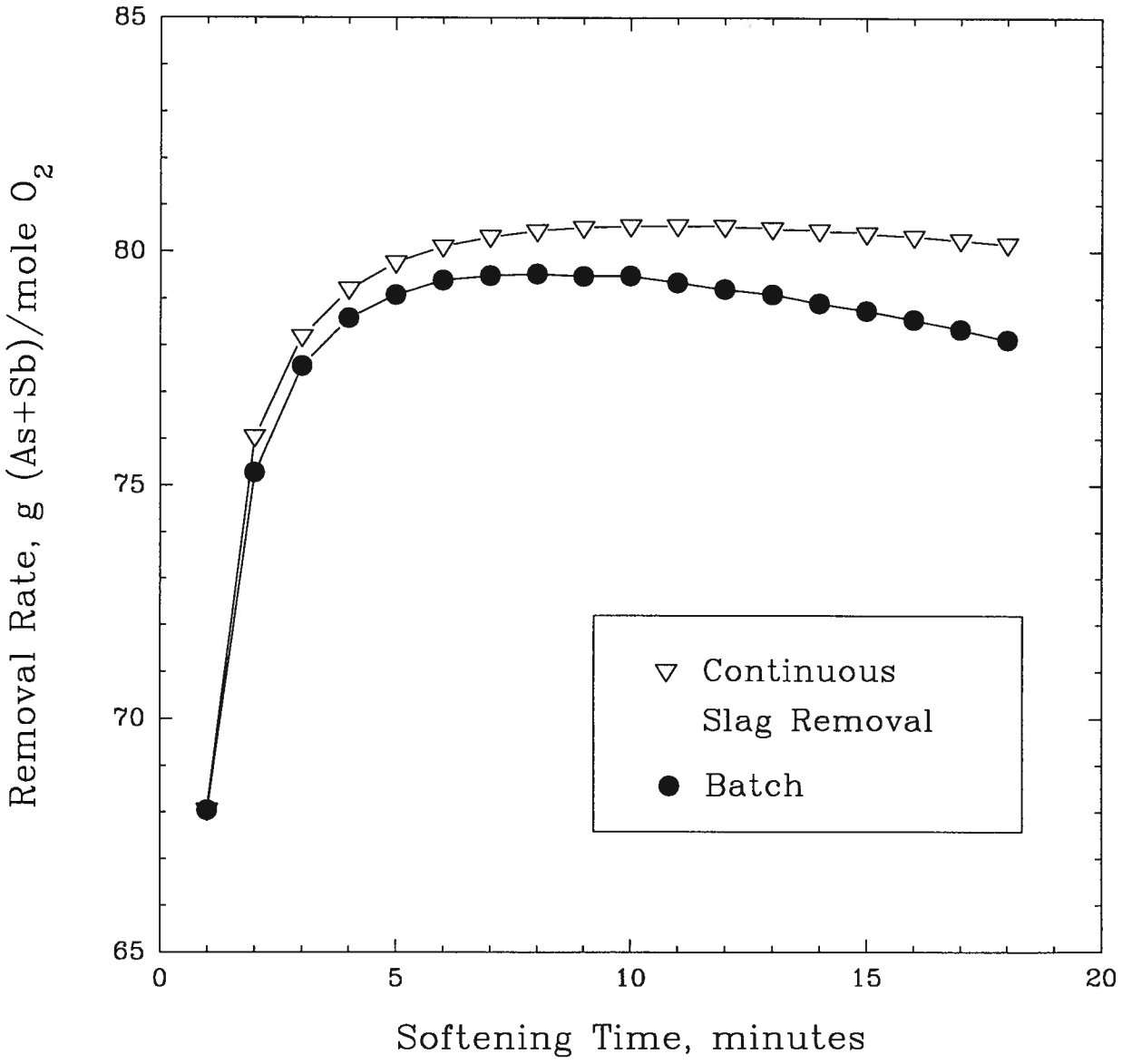

Figure 6.3 - As+Sb removal during a softening cycle in batch and continuous slag removal modes (computed from model simulations).

drops, the softening efficiency also falls and more lead is oxidized to PbO (see Figure 6.4). In a normal 18 minute cycle, starting with oxygen free lead, this would mean that roughly 57% of the oxygen consumed reacts to remove antimony and arsenic.

Continuous removal of the slag during softening, however, leads to slightly higher efficiency because the high antimony and arsenic slag formed in the earlier stages of the cycle is removed and does not back react with lead as time goes on (see Figures 6.3 and 6.5). Under these conditions, about 60% of the oxygen consumed reacts to remove antimony and arsenic.

The improvement provided by continuously removing the slag is very small, there is only a 3% increase in oxygen utilized to remove As and Sb. This is due to the limited variation range of bullion composition during a cycle. The difference between $(As+Sb)_{start}$ and $(As+Sb)_{end}$, where (As+Sb) corresponds to the wt% of As+Sb in the bullion, is less than 0.1 wt%. This means that the slag composition in equilibrium with the bullion in the early stages of the cycle is only slightly different than the final slag composition. Thus, even though the activity coefficients of the slag species are fitted to match the final slag composition, they still provide a reasonable estimate over the whole cycle. This leads to the conclusion that the benefits of continuously removing the slag would only justify the additional operating requirements if large variations in bullion composition were occurring during a cycle.

Temperature plays a role in determining softener efficiency as shown in Figure 6.6. The activity coefficients of the slag species were calculated at temperatures other than 615°C assuming that $RT \ln \gamma$ is constant. Increasing temperature results in a decrease in process efficiency. This

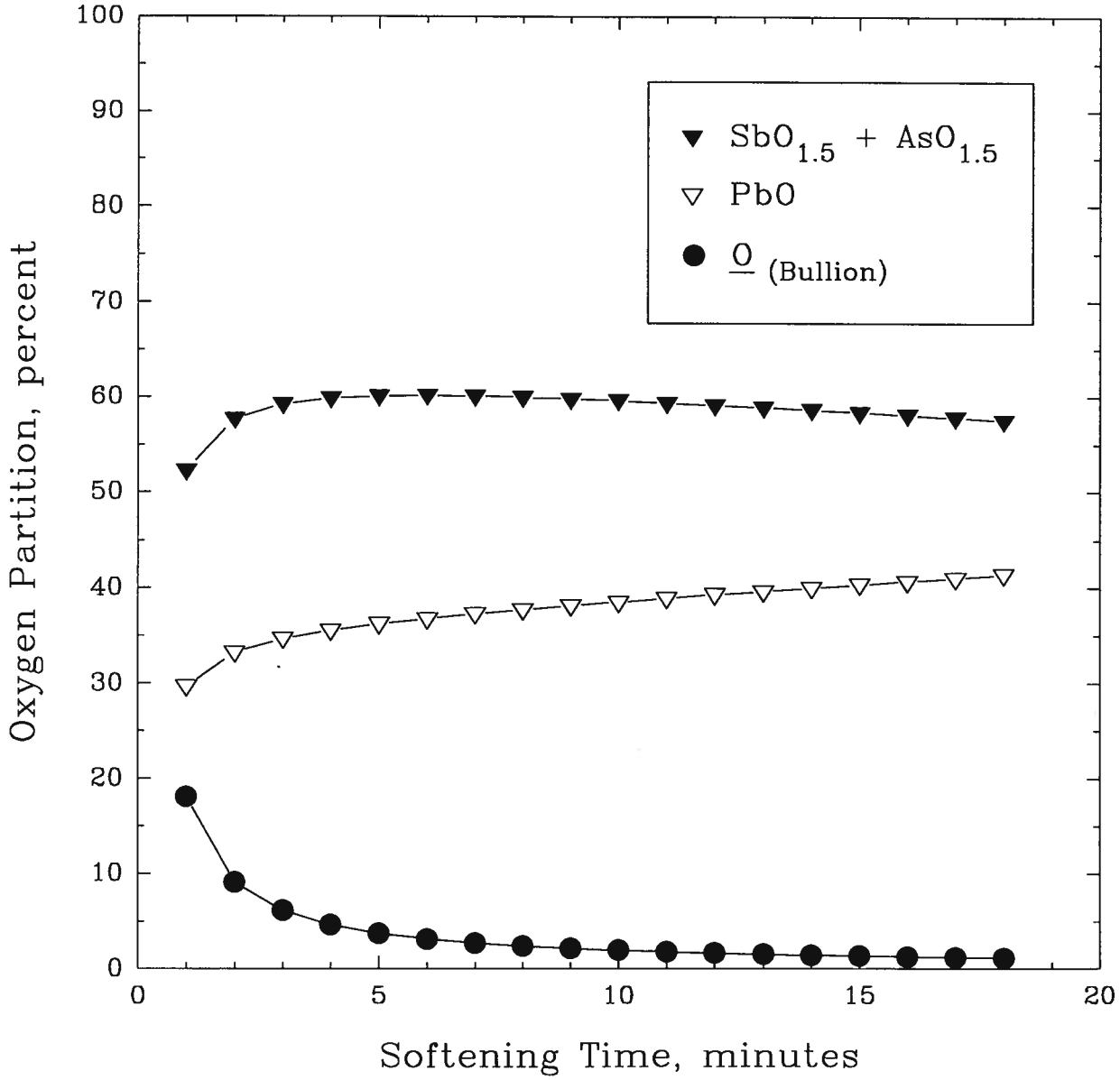

Figure 6.4 - Oxygen partition during a softening cycle in batch mode (computed from model simulations).

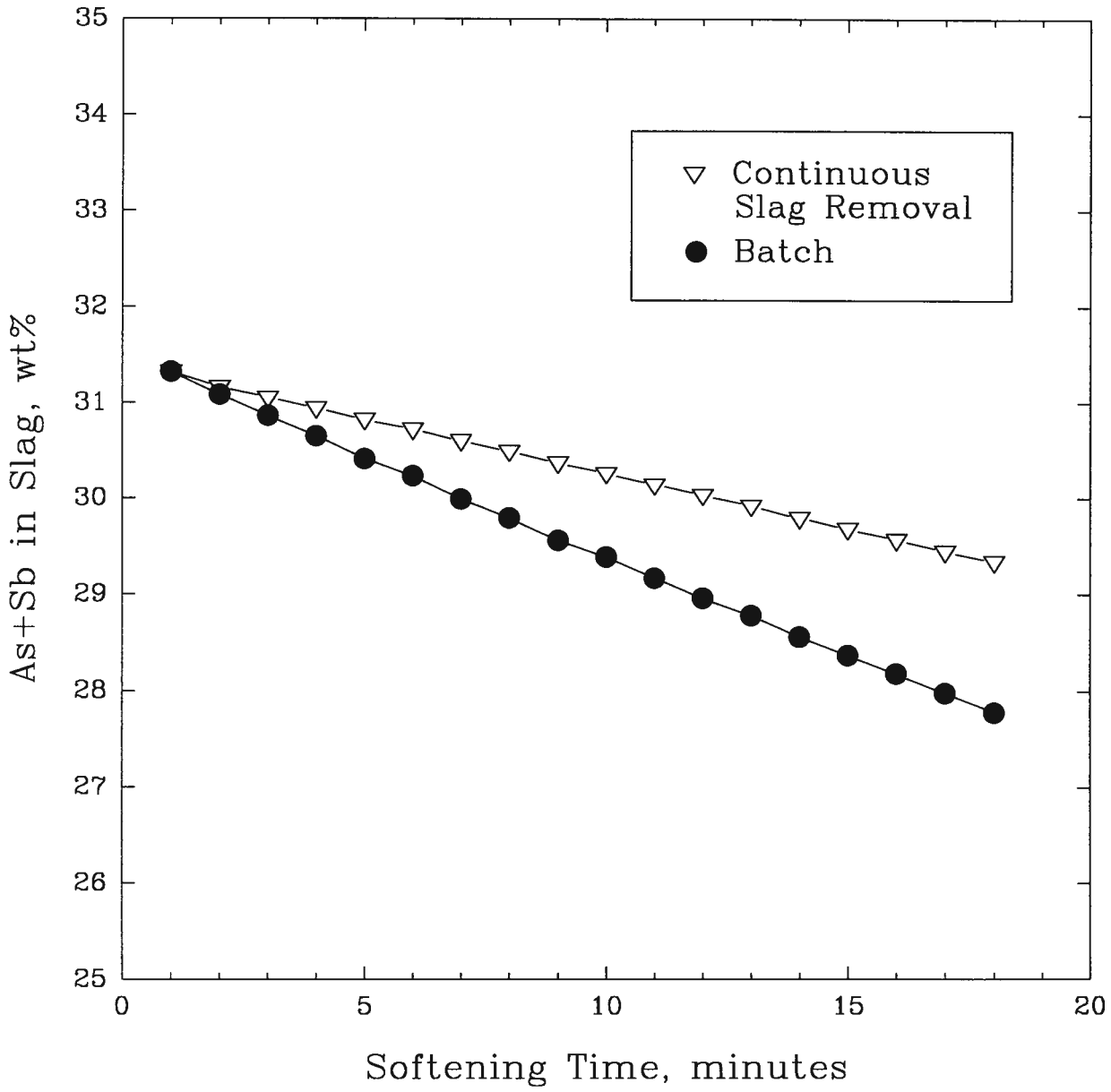

Figure 6.5 - Evolution of the slag composition during a softening cycle in batch and continuous slag removal modes (computed from model simulations).

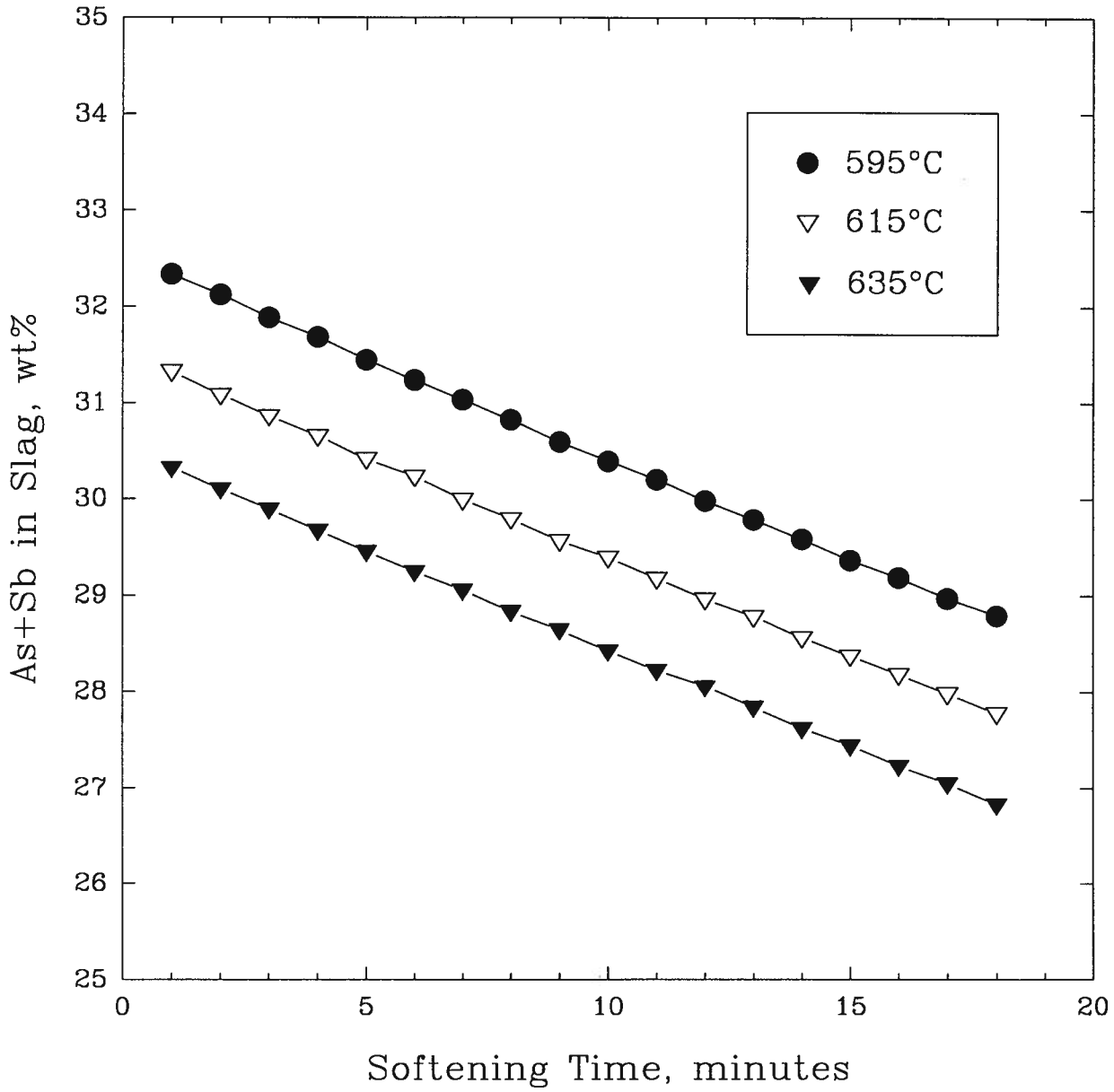

Figure 6.6 - Effect of temperature on the slag composition during a softening cycle in batch mode (computed from model simulations).

arises due to changes in equilibrium constants of Reactions (III) and (IV) with temperature, see Table 6.8.

$$\underline{Sb}_{(Bullion)} + 3/4\ O_{2\,(g)} \leftrightarrow SbO_{1.5\,(s)} \qquad \text{(III)}$$

and

$$\underline{As}_{(Bullion)} + 3/4\ O_{2\,(g)} \leftrightarrow AsO_{1.5\,(l)} \qquad \text{(IV)}$$

Table 6.8 - Equilibrium constants of As and Sb oxidation (Reactions (III) and (IV)).

Temperature (°C)	$\mathbf{K_{III}}$	$\mathbf{K_{IV}}$
600	1.56×10^{14}	3.93×10^{13}
625	3.85×10^{13}	1.11×10^{13}
650	1.03×10^{13}	3.35×10^{12}
675	2.94×10^{12}	1.08×10^{12}
700	8.99×10^{11}	3.70×10^{11}

6.2.4 Batch Process Operation

The analysis of the process with the model permitted the identification of a number of important parameters. However, it cannot be emphasized enough that any conclusions drawn from the analysis are subject to the assumption of thermodynamic equilibrium. With this in mind, the following remarks concerning process operation can be made.

Temperature

Although higher temperatures may assist with process kinetics, from a thermodynamic perspective lower temperatures favor As+Sb deportment into the slag. Operating at the lowest possible temperature is thus preferred. Observations during the plant visits showed that temperature is also a key issue regarding lance life. High temperatures in the vessel increase the corrosiveness of the slag and reduce the life span of the lances. In 1987, H. Salomon-De-Friedberg[96] examined daily assays of various softener streams in an attempt to assess relationships that might explain elemental deportment and lance life. The prominent conclusion of his analysis was that the arsenic level in the input bullion determined softener performance and lance life. More specifically, arsenic levels in input bullion higher than 0.6 wt% at 620°C, and higher than 0.5 wt% at 640°C drastically reduced lance life. During the visits in March, June, and October 1994, the arsenic content in the bullion never exceeded 0.5 wt%, but lance consumption increased on several occasions, including one instance where it reached 150 lances per shift. It was observed that increased lance consumption was always associated with high temperatures in the vessel. Two types of lance failure can occur, caused either by metal ignition with the oxygen stream, or by PbO corrosion at the slag level. The first type could be explained by the "arsenic level effect". As suggested by Salomon-De-Friedberg, the higher the temperature, the lower the tolerable level. The second type is directly correlated to

the corrosiveness of the slag which is strongly dependent on temperature. Temperature control in the softener thus appears to be critical, temperature playing an important role in softener performance and influencing considerably lance life. It should be pointed out, however, that temperatures very close to the slag melting point would render the softener very vulnerable to minor impurity elements such as tin, which can considerably lower the slag freezing point even when present in minute amounts.

Cycle length

The process analysis showed that short cycles, in the order of 15 minutes, are preferred to take advantage of the higher removal rate of As and Sb in the early stages. When the softener runs under the "normal operating conditions" as defined during the plant trials and presented in Chapter 5, the duration of a cycle is about 15 to 20 minutes.

As+Sb level

A high level of combined As+Sb favors high slag quality minimizing Pb oxidation. Depending on the softening capacity, i.e. the ability to remove sufficient amounts of As+Sb with short cycles while meeting the target, As+Sb should be increased rather than lowered to boost the efficiency. Fast kinetics at low levels are effective only within the range 0.02 to 0.06 wt%, which is too low in a partial softening process to be practical.

As/Sb ratio

With respect to lance protection, low As content is preferable.

6.3 Continuous Single Pass Softening Process

In order to simulate the process, the equilibrium model developed for the batch process was modified to continuous softening through a number of important assumptions. The model was then used to analyze the continuous, single pass softening route for a variety of conditions. A control strategy was devised as a result of the analysis. The first section deals with the assumptions of the model, the second covers the process analysis, while the last presents the control strategy.

6.3.1 Assumptions

When modifying the equilibrium model developed for the batch process, the following important assumptions were made:

- the bullion is fully backmixed,
- the slag is fully backmixed, and
- isothermal conditions prevail.

Work on the existing softener showed that the slag phase is relatively well mixed. Bullion mixing in the continuous process would depend on flow rate and vessel geometry. With mechanical stirring it could be kept close to backmixed conditions if desired. Without deliberate mixing however, there is a likelihood that there would be compositional gradients that would affect output bullion composition. At this stage of the analysis the heat balance was ignored in order to clarify the process chemistry. Furthermore, a heat balance would depend on a host of factors such as vessel size, refractory thickness, and use of natural gas for heating the freeboard.

The critical model parameters used in the analysis are given in Table 6.9. Given the uncertainty at this point as to the dependence of the slag activity coefficients on temperature and composition these values were held constant at levels that give reasonable predictions of the batch reactor performance at higher As+Sb content. To simulate operating conditions, the model calculation was carried out for short time steps (1 min) starting at an arbitrary bullion and slag composition. During each time step the appropriate weight of input bullion is added and then the amount of O_2 injected is equilibrated with the bullion and slag present. The excess bullion and slag are then removed and the process repeated until steady state is reached. Thus, although the results presented in this thesis deal only with steady state, the model is capable of simulating transient behaviour.

Table 6.9 - Continuous softening model parameters.

	Activity coefficient
Bullion	
Pb	1
$\underline{Sb}$	0.78
$\underline{As}$	1
$\underline{O}$	dependent on composition
Slag	
PbO	0.24
$SbO_{1.5}$	0.42
$AsO_{1.5}$	0.05

6.3.2 Process Analysis

Continuous single pass softening was analyzed for a variety of conditions as summarized in Table 6.10. In the base case, 15.5 tph of bullion with 2.9 wt% As+Sb is treated with 40 Nm^3/h of oxygen at 615°C. The predicted output composition is 1.73 wt% As+Sb, in the middle of the target range of 1.5 to 2.0 wt% As+Sb.

Table 6.10 - Continuous softening model parameters.

	Base	Range
Bullion		
output target As+Sb (wt%)	1.73	1.5 - 2.0
input As+Sb (wt%)	2.9	2.3 - 3.5
input flow (tph)	15.5	10.3 - 25.8
Oxygen		
injection rate (Nm^3/h)	40	32 - 56
Temperature (°C)	615	595 - 635

Figure 6.7 shows the effect of impurity level in input bullion on output bullion composition. As expected, output impurity level increases linearly with impurity level. The slope of the lines is approximately 0.82 which indicates that a 1% rise in impurity level results in roughly a 0.82% rise in output impurity level. This is due to the increasing thermodynamic efficiency of impurity removal as impurity level in softener bullion rises. As suggested by Reactions (III) and (IV),

$$\underline{Sb}_{(Bullion)} + 3/4\ O_{2\,(g)} \leftrightarrow SbO_{1.5\,(s)} \quad \text{(III)}$$

$$\underline{As}_{(Bullion)} + 3/4\ O_{2\,(g)} \leftrightarrow AsO_{1.5\,(l)} \quad \text{(IV)}$$

increasing the concentrations (activities) of $[Sb]_{Pb}$ and $[As]_{Pb}$ would shift the equilibrium to the right and put more Sb and As into the slag phase. This effect is illustrated in Figure 6.8.

It is interesting to note that there is not a direct proportionality between As+Sb in slag and bullion as might be suggested by the equilibrium constants of Reactions (III) and (IV),

$$[SbO_{1.5}] = K_{III}\,[Sb]\,P_{O_2}^{3/4} \quad (6.13)$$

and

$$[AsO_{1.5}] = K_{IV}\,[As]\,P_{O_2}^{3/4} \quad (6.14)$$

This arises because as As+Sb increases in bullion the oxygen dissolved in bullion, and hence P_{O_2}, decreases. Figure 6.9 shows the variation of $P_{O_2}^{3/4}$ with impurity level.

The other feature to note from Figure 6.7 is the effect of O_2 injection rate on impurity level. Increasing O_2 injection results in an almost proportionate rise in impurity removal. However, there is a reduction in efficiency as illustrated in Figure 6.10 where absolute impurity removal in grams of As+Sb is plotted against O_2 injection rate. Efficiency falls, in this case, for the same reasons it rises with output impurity level. As O_2 injection rate increases, more impurity is removed from the bullion and output bullion impurity level falls. At lower $(As+Sb)_{Pb(l)}$ the slag is not as rich in As+Sb and an increased fraction of O_2 reacts to form PbO.

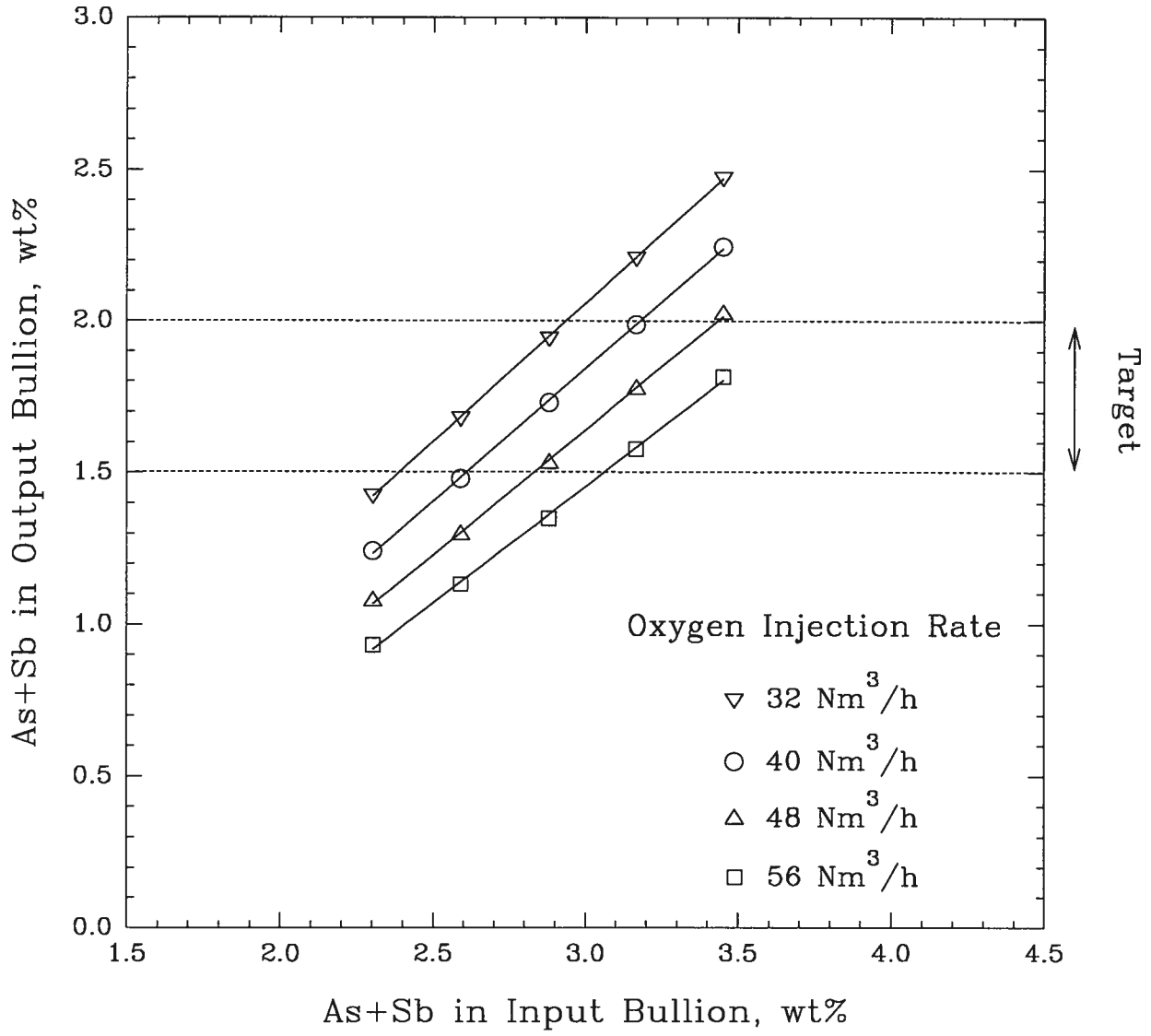

Figure 6.7 - Effect of impurity level and O_2 injection rate on output bullion quality (615°C, 15.5 tph input bullion).

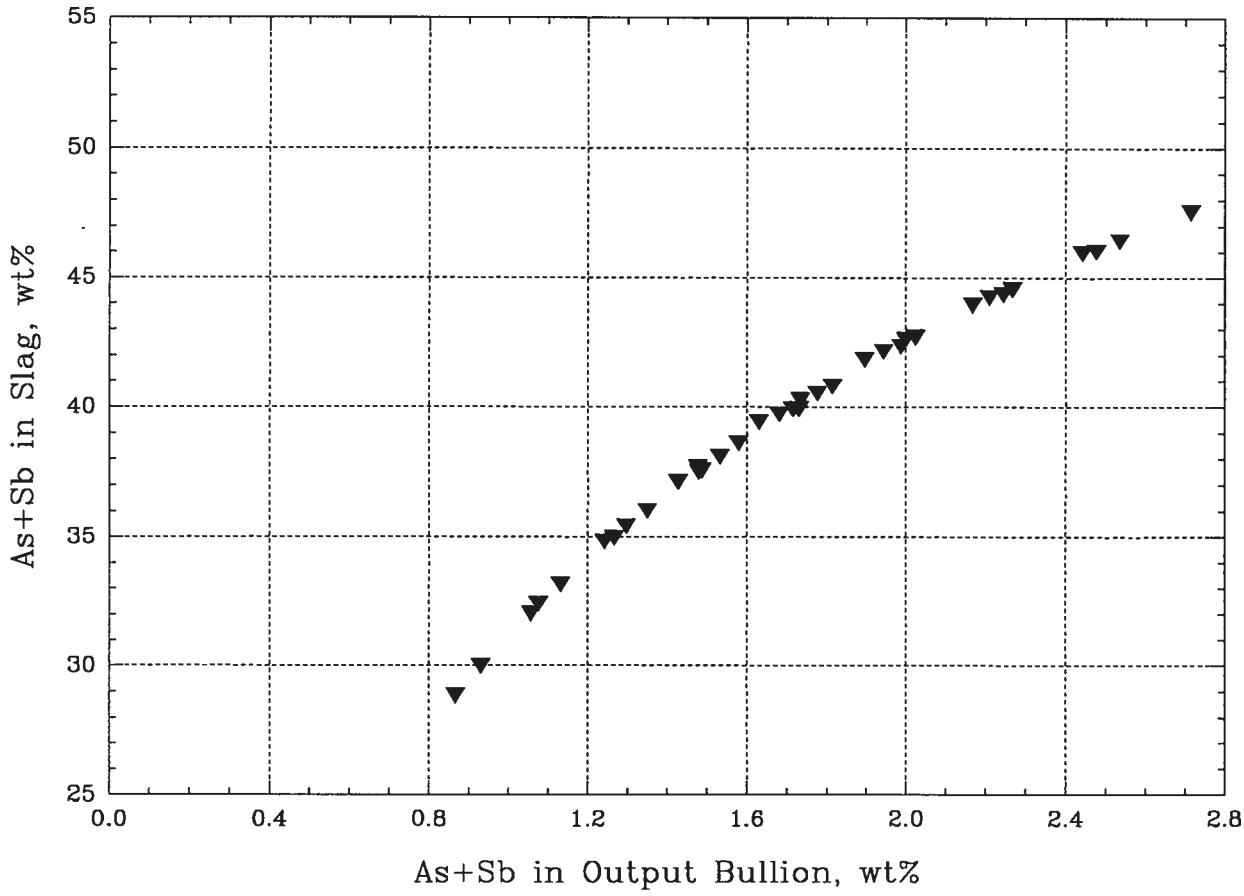

Figure 6.8 - Relationship between slag composition and impurity level in output bullion (615°C).

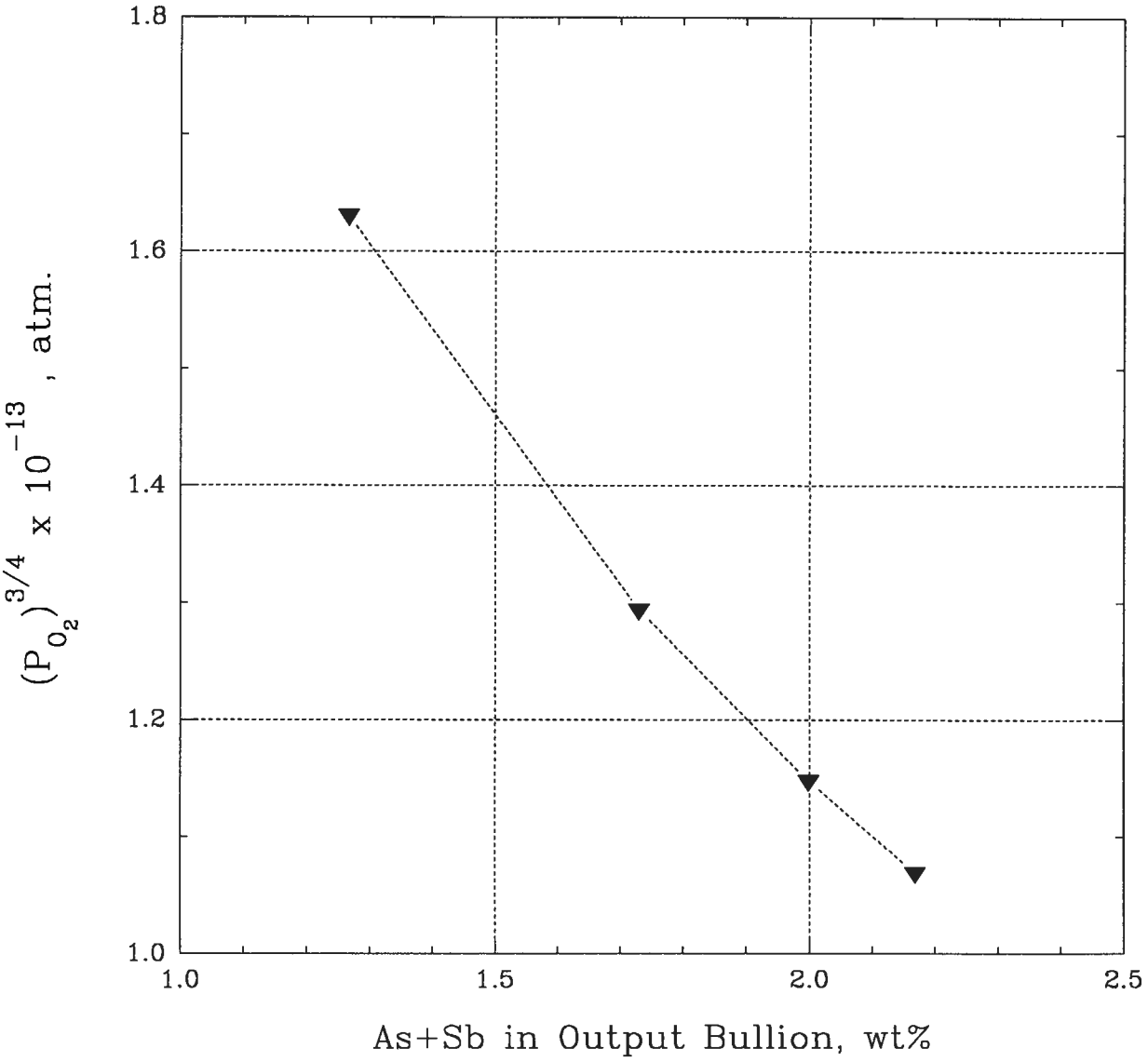

Figure 6.9 - Variation of $P_{O_2}^{3/4}$ with impurity level in output bullion (615°C).

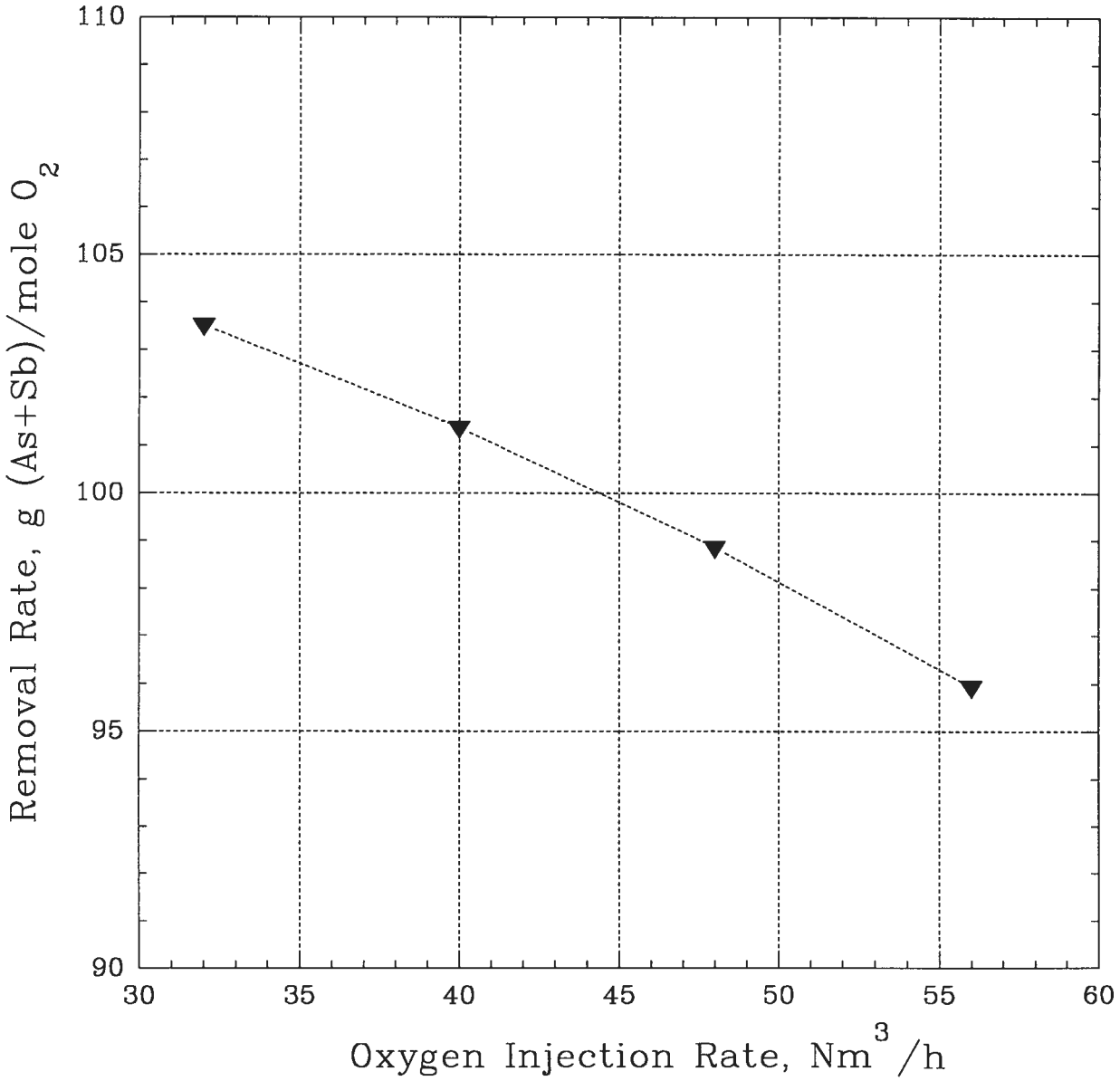

Figure 6.10 - Sensitivity of impurity removal rate to O_2 injection rate (615°C, 15.5 tph input bullion).

A comparison between Figures 6.10 and 6.3 shows that continuous single pass softening presents efficiency gains with respect to batch softening: removal rates in the order of 100 g (As+Sb)/mole O_2 and 80 g (As+Sb)/mole O_2 for the continuous and batch routes, respectively.

The effect of bullion flow rate is shown in Figure 6.11. As the flow is increased at a given impurity level, the impurity level in the output bullion rises. The effect is not linear, however. This results from the relatively constant rate of As+Sb removal. The output $(As+Sb)_{Pb(l)}$ is given by,

$$\%\ (As+Sb)_{out} = \%\ (As+Sb)_{in} - \frac{a}{f} \times 100\% \qquad (6.15)$$

where "a" is the As+Sb removal rate in tph, and "f" is the bullion flow rate in tph. Therefore doubling the bullion flow basically cuts the change in $\%\ (As+Sb)_{out}$ in half. Again, however, there is a secondary effect which arises as output $\%\ (As+Sb)_{out}$ increases. As discussed above, as % (As+Sb) in output bullion increases the process becomes more efficient due to an increase in % (As+Sb) in slag, see Figure 6.8.

Temperature plays a role in determining softener efficiency as shown in Figure 6.12. Increasing temperature results in a decrease in process efficiency. As previously mentioned, this arises due to changes in equilibrium constants of Reactions (III) and (IV) with temperature, see Table 6.8. It is clear that monitoring of softener temperature will be an important part of the control system.

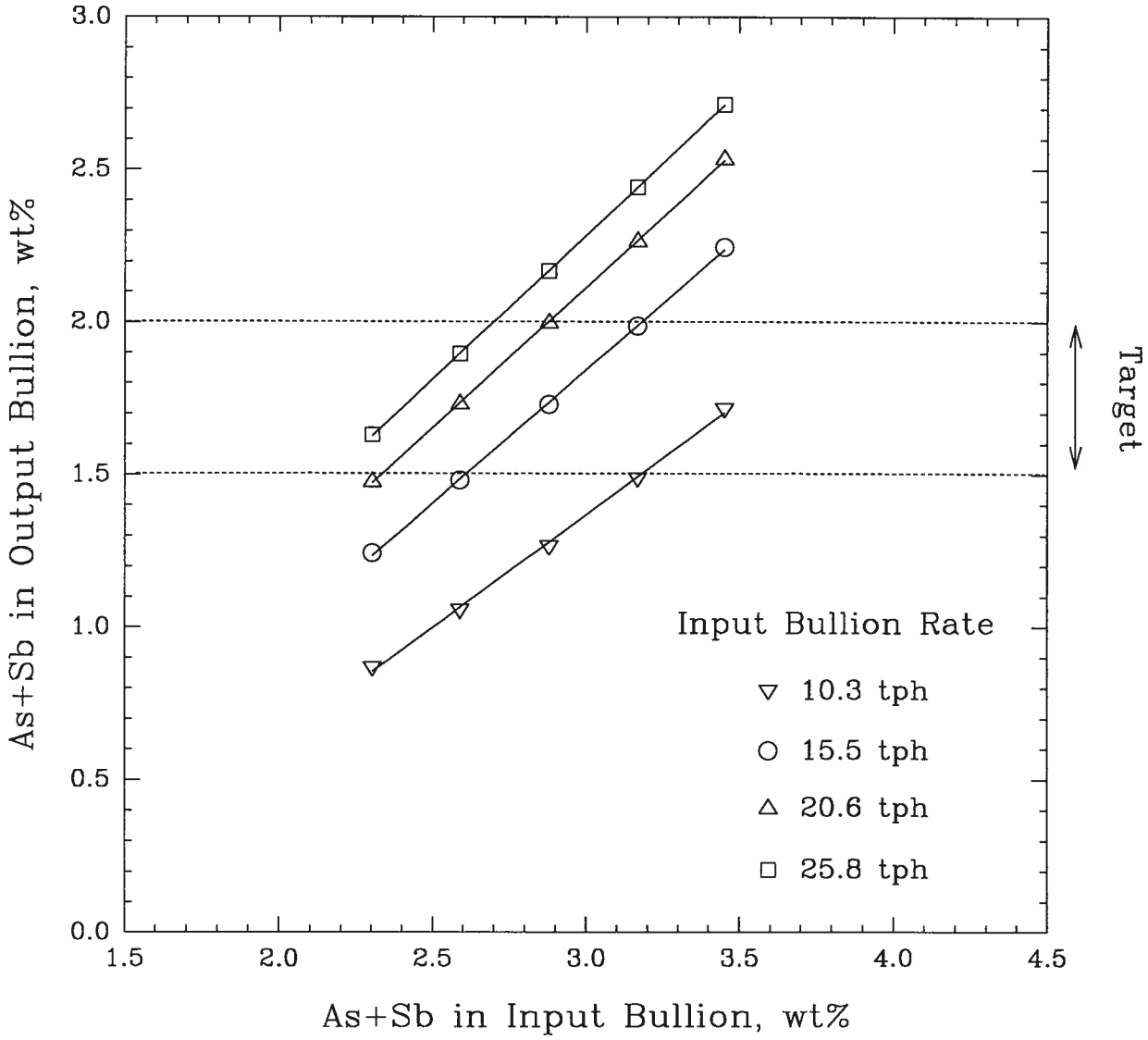

Figure 6.11 - Effect of bullion flow rate on impurity level in output bullion (615°C).

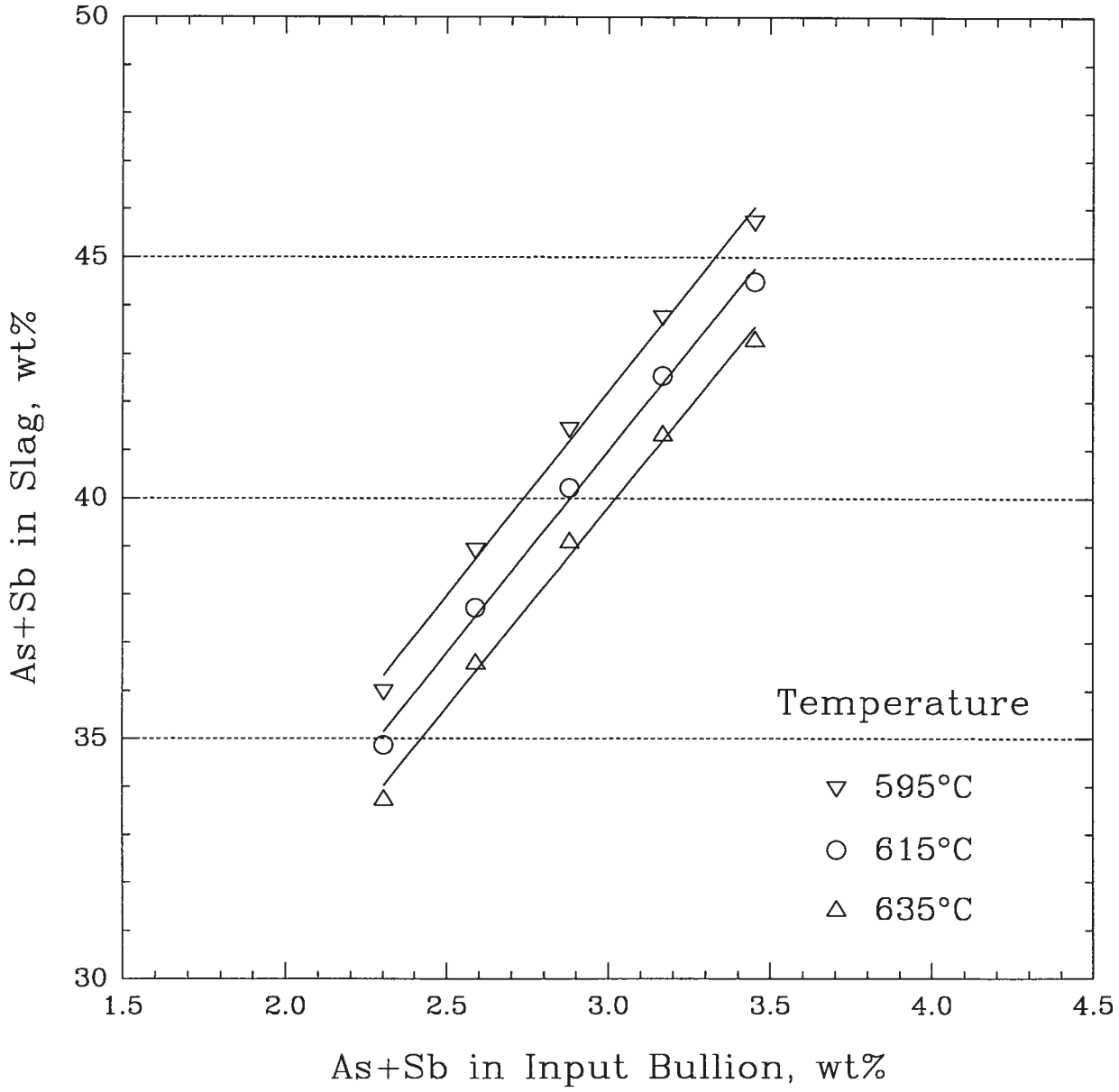

Figure 6.12 - Effect of temperature on impurity level in output bullion (40 Nm^3/h O_2, 15.5 tph bullion).

6.4 Control Strategy

The above calculations show that the concept of continuous single pass softening will meet the target set for lead softening, assuming the process operates close to thermodynamic equilibrium. A simple feedback system would control O_2 injection into the softener on the basis of the measured level of As+Sb in the output bullion. If the % (As+Sb) in the bullion increased, the O_2 injection rate would be increased to keep the As+Sb within a target range.

Based on data presented in this Chapter, a control algorithm could be developed to regulate O_2 flow to a continuous softener. The essential elements of a control system would be:

- a probe to measure As+Sb in the bullion output stream,
- a temperature probe in the softener, and
- a controller to control (1) O_2 injection rate and (2) burners/coolers in the softener.

The critical measurement of combined arsenic and antimony level in the lead bullion would be provided by the oxygen probe, whose design was described in Chapter 4 and industrial calibration was presented in Chapter 5. The simple feedback system described above, although providing the necessary control to keep the As+Sb within the target range, would not address the aspect of process optimization. The thermodynamic model could then be incorporated in the controller, provided further development was carried out to adjust for the idealized assumptions built into the model. Once part of the controller, the model would have the powerful role of providing the necessary data to run the process by predicting the optimum process parameters in response to the continuously

changing bullion characteristics. Contrary to a simple feedback control system, which would only adjust the O_2 injection rate to achieve bullion control, the model would be able to predict the effect of adjusting a number of process parameters to a change in bullion quality. For example, in response to an increase in emf, i.e. an increase of impurity level, the model would simulate the effect of an increase in O_2 injection rate, a decrease of input bullion flow, and a decrease of temperature. Based on the computations, the best alternative to meet the bullion target, with the highest oxygen efficiency and the best slag quality, would be suggested to the operator. In this manner, the operator would be able to take the most appropriate action to ensure process efficiency while meeting the composition target.

CHAPTER 7

SUMMARY AND RECOMMENDATIONS

7.1 Summary

An oxygen probe for continuous measurements in molten lead has been designed in the laboratory prior to being tested in an industrial environment. A commercially available yttria stabilized zirconia serves as solid electrolyte. The reference system is composed of a Cu-Cu_2O mixture. Both lead wire and conducting lead (probe housing) are made of 316 stainless steel. Sealing is achieved by means of a high temperature magnesia cement. An additional plug of copper powder, isolated from the reference system by a layer of alumina powder, serves as oxygen getter to eliminate oxygen ingress from the atmosphere. The extremity of the lead wire that is inserted into the probe is coated with cement to avoid any short-circuit with the Cu plug. These features were decisive in the success of the probe which provides a continuous measurement for several consecutive days. Once it was established that the probe was giving satisfactory measurements in the laboratory, i.e. quick response, proper response to temperature changes and oxygen potential changes, a testing campaign was carried out in the plant. The campaign was successful and a correlation between measured emf and As+Sb bullion content was established as follows

$$(wt\%)_{As+Sb} = -1.396 + 10.45 \times 10^{-3} (mV)_{meas} \qquad \pm 0.05\ (wt\%)$$

where $(wt\%)_{As+Sb}$ is the combined As+Sb bullion content in wt%, and $(mV)_{Measured}$ is the measured emf in mV.

Since any control decision would be based on the probe readings, it is crucial to regularly ensure the proper functioning of the probe. A method based on the thermal arrest technique has been tested and calibrated to provide for a rapid assessment of the probe reliability. The following correlation between liquidus temperature and As+Sb bullion content was obtained

$$(wt\%)_{As+Sb} = 37.57 - 0.117\,(°C)_{Liquidus} \qquad \pm 0.15\,(wt\%)$$

where $(wt\%)_{As+Sb}$ is the combined As+Sb bullion content in wt%, and $(°C)_{Liquidus}$ is the measured emf in mV. In order to take into account any long term changes in bullion characteristics, i.e. amount of As+Sb relative to the total impurity content, this relationship should to be re-assessed on a regular basis. Such updating would only involve a simple analysis of daily plant assays.

A thermodynamic model of the current semi-batch process was developed. An analysis of the process showed that a thermodynamic model can be used to represent process operation, and an equilibrium analysis gave a reasonable fit to operating data. The model developed for semi-batch softening was modified to continuous softening in order to simulate continuous single pass softening. The preliminary calculations showed that the concept of continuous single pass softening will meet the target set for lead softening, assuming the process will operate close to thermodynamic equilibrium. A slag high in As+Sb can be produced at bullion compositions in the target range for electrorefining. Based on the data presented in this thesis, a simple feedback control algorithm could be developed to regulate O_2 injections to a continuous softener on the basis of the measured level of As+Sb in output bullion. This critical measurement would be provided by the oxygen probe designed for this project.

7.2 Recommendations

This thesis has served as an attempt to explore the option of continuous single pass softening which would considerably simplify the softening circuit and lead to a bullion of consistent quality. Such a revision relies on the ability to continuously monitor the bullion quality, and on the understanding of process fundamentals.

Although successful in the plant, the oxygen probe would require a number of modifications in order to improve its reliability in an industrial environment. These modifications would include

(1) improving the thermal shock resistance by a proper preheating prior to immersion,

(2) improving the slag and sludge protection, and

(3) improving the resistance to liquid lead infiltrations.

The assessment of a control strategy, which would be based on a continuous measurement of the bullion quality, requires a proper understanding of the process. A model was developed to help understand the basic reactions assuming thermodynamic equilibrium. Further development of the model should be made to

(1) adjust for deviations from idealized assumptions,

(2) include certain kinetic effects, and

(3) include a heat balance.

Some laboratory tests should also be performed to develop a better model of the slag thermochemistry and to verify that the thermodynamic model applies to softening at high As+Sb levels.

REFERENCES

(1) T.R.A. Davey, "The Physical Chemistry of Lead Refining", Lead-Zinc-Tin'80, J.M. Cigan, T.S. Mackey and T.J. O'Keefe, Eds., The Met. Soc. of AIME, New York, 1980, pp. 477-507.

(2) J.F. Castle and J.H. Richards, "Lead Refining: Current Technology and a New Continuous Process", Advances in Extractive Metallurgy, M.J. Jones, Ed., Inst. Min. Met., London, 1977, pp. 217-234.

(3) G.R. Larouche, "Antimonial and Arsenial Lead Production at Cominco Trail Operations", Primary and Secondary Lead Processing, M.L. Jaeck, Ed., The Met. Soc. of CIM, 1990, pp. 103- 109.

(4) E.R. Freni, "Electrolytic Lead Refining in Sardinia", J. Metals, November 1965, pp. 1206-1214.

(5) C.A. Aranda and P.J. Taylor, "Electrolytic Lead Refining as Practiced by the Cerro de Pasco Corporation at La Oroya, Peru", Extractive Metallurgy of Lead and Zinc, C.H. Catterill and J.M. Cigan, Eds., Vol. II, The Met. Soc. of AIME, New York, 1970, pp. 891-915.

(6) D. Shen, "Lead Electrorefining at Shenyang Smelter, China", Mineral Processing and Extractive Metallurgy, M.J. Jones and P. Gill, Eds., Inst. Min. Met., London, 1984, pp. 599-605.

(7) J.L. Leroy, P.J. Lenoir and L.E. Escoyez, "Lead Smelter Operation at N.V. Metallurgie Hoboken S.A.", Extractive Metallurgy of Lead and Zinc, C.H. Catterill and J.M. Cigan, Eds., Vol. II, The Met. Soc. of AIME, New York, 1970, pp. 824-852.

(8) K. Emicke, G. Holzapfel and E. Kniprath, "Lead Refinery and Auxiliary By-Product Recoveries at Norddeutsche Affinerie (N.A.)", Extractive Metallurgy of Lead and Zinc, C.H. Catterill and J.M. Cigan, Eds., Vol. II, The Met. Soc. of AIME, New York, 1970, pp. 867-890.

(9) J.E. Bowers and R.D. Johnston, "Continuous Refining of Secondary Lead", Mineral Processing and Extractive Metallurgy, M.J. Jones and P. Gill, Eds., Inst. Min. Met., London, 1984, pp. 63-71.

(10) R.N. Gilges, E.K. Hudson and F.E. Pierce, "Lead Refining Practice at Bunker Hill", TMS Paper A81-35, 1981.

(11) G.K. Williams, "Development and Application of the Continuous Lead Refining Process", McCarron, Bird and Co., Ed., Melbourne, Australia.

(12) G.K. Williams, "Continuous Lead Refining at Port Pirie, South Australia", Trans. Am. Inst. Min. Engrs., Vol. 121, 1936, pp. 226-263.

(13) F.A. Green, "The Refining of Lead and Associated Metals at Port Pirie, South Australia", The Refining of Non-Ferrous Metals, The Inst. Min. Met., London, 1950, pp. 297-325.

(14) J. Blanderer, "The Refining of Lead by Oxygen", J. Metals, December 1984, pp. 53-54.

(15) G.C. Quigley and J.V. Happ, "Kinetics of Arsenic Removal From Lead Bullion", Research and Development in Extractive Metallurgy, Adelaide Branch, AusIMM, Adelaide, South Australia, May 1987, pp. 187-195.

(16) E.T. de Groot, M.T. Martin and G.W. Toop, "Partial Softening of Lead Bullion with Oxygen", Non-Ferrous Smelting Symposium, AusIMM-IE Aust Port Pirie Combined Group, Port Pirie, South Australia, September 1989, pp. 61-63.

(17) K. Kiukkola and C. Wagner, "Measurements on Galvanic Cells Involving Solid Electrolytes", J. Electrochem. Soc., Vol. 104, 1957, pp. 379-387.

(18) G.G. Richards, D. Dreisinger, E. Peters and J.K. Brimacombe, "Mathematical Modelling of Zinc Processes", Computer Software in Chemical and Extractive Metallurgy, W.T. Thompson, F. Ajersch and G. Eriksson, Eds., The Met. Soc. of CIM, Montreal, Canada, 1988, pp. 223-252.

(19) K.T. Jacob and T. Mathews, "Solid State Electrochemical Sensors in Process Control", Indian J. Technology, Vol. 28, June-August 1990, pp. 413-427.

(20) G.R. Fitterer, "Progress in the Development of a Device for Direct Determination of Oxygen in Liquid Steel", J. Metals, August 1966, pp. 961-66.

(21) G.R. Fitterer, "Further Development of the Electrolytic Method for the Rapid Determination of Oxygen in Liquid Steels", J. Metals, September 1967, pp. 92-96.

(22) G.R. Fitterer, C.D. Cassley and V. Vierbicky, "The Rapid Determination of Oxygen in Commercial Steel With the Solid Electrolyte Probe", J. Metals, June 1968, pp. 74-78.

(23) R.J. Fruehan, L.J. Martonik and E.T. Turkdogan, "Development of a Galvanic Cell for the Determination of Oxygen in Liquid Steel", Met. Trans., Vol. 245, 1969, pp. 1501-1509.

(24) C.K. Russell, R.J. Fruehan and R.S. Rittiger, "Probing for More Than Temperature", J. Metals, November 1971, pp. 44-47.

(25) D.A. Dukelow, J.M. Steltzer and G.F. Koons, "Oxygen Sensor: A New Base for Deoxidation Practices?", J. Metals, December 1971, pp. 22-25.

(26) E.T. Turkdogan and R.J. Fruehan, "Review of Oxygen Sensors for Use in Steelmaking and of Deoxidation Equilibria", Can. Met. Quarter., Vol. 11, 1972, pp. 371-382.

(27) M. Kawakami, K.S. Goto and M. Matsuoka, "A Solid Electrolyte Oxygen Sensor for Steelmaking Slags of the Basic Oxygen Converter", Met. Trans., Vol. 11B, 1980, pp. 463-69.

(28) D. Janke, "Fundamental Aspects of the Electrochemical Oxygen Measurement in Molten Iron and Iron Alloys", Applications of Solid Electrolytes, T. Takahashi and A. Kozawa, Eds., JEC Press, Cleveland, 1980, pp. 154-163.

(29) K.I. Suzuki and K. Sanbongi, "Application of Oxygen Probes to Steelmaking Process", Applications of Solid Electrolytes, T. Takahashi and A. Kozawa, Eds., JEC Press, Cleveland, 1980, pp. 164-170.

(30) T. Kawawa, R. Imai and H. Tokunaga, "Problems in Application of Oxygen Probes in Steelmaking Process", Applications of Solid Electrolytes, T. Takahashi and A. Kozawa, Eds., JEC Press, Cleveland, 1980, pp. 171-176.

(31) M. Matsuoka and I. Ikedo, "Recent Applications of Our Oxygen Probe for Sub-Lance System in Japanese Steelmaking Industry", Applications of Solid Electrolytes, T. Takahashi and A. Kozawa, Eds., JEC Press, Cleveland, 1980, pp. 177-180.

(32) W. Pluschkell, "Application of Oxygen Concentration Cells to Steel Making Problems", Applications of Solid Electrolytes, T. Takahashi and A. Kozawa, Eds., JEC Press, Cleveland, 1980, pp. 181-192.

(33) K.S. Goto, K. Nagata and S. Yamaguchi, "A Review of New Uses for Oxygen Sensors for Iron and Steelmaking Slags", Iron and Steelmaking, November 1983, pp. 43-52.

(34) K.S. Goto, "Use of Oxygen Sensors for Steelmaking in Japan", Scan. J. Met., Vol. 12, 1983, pp. 43-44.

(35) S. Ariga and H. Ogawa, Report no 17 of 2nd National Meeting of Oxygen Probes for Steelmaking, Tokyo, July 1977.

(36) T. Hiromoto, T. Saeki, Y. Igaki, T. Nisugi and K. Ishikura, "Development and Application of Oxygen Sensors to Steelmaking", J. Iron Steel Inst. Japan (Tetsu-to-Hagane), Vol. 63 , December 1977, pp. 2326-2334.

(37) K.S. Goto, "Solid State Electrochemistry and its Applications to Sensors and Electronic Devices", Materials Science Monographs, No 45, Elsevier, 1988.

(38) J. Dompas and J. Van Melle, "Operation of EMF Oxygen Probes in a Copper Refinery", J. Inst. Metals, Vol. 98, 1970, pp. 304-309.

(39) J.M. Dompas and P.C. Lockyer, "Oxygen Control in Liquid Copper by the Oxycell", Met. Trans., Vol. 3, 1972, pp. 2597-2604.

(40) W.T. Thompson and P. Tarassoff, "Determination of Oxygen in Copper with an Emf Probe", Can. Met. Quarter., Vol. 10, No 4, 1971, pp. 315-321.

(41) J.M. Floyd and D.S. Conochie, "Trials of Oxy-Probes in Liquid Converter Slags", C.S.I.R.O. Division of Chemical Engineering, 1976.

(42) N. Kemori, Y. Shibata and M. Tomono, "Application of Oxygen Probes to a Copper Flash Smelting Furnace", Met. Rev. of MMIJ, Vol. 4, No 1, 1987, pp. 40-52.

(43) O.M. Sreedharan, C. Mallinka and J.B. Gnanamoorthy, "Metallurgical Application of Solid Electrolyte Oxygen Sensors: A Review", Bull. Electrochem., Vol. 2, No 3, 1986, pp. 297-302.

(44) C.B. Alcock and T.N. Belford, "Thermodynamics and Solubility of Oxygen in Liquid Metals from E.M.F. Measurements Involving Solid Electrolytes, Part I - Lead", Trans. Faraday Soc., Vol. 60, 1964, pp. 822-835.

(45) G.G. Charette and S.N. Flengas, "Thermodynamic Properties of the Oxides of Fe, Ni, Pb, Cu, and Mn, by EMF Measurements", J. Electrochem. Soc., Vol. 115, 1968, pp. 796-804.

(46) R. Szwarc, K.E. Oberg and R.A. Rapp, "The Diffusivity and solubility of Oxygen in Liquid Lead from Electrochemical Measurements", High Temperature Science, Vol. 4, 1972, pp. 347-356.

(47) G.K. Bandyopadhyay and H.S. Ray, "Kinetics of Oxygen Dissolution in Molten Lead", Met. Trans., Vol. 2, 1971, pp. 3055-3061.

(48) K.T. Jacob and J.H.E. Jeffes, "Thermodynamics of Oxygen in Liquid Copper, Lead and Copper Lead Alloys", Trans. Inst. Min. Met., Vol. 80, 1971, pp. C32-C41.

(49) S. Otsuka and Z. Kozuka, "Activities of Oxygen in Liquid Lead and Antimony from Electrochemical Measurements", Met. Trans., Vol. 10B, 1979, pp. 565-574.

(50) S. Otsuka and Z. Kozuka, "Further Study on the Activities of Oxygen in Liquid Lead and Antimony by a Modified Coulometric Titration Method", Met. Trans., Vol. 12B, 1981, pp. 616-620.

(51) A. Taskinen, "Oxygen Metal (Ag, Au, Bi, Cu, In, Ni, Sb, Sn, Te) Interaction in Dilute Molten Lead Alloys", Acta Polytech. Scand., No 146, 1881.

(52) L. Fontainas, D. Verhulst and P. Bruwier, "Oxygen Potential Measurements in Lead Smelter Slags by Means of Disposable Solid Electrolyte Probes", Can. Met. Quart., Vol. 24, 1985, pp. 47-52.

(53) Ja. Dekeyser, F. Casteels, H. Tas, M. Soenen and M. Alberty, "On-Line Monitoring and Control in Dynamic Lithium and Static Lithium-Lead", Proceedings 13th Conference on Fusion Technology, Italy, 1984, pp. 1037-1044.

(54) Ja. Dekeyser, F. Casteels, H. Tas, N. Rumbaut and M. Soenen, "On-Line Monitoring and Control of Non-Metallic Impurities in Lithium and Sodium", Liquid Metal Engineering and Technology, Brit. Nuclear Energy Soc., London, 1985, pp. 163-170.

(55) F. De Schutter, Ja. Dekeyser, H. Tas and S. De Burbure, "Compatibility and Performance of Electrochemical Oxygen and Lithium Monitors in Liquid Pb-17Li", J. Nuclear Materials, Vol. 155-157, 1988, pp. 744-748.

(56) F. De Schutter, Ja. Dekeyser, J. Luyten and H. Tas, "Monitoring System for Chemical Characterization of Liquid Breeder Alloys", Sensors and Actuators, Vol. B1, 1990, pp. 446-450.

(57) F. De Schutter, Ja. Dekeyser, R. Deknock, R. Jacobs and H. Tas, "Electrochemical Sensors for Oxygen and Lithium Detection in Pb-17Li", Fusion Engineering and Design, Vol. 14, 1991, pp. 241-248.

(58) J.C. Dekeyser and F. De Schutter, "Development of Electrochemical Sensors for Pb-17Li", Final Report 89-92, Energy Division of the Vlaamse Instelling voor Technologisch Onderzoek (VITO), March 1993.

(59) Z. Kozuka, "Oxygen Potentials in Molten Metals, Mattes and Gases", Australia Japan Extractive Metallurgy Symposium, AusIMM, Sydney, Australia, 1980, pp. 335-341.

(60) R.C. Bell, G.H. Turner and E. Peters, "Fuming of Zinc from Lead Blast Furnace Slag", J. Metals, March 1955, pp. 472-477.

(61) H.H. Kellogg, "A Computer Model of the Slag-Fuming Process for Recovery of Zinc Oxide", Trans. Met. of AIME, Vol. 239, 1967, pp. 1439-1449.

(62) R.J. Grant and L.J. Barnett, "Development and Application of the Computer Model of the Slag Fuming Process at Port Pirie", South Australia Conference 1975, AusIMM, Melbourne, 1975, pp. 247-265.

(63) A.K. Kyllo and G.G. Richards, "A Mathematical Model of the Nickel Converter: Part I. Model Development and Verification", Met. Trans., Vol. 22B, 1991, pp. 153-161.

(64) S. Goto, "Copper Metallurgy - Practice and Theory", IMM, London, 1974, pp. 23-34.

(65) W.B. White, S.M. Johnson and G.B. Dantzig, "Chemical Equilibrium in Complex Mixtures", J. Chem. Phys., Vol. 28, May 1958, pp. 751-755.

(66) R.C. Oliver, S.E. Stephanou and R.W. Baier, "Calculating Free-Energy Minimization", Chem. Eng., February 1962, pp. 121-128.

(67) G. Eriksson, "Thermodynamic Studies of High Temperature Equilibria, III. SOLGAS, a Computer Program for Calculating the Composition and Heat Condition of an Equilibrium Mixture", Acta Chem. Scand., Vol. 25, 1971, pp. 2651-2658.

(68) G. Eriksson and E. Rosen, "Thermodynamic Studies of High Temperature Equilibria, VIII. General Equations for the Calculation of Equilibria in Multiphase Systems", Chem. Scripta, Vol. 4, 1973, pp. 193-194.

(69) A.Y. Vartiainen, P.A. Taskinen and A.T. Jokilaakso, "Thermochemical Description of Antimony and Arsenic in the Suspension Stage of the Outokumpu Flash Smelting Furnace", H.H. Kellogg International Symposium, QuantitativeDescription of Metals Extraction Processes, N.J. Themelis and P.F. Duby, Eds., TMS, 1991, pp. 45-67.

(70) G.G. Richards, J.K. Brimacombe and G.W. Toop, "Kinetics of the Zinc Slag Fuming Process: Part I. Industrial Measurements", Met. Trans. B, Vol. 16B, 1985, pp. 513-527.

(71) G.G. Richards and J.K. Brimacombe, "Kinetics of the Zinc Slag Fuming Process: Part II. Mathematical Model", Met. Trans. B, Vol. 16B, 1985, pp. 529-540.

(72) G.G. Richards and J.K. Brimacombe, "Kinetics of the Zinc Slag Fuming Process: Part III. Model Prediction and Analysis of Process Kinetics", Met. Trans. B, Vol. 16B, 1985, pp. 541-549.

(73) S.L. Cockcroft, G.G. Richards and J.K. Brimacombe, "High-Pressure Coal Injection in Zinc Slag Fuming", Met. Trans. B, Vol. 20B, 1989, pp. 227-235.

(74) J.W. Patterson, "Conduction Domains for Solid Electrolytes", J. Electrochem. Soc., Vol. 118, 1971, pp. 1033-1039.

(75) C.B. Choudhary, H.S. Maiti and E.C. Subbarao, "Defect Structure and Transport Properties", in Solid Electrolytes and Their Applications, E.C. Subbarao, Ed., Plenum Press, 1980, pp. 1-80.

(76) T.H. Etsell and S.N. Flengas, "The Electrical Properties of Solid Oxide Electrolytes", Chemical Reviews, Vol. 70, 1970, pp. 339-376.

(77) H.L. Tuller and A.S. Novick, "Doped Ceria as a Solid Oxide Electrolyte", J. Electrochem. Soc., Vol. 122, 1975, pp. 255-259.

(78) H.S. Maiti and E.C. Subbarao, "Electrical Conduction in CaO-Doped Thoria Electrolytes", J. Electrochem. Soc., Vol. 123, 1976, pp. 1713-1718.

(79) P.M. Mc Geehin and A. Hooper, "Review of Fast Ion Conduction Materials", J. Mater. Sc., Vol. 12, 1977, pp. 1-27.

(80) A. Hooper, "Fast Ionic Conductors", Contemp. Phys., Vol. 19, 1978, pp. 147-168.

(81) E.C. Subbarao and H.S. Maiti, "Solid Electrolytes with Oxygen Ion Conduction", Solid State Ionics, Vol. 11, 1984, pp. 317-338.

(82) A.J. Burggraaf, B.A. Boukamp, I.C. Vinke and K.J. de Vries, "Recent Developments in Oxygen-Ion Conducting Solid Electrolyte and Electrode Materials", Adv. Sol. State Chem., Vol. 1, 1989, pp. 259-293.

(83) Nippon Kagaku Togyo Co. Ltd., Marketing pamphlet.

(84) W.L. Worrell and J.L. Iskoe, "Kinetics of Oxygen Transfer at the Interface Between a Zirconia-Based Electrolyte and a Metal-Metal Oxide Electrode", Fast Ion Transport in Solids, W. Van Gool, Ed., IUPAC, North-Holland, Amsterdam, 1973, pp. 513-521.

(85) I. Barin and O. Knacke, "Thermochemical Properties of Inorganic Substances", Springer-Verlag, Berlin, 1973.

(86) O. Kubaschewski and C.B. Alcock, "Metallurgical Thermochemistry", 5th Ed., Pergamon Press, 1979.

(87) Y.K. Rao, "Stoichiometry and Thermodynamics of Metallurgical Processes", Cambridge University Press, 1985.

(88) L. Pankratz, "Thermodynamic Properties of Elements and Oxides", Bulletin No 672, US Bureau of Mines, 1982.

(89) I. Barin, "Thermochemical Data of Pure Substances", VCH, Weinheim, Germany, 1989.

(90) K. Itagaki, T. Shimizu and M. Hino, "Thermodynamic Studies of the Liquid Lead-Arsenic System", Report No 767, Research Institute of Mineral Dressing and Metallurgy, Tohoku University, Japan, 1978.

(91) R. Hultgren, P.D. Desai, D.T. Hawkins, M. Gleiser and K.K. Kelley, "Selected Values of the Thermodynamic Properties of Binary Alloys", America Society for Metals, 1973.

(92) H. Seltz and B.J. De Witt, "A Thermodynamic Study of the Lead-Antimony System", J. Am. Chem. Soc., Vol. 61, 1939, pp. 2594-2597.

(93) A.D. Zunkel and A.H. Larson, "Slag-Metal Equilibria in the Pb-PbO-Sb2O3 System", Trans. Met. Soc. AIME, Vol. 239, 1967, pp. 473-477.

(94) E. Sugimoto, S. Kuwata and S. Kozuka, "Activity Measurements in the Pb-Sn and Pb-Sb Alloys by E.M.F. Method with Y2O3 Doped Stabilized Zirconia at Low Temperatures", Nippon Kogyo Kaishi, Vol. 98, May 1982, pp. 39-45.

(95) V. Chaskar, "Thermodynamics of Softener Slags", unpublished work, University of British Columbia, Vancouver, Canada, 1995.

(96) H. Salomon-De-Friedberg, "Softener Metallurgy", Cominco Metals Development, Internal Memorandum No 840-10, June 1987.

APPENDIX 1

EXPERIMENTAL EQUIPMENT

Custom-made Furnace Specifications

Dimensions	1.0 m x 0.5 m x 0.5 m
Heating element	Chromel A-1 ribbon
Number of windings	104 with variable pitch as follows (from top to bottom): 7 in. with 4 windings/in. 4 in. with 31/2 windings/in. 8 in. with 21/2 windings/in. 4 in. with 31/2 windings/in. 7 in. with 4 windings/in.
Insulating materials	
Inner core	Solid alumina particles (with traces of titanium oxide)
Walls	Diatomite insulating bricks (Diatherm 23) Fiber frax
Measured resistance	12.4 Ω
Maximum temperature	1100°C
Hot zone (± 1°C)	~ 10 cm
Chamber diameter	~ 7 cm
Electromagnetic shield	Stainless steel foil
Other specifications	• Water cooled top and bottom gas-tight caps to allow control of the atmosphere • Power supply unit • Temperature controller (Omega CN9000 Series) • S-type control thermocouple

Corning 130 pH and Millivolt Meter

Specifications

Range	0 to ± 1800 mV
Resolution	0.1 mV
Relative accuracy	± 0.2 mV
Repeatability	± 0.1 mV
Recorder output	Adjustable
Modes	STANDBY, pH, REL mV, mV
Input impedance	$> 10^{12}$ ohms

DAS-8 Board

Features

- 8 analog input channels
- 12-bit resolution
- 7 digital I/O bits (4 out, 3 in)
- 4000 samples per second using Call Driver
- On-board sample pacer clock

Specifications

Number of channels	8, single-ended
Resolution	12 bits (2.4 mV/bit)
Accuracy	0.01% of reading ± bit
Full scale	±5 volt
A/D type	Successive approximation
Linearity	±1 bit
Coding	Offset binary
Overvoltage	Continuous single channel to ±35 V
Input impedance	10^7 ohms
Input current	100 nA max at 25°C

Exp-16 Channel Multiplexer

Features

- Expands any analog input to 16 differential inputs
- Cold-junction compensation for thermocouples
- Open thermocouple detection
- Shunt terminals for current measurement
- Daisy-chain up to 8 boards
- Instrumentation amplifier with switch-selectable gains of 0.5, 1, 2, 10, 50, 100, 200, and 1000
- Input filtering

Specifications

Input bias current	2 nA typ, 6 nA max
Temperature coefficient	5 ppm typ, 15 ppm max
Overvoltage protection	±30 V continuous
Common mode voltage	±10 V max
Analog output voltage	±5 V max
Analog output current	20 mA max
Cold-junction compensation	+24.4 mV/°C (.1°C/bit) 0.0 V at 0.0°C
Thermocouple types accepted	J, K, T, E, S, R, B

APPENDIX 2

PLANT DATA

	Sb wt%	As wt%	Bi wt%	Cu wt%
Input bullion - cycle 1	1.20	0.18	0.35	0.08
Softener bullion - Start of cycle 1	0.77	0.07	0.31	0.11
Softener bullion - End of cycle 1	0.72	0.07	0.33	0.11
Slag sample - End of cycle 1	24.1	6.9	-	-

Table A2.1 - Assays of input and output bullion, and slag from cycle 1 (June test).

	Sb wt%	As wt%	Bi wt%	Cu wt%
Input bullion - cycle 2	1.19	0.18	0.35	0.09
Softener bullion - Start of cycle 2	0.78	0.08	0.32	0.11
Softener bullion - End of cycle 2	0.71	0.06	0.31	0.11
Slag sample - End of cycle 2	24.3	6.9	-	-

Table A2.2 - Assays of input and output bullion, and slag from cycle 2 (June test).

	Sb wt%	As wt%	Bi wt%	Cu wt%
Input bullion - cycle 3	1.16	0.17	0.34	0.10
Softener bullion - Start of cycle 3	0.77	0.07	0.31	0.11
Softener bullion - End of cycle 3	0.69	0.06	0.32	0.11
Slag sample - End of cycle 3	24.1	6.9	-	-

Table A2.3 - Assays of input and output bullion, and slag from cycle 3 (June test).

	Sb wt%	As wt%	Bi wt%	Cu wt%
Input bullion - cycle 4	1.13	0.16	0.32	0.11
Softener bullion - Start of cycle 4	0.78	0.08	0.32	0.11
Softener bullion - End of cycle 4	0.67	0.05	0.29	0.11
Slag sample - End of cycle 4	24.4	6.9	-	-

Table A2.4 - Assays of input and output bullion, and slag from cycle 4 (June test).

	Sb wt%	As wt%	Bi wt%	Cu wt%
Input bullion - cycle 5	1.13	0.16	0.32	0.10
Softener bullion - Start of cycle 5	0.75	0.07	0.30	0.11
Softener bullion - End of cycle 5	0.68	0.06	0.31	0.11
Slag sample - End of cycle 5	24.5	6.9	-	-

Table A2.5 - Assays of input and output bullion, and slag from cycle 5 (June test).

	Sb wt%	As wt%	Bi wt%	Cu wt%
Input bullion - cycle 6	1.13	0.16	0.33	0.10
Softener bullion - Start of cycle 6	0.72	0.06	0.31	0.10
Softener bullion - End of cycle 6	0.68	0.06	0.31	0.11
Slag sample - End of cycle 6	24.5	6.9	-	-

Table A2.6 - Assays of input and output bullion, and slag from cycle 6 (June test).

	Sb wt%	As wt%	Bi wt%	Cu wt%
Input bullion - cycle 1	0.93	0.21	0.26	0.07
Softener bullion - Start of cycle 1	0.68	0.10	0.25	0.07
Softener bullion - End of cycle 1	0.62	0.08	0.26	0.08
Slag sample - End of cycle 1	18.7	8.6	-	-

Table A2.7 - Assays of input and output bullion, and slag from cycle 1 (October test).

	Sb wt%	As wt%	Bi wt%	Cu wt%
Input bullion - cycle 2	0.91	0.20	0.26	0.08
Softener bullion - Start of cycle 2	0.67	0.09	0.25	0.08
Softener bullion - End of cycle 2	0.61	0.08	0.26	0.08
Slag sample - End of cycle 2	18.8	8.5	-	-

Table A2.8 - Assays of input and output bullion, and slag from cycle 2 (October test).

	Sb wt%	As wt%	Bi wt%	Cu wt%
Input bullion - cycle 3	0.89	0.19	0.26	0.07
Softener bullion - Start of cycle 3	0.66	0.09	0.26	0.07
Softener bullion - End of cycle 3	0.59	0.08	0.25	0.08
Slag sample - End of cycle 3	18.8	8.6	-	-

Table A2.9 - Assays of input and output bullion, and slag from cycle 3 (October test).